Equilibre magnétohydrodynamique des protubérances solaires

Jean-Marie Malherbe

UNIVERSITE DE PARIS VII

THESE

DE

DOCTORAT DE TROISIEME CYCLE

présentée

par

Jean-Marie MALHERBE

EQUILIBRE MAGNETOHYDRODYNAMIQUE DES PROTUBERANCES SOLAIRES

Soutenue le 15 AVRIL 1983 devant la commission d'examen :

J. HEYVAERTS	Président
P. MEIN	Examinateurs
S. SAHAL-BRECHOT	
B. SCHMIEDER	
J.P. ZAHN	

REMERCIEMENTS

Le présent travail m'a été proposé par P. MEIN et B. SCHMIEDER. Outre leur contribution, ils en ont assuré la direction scientifique toujours avec une grande compétence, disponibilité et dynamisme. Qu'ils en soient ici vivement remerciés.

J'ai collaboré aussi parfois avec N. MEIN, E. RIBES, G. SIMON et J.C. VIAL dont les suggestions m'ont toujours été bénéfiques. Je leur en suis reconnaissant, ainsi qu'à M.J. MARTRES, pour les fréquentes discussions que nous avons eues.

La partie théorique de cette thèse est le fruit du travail commencé pendant mon séjour à l'Université de St Andrews, en Ecosse. Je remercie E. PRIEST de m'y avoir réservé un si bon accueil et d'avoir guidé si efficacement mes premiers pas en modellisation. Ma plus profonde gratitude va aussi à J. HEYVAERTS dont les nombreux conseils m'ont été profitables et sans l'impulsion de qui notre modèle de protubérance n'aurait pu voir le jour.

Je tiens aussi à exprimer mes remerciements à tous les membres de mon jury, qui m'ont fait l'honneur d'accepter de juger ce travail.

Je voudrais remercier C. COUTARD, R. HELLIER et A. MIGUEL pour la qualité des observations Hα au DPSM, ainsi que P. MICHENEAU pour son assistance dans l'élaboration de mes nombreux programmes.

Je suis redevable à D. DURAIN, C. BRECHET, G. SERVAJEAN et J.R. FREMY de leur aide matérielle, ainsi qu'à G. PRIEUR d'avoir assuré la dactylographie du manuscrit.

Enfin, mes remerciements s'étendent à toutes les personnes non citées, qui, par leur concours ou par leurs conseils, m'ont permis de mener à bien, je l'espère, ce travail.

MEUDON, Février 1983

RESUME

Nous étudions le champ des vitesses (Partie I) et les instabilités (partie II) dansles protubérances solaires à partir d'observations en Hα (DPSM de la Tour Solaire de Meudon) et C IV (spectropolarimètre UV à bord du satellite SMM). Nous proposons ensuite un modèle théorique (partie III) basé sur nos résultats dynamiques et les mesures Hanlé de champ magnétique de Leroy (Pic du Midi).

Première partie :

Nous analysons et comparons les mouvements stationnaires et les oscillations de vitesse en Hα dans un filament (article 1, communication 1) et en C IV dans la zone de transition (communication 1). Des mouvements ascendants sont décelés, dans les deux raies, à l'emplacement de la protubérance. Les oscillations chromosphériques y sont fortement réduites en Hα , suggérant une réflexion sous le filament. Par contre, on y détecte des oscillations en C IV, pouvant être attribuées à une contribution prépondérante de la région de transition chromosphère-couronne sur l'interface protubérance-couronne.

L'observation centre bord (article 2) d'un filament en Hα conduit à 2 types de circulations possibles, selon la durée de vie des mouvements : montée de matière à travers la protubérance et alimentation sur les bords (durée de vie de quelques jours, modèle proposé en 3ème partie), ou bien organisation en boucles de vitesse (durée de vie de quelques dizaines de minutes, modèle de Ribes et Unno, 1980).

Seconde partie :

Deux mécanismes de "disparitions brusques" en Hα , thermique et dynamique, ont été mis en évidence. Dans le premier cas (communication 2), la comparaison entre profils observés à l'emplacement du filament et profils théoriques, calculés par transfert radiatif dans un modèle d'atmosphère (VAL + Protubérance), suggère un processus de chauffage du plasma. Dans le second cas (communication 3), la disparition,

hautement dynamique, s'accompagne d'éjections de matière accélérée à des vitesses supersoniques (100 km s^{-1}) dans des tubes de champ magnétique.

Troisième partie :

Nous proposons un modèle théorique de protubérance quiescente basé sur les résultats observationnels les plus récents, à savoir :

a - champ de vitesses : mouvements ascendants dans le filament, alimentation coronale sur les bords (article 2)

b - champ magnétique : support de Kuperus-Raadu plus probable que Kippenhahn-Schlüter (Leroy, 1982)

c - formation des filaments : au-dessus des frontières entre cellules de polarités opposées animées de mouvements d'approche (ceintures polaires par exemple).

Etudiant la magnétostatique de plusieurs modèles construits à l'aide des fonctions holomorphes, ainsi que leur évolution engendrée par des circulations photosphériques, nous montrons que seul un modèle de type Kuperus-Raadu à reconnections magnétiques stationnaires, dont les pieds des lignes de force sont entrainés par des mouvements convergents, peut rendre compte des conclusions (a, b, c). La dynamique du flux ascendant transporté dans le filament par le champ magnétique est modellisée (article 3). Les processus de condensation stationnaire et de refroidissement du plasma coronal alimentant la protubérance sur ses bords, au dessus du point de reconnection, ainsi que sa dynamique, sont explicités (article 4).

ABSTRACT

Velocity fields (part 1) and instabilities (part 2) in solar prominences are studied from observations in Hα (MSDP at the Meudon Solar Tower) and C IV (UVSP aboard the SMM satellite). A theoretical model (part 3) is proposed to account for our dynamical results and Hanlé magnetic field measurements by Leroy (at Pic du Midi).

Part 1 :

Steady flows and velocity oscillations are analysed in Hα filaments (paper 1 and communication 1) and, at the same place, in the C IV transition zone (communication 1). Hα and C IV results are compared. Upward motions are found, in both lines, at the prominence location. Chromospheric oscillations are strongly reduced in the Hα filament, suggesting a reflection below, while, in the C IV corresponding region, oscillations are detected : they are more likely due to the chromosphere-corona transition layer than to the prominence-corona one.

Centre to limb observations (paper 2) of a Hα filament leads to different types of material circulations, according to their life time : long-lived motions (a few days) suggest upflows accross filaments and a fast input of plasma on both sides (model of part 3) ; while short-lived ones may be interpreted in terms of velocity loops (model of Ribes and Unno, 1980).

Part 2 :

We give evidence of two mechanisms, thermal and dynamical, for "disparitions brusques". In the first case (communication 2), the comparison between Hα profiles, observed during a filament dissapearance, and computed by radiative transfer (atmospheric model VAL + prominence) suggests a heating process. In the second case (communication 3), the instability is highly dynamic : ejecta of Hα material accelerated to supersonic velocities (100 km s^{-1}) inside magnetic tubes are analysed.

Part 3 :

A model for quiescent solar prominences is proposed to explain the most recent observational results , namely :

a - velocity fields : upflows accross filaments and coronal input on both edges (paper 2)

b - magnetic fields : Kuperus-Raadu supports seem to be more frequent than Kippenhahn-Schlüter ones (Leroy, 1982)

c - prominence formation : it often occurs above boundaries between giant and approaching together cells of opposite polarities (as in polar crowns).

We study the magnetostatics of several models built with the help of holomorphic functions . Then, we investigate their evolution, through series of equilibria, due to photospheric flows. We show that conclusions (a, b, c) may well be explained by a stationary reconnection model of Kuperus-Raadu type, in which the foot points of magnetic lines are submitted to converging motions. The dynamics of cold material carried up accross the filament by the magnetic field is presented (paper 3). The steady condensation and cooling processes, and the dynamics of the coronal plasma flowing along field lines and entering the prominence on both sides of the sheet, just above the reconnection site, are investigated (paper 4).

TABLE DES MATIERES

I - INTRODUCTION I

II - LE CHAMP DES VITESSES DANS LES PROTUBERANCES QUIESCENTES 8

1 - Etat des observations du champ magnétique et du champ des vitesses 9

2 - Contribution personnelle : mouvements stationnaires et oscillations

. Présentation I8

. Article 1 (Astron. Astrophys., 1981, 102,124) : "Dynamics in the filaments - I - Oscillations in a quiescent filament" 20

. Communication 1 (SMM Workshop, Janvier 1983) : "Dynamics of solar filaments : mass motions and oscillations in Hα and C IV" 25

. Article 2 (Astron. Astrophys., 1983, sous presse) "Dynamics of solar filaments - II - mass motions in an active region filament from Hα centre to limb observations" 45

III - LES INSTABILITES DANS LES PROTUBERANCES - DISPARITIONS BRUSQUES. 55

1 - Etat des observations et des modèles 56

2 - Contribution personnelle : deux mécanismes de disparitions brusques

. Présentation 63

. Communication 2 (24è COSPAR, Mai 1982) : "Heating of preflare filaments" 66

. Communication 3 (24è COSPAR, Mai 1982) : "Mass motions in preflare filaments" 78

IV - UN MODELE DYNAMIQUE DE PROTUBERANCE QUIESCENTE 86

1 - Etat des modèles : formation des filaments, magnétostatique et dynamique 87

2 - Contribution personnelle : construction d'un nouveau modèle

. Présentation 95

. Article 3 (Astron. Astrophys., 1983, sous presse) "Current sheet models for solar prominences - I - Magnetostatics of support and evolution through quasi-static models" 96

. Article 4 (soumis à Astron. Astrophys.) : "Current sheet models for solar prominences -II- Energetics and condensation process" I3I

V - CONCLUSIONS ET PERSPECTIVES I54

- Références bibliographiques I57

- Références des articles et communications constituant la thèse. I60

I - INTRODUCTION

I - 1 - BREF HISTORIQUE

Bien que la première "description" des protubérances ait été donnée par Vassénius en 1733, "ce fut pendant l'éclipse du 8 Juillet 1842 que l'attention des astronomes fut attirée par ces protubérances, qui s'élancent autour de la lune comme des flammes gigantesques, de couleur rose ou fleur de pêcher" (Secchi, 1875). D'abord considérées comme de "pures illusions d'optique, mirages produits à la surface de la lune", elles furent prises ensuite pour des "montagnes, des flammes ou des nuages" à la surface du soleil. Secchi rapporte : " le nombre des protubérances était incalculable. Le soleil nous parut tout environné de flammes ; elles étaient tellement multipliées qu'il nous paraissait impossible de les compter". Face à ces difficultés et à la grande "vivacité" des protubérances, Secchi substitua en 1860 la photographie à l'observation directe. Mais le plus gros progrès fut consécutif à l'utilisation d'un spectroscope à fente étroite qui permit, durant l'éclipse du 18 Août 1868, d'identifier les protubérances à d'énormes masses de gaz. Cette éclipse, écrit Secchi, "sera une date mémorable dans l'histoire de l'astronomie, car c'est alors que M. Janssen apprit aux savants à étudier en tous temps les protubérances". En effet, le lendemain, Janssen, pointant son instrument vers le bord du disque solaire, découvrait que leur observation hors éclipse était possible, grâce à la spectroscopie.

Dès lors, l'étude systématique des protubérances a commencé, s'est étendue à toutes les longueurs d'onde du spectre électromagnétique et se poursuit aujourd'hui à l'aide d'instruments puissants :

- au sol, en optique avec de grands spectrographes à haute dispersion (Double Passage Soustractif Multicanal de la Tour Solaire de Meudon) ou, plus simplement, à l'aide de filtres monochromatiques (héliographe à 3 longueurs d'onde de Meudon) et en radio (radiohéliographe et radiospectrographe multicanal numérique de Nançay).
- en ballon, tir fusée ou mieux, sur orbite, avec de plus petits instruments, souvent moins performants, mais permettant d'explorer les domaines UV, X et γ du spectre solaire (SMM).

I - 2 - INTERÊT SCIENTIFIQUE DE CETTE ETUDE DES PROTUBÉRANCES SOLAIRES.

Le Soleil est la seule étoile qui nous fournit des données à haute résolution spatiale. Les processus physiques qu'on y rencontre sont ceux, évidemment, que l'on s'attend à reconnaître dans d'autres atmosphères stellaires. Le soleil peut donc servir de test et de guide à l'élaboration des théories stellaires. La dégradation des observations solaires par intégration sur le disque et la comparaison aux étoiles peut fournir des renseignements précieux sur la structure globale des atmosphères. Inversement, la résolution spatiale du soleil peut souvent aider à déterminer l'origine et la nature des mécanismes physiques mis en jeu sur les étoiles (champs magnétiques, éruptions, etc...).

D'autre part, le Soleil est un véritable laboratoire de physique des plasmas et magnétohydrodynamique dont les conditions "expérimentales" (le chercheur n'en est pas maître) sont impossibles à réaliser sur Terre. L'étude du plasma solaire est donc complémentaire, par exemple, de celle du Tokamak, dans lesquels certains processus peuvent être communs : un bon exemple est fourni par le phénomène de reconnection magnétique, engendrant des éruptions solaires, ou des disruptions dans les tokamaks (Dubois et Samain, 1980).

a - Relation avec le chauffage des couches extérieures de l'atmosphère solaire

L'atmosphère solaire présente une remontée de température dans ses couches extérieures (4300 K au pied de la chromosphère à plus de 10^6K dans la couronne), que l'on peut interpréter par un chauffage dû à la dissipation d'ondes de choc. Ces chocs pourraient résulter de la transformation d'ondes acoustiques, engendrées par la turbulence au sommet de la zone convective : la densité atmosphérique décroissant avec l'altitude, l'amplitude des oscillations augmente et les effets non linéaires (raidissement du front d'onde) apparaîssent (revue de Jordan, 1981).

Mais des résultats récents (Mein et Schmieder, 1981) ont montré que le chauffage ne pouvait pas s'expliquer par un simple modèle homogène et stratifié. On doit tenir compte de la structure hétérogène de la chromosphère (réseau, cellules, plages, protubérances...) et encore plus de la couronne (trous coronaux, boucles, arches...). Ces hétérogénéités étant déterminées par l'organisation du champ magnétique, dans lequel le plasma est gelé (dû à sa forte conductivité), le transport de l'énergie mécanique, la propagation et la dissipation d'ondes MHD dans les tubes de flux doivent être examinés (revue de B. Roberts, 1980), ainsi que les effets dissipatifs des ondes de surface (revue de Kuperus et Heyvaerts, 1980). L'étude des filaments en temps que structures dominées par les forces magnétiques, peut contribuer à la compréhension de ces mécanismes. Nous présentons (chapitre II) pour la première fois, une analyse et une comparaison des oscillations dans les filaments (article 1, communication 1) et la zone de transition (communication 1).

b - Relation avec les instabilités et le déclenchement des éruptions.

La disparition des protubérances est souvent suivie d'une éruption en double filet ou "two ribbon flare". Les mécanismes régissant la simple "disparition brusque" d'un filament quiescent pourraient bien être les mêmes que ceux gouvernant le déclenchement des éruptions, la principale différence résidant dans l'énergie magnétique mise en jeu et l'échelle spatiale (revue de Priest, 1981). On a donc tout intérêt à étudier les processus de déstabilisation des filaments, tant observationnellement que théoriquement, car leur configuration magnétique est plus simple, en général, que celle des éruptions. Nous abordons cet aspect au chapitre III (communications 2 et 3) en mettant en évidence et quantifiant deux processus bien distincts de "disparitions brusques", thermique et dynamique, déjà suggérés par Mouradian et al., (1980)

c - L'équilibre des protubérances

Bien entendu, le succès de l'étude des instabilités dépend étroitement du degré de connaissance que nous avons de l'équilibre des protubérances. De nombreux modèles concernant la formation et la magnétostatique des filaments ont déjà été proposés (revue du chapitre IV). Mais les observations les plus récentes (Martres et al, 1981) indiquent que l'équilibre n'est pas statique mais dynamique, avec des mouvements permanents, ce qui implique de plus un processus de condensation et de refroidissement stationnaires du plasma alimentant la protubérance. Les difficultés inhérentes à ce couplage entre le mouvement et les mécanismes de condensation, alliées à l'insuffisance des observations disponibles (nécessitant une étude statistique et quantitative du champ des vitesses dans un champ à 2 dimensions suffisamment grand avec de bonnes résolutions temporelles et spatiales, ce dont peu d'instruments sont capables) font que ce domaine de recherche, malgré son importance capitale pour l'étude ultérieure des instabilités, reste encore peu exploré . Si quelques résultats observationnels ont été obtenus (chapitre II-1), aucun modèle théorique parmi les rares existants (Uchida, 1980 ; Ribes et Unno, 1980) n'est vraiment satisfaisant. Le présent travail tente d'y remédier.

I - 3 - CONSTRUCTION D'UN MODÈLE DYNAMIQUE DE PROTUBÉRANCE SOLAIRE.

L'élaboration d'un modèle d'équilibre dynamique et thermique de protubérance requiert une bonne connaissance du champ magnétique et du champ des vitesses qui y règnent.

Pour le champ magnétique, nous nous sommes fiés aux récents résultats de Leroy et al (1982), obtenus par effet Hanlé au Pic du Midi, méthode beaucoup plus riche en informations que les techniques magnétographiques classiques (effet Zeeman).

Le Chapitre II de ce mémoire est consacré à l'étude statistique et quantitative du champ des vitesses dans les filaments, à l'aide d'observations C IV au spectropolarimètre UV du satellite SMM, et, surtout, d'observations Hα au spectrographe (Mein, 1977) à Double Passage Soustractif Multicanal (DPSM) de la tour solaire de Meudon. Cette technique est beaucoup plus puissante qu'une spectrographie classique à fente fine, pour une étude de la dynamique solaire, car elle permet d'obtenir, toutes les 5 secondes, à l'aide de 9 canaux distants de 0.3 Å, les profils Hα (d'où nous déduisons les fluctuations d'intensité et les "Dopplershifts") simultanément en tous les points (28000) d'un champ à 2 dimensions de 8' x 1', résolu spatiallement à 1". A l'aide d'observations centre bord (article 2) nous avons pu mettre en évidence un modèle de circulations globales stationnaires, par reconstitution du champ des vitesses à 3 dimensions, dans lequel la protubérance est traversée par un flux montant avec une entrée de nouveau plasma sur chacun de ses deux bords. Mais actuellement, aucun modèle théorique n'est capable d'en rendre compte.

Un défaut commun à tous les modèles, jusqu'ici, a été de décrire le mouvement à l'aide d'un mécanisme de siphon dans un champ magnétique statique. L'évolution du support n'a jamais été envisagée, sauf par Raadu (1979), et, encore moins, son influence sur la dynamique. Or, cette évolution semble observationnellement très probable, car les filaments se forment au dessus des lignes d'inversion entre cellules de polarités

magnétiques opposées animées, dans la ceinture polaire au moins, de vitesses d'approche, entrainant les pieds des lignes de force supportant la structure.

Nous présentons plusieurs modèles de support magnétique à champ potentiel, construits à l'aide de fonctions holomorphes simples (chapitre IV, article 3). Etudiant leur évolution sous l'influence de mouvements photosphériques convergents, nous concluons, pour expliquer nos observations de vitesses, que le support magnétique doit être du type Kuperus-Raadu, auquel Leroy accorde par ailleurs la plus forte probabilité.

Nous proposons donc un modèle stationnaire dans lequel le chaud plasma coronal se condense et se refroidit, guidé par les lignes de force, en approchant la protubérance, au-dessus du point de reconnections de la structure. La matière froide est ensuite transportée au travers du filament par les mouvements ascendants du champ magnétique. La dynamique est étudiée dans l'article 3. Les processus de condensation, ainsi que la dynamique du plasma coronal alimentant la protubérance sont l'objet de l'article 4.

I - 4 - ORGANISATION DU PRÉSENT MÉMOIRE

Ce travail est divisé en trois chapitres : champ des vitesses dans les protubérances quiescentes (chapitre II), instabilités et disparitions brusques (chapitre III) et modèle dynamique de filament (chapitre IV). Chacun de ces 3 chapitres est divisé en deux parties : dans la première, nous présentons une brève revue de l'état des observations ou des modèles, de façon à situer notre contribution personnelle, exposée dans la seconde partie, à l'aide d'articles acceptés (1,2, et 3) ou soumis (4), et de communications à des colloques internationaux (1,2 et 3).

II - LE CHAMP DES VITESSES DANS LES PROTUBERANCES QUIESCENTES.

"LES PROTUBERANCES SE PRÉSENTENT SOUS DES ASPECTS SI BIZARRES ET SI CAPRICIEUX QU'IL EST ABSOLUMENT IMPOSSIBLE DE LES DÉCRIRE AVEC QUELQUE EXACTITUDE"

SECCHI, 1875, " LE SOLEIL"

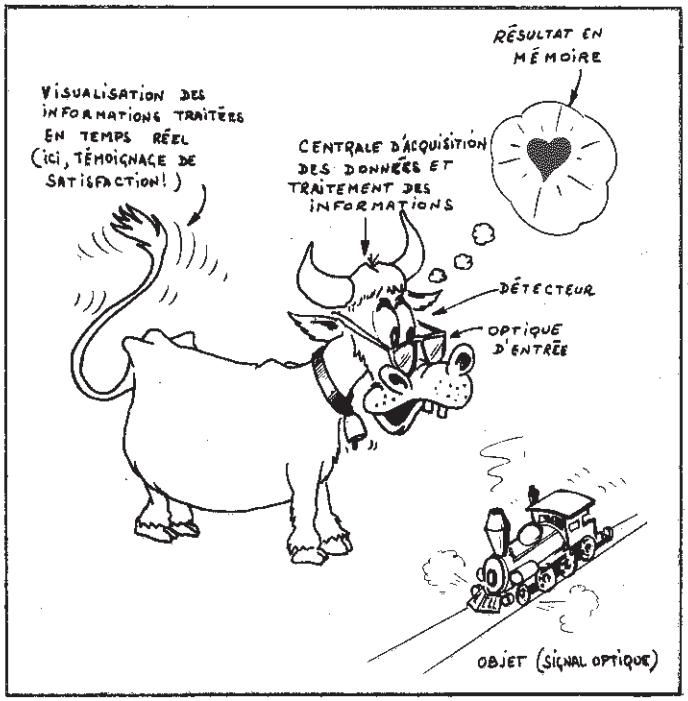

II - 1 - ETAT DES OBSERVATIONS DU CHAMP MAGNETIQUE ET DU CHAMP DES VITESSES.

Les protubérances (filaments) sont très schématiquement, d'énormes feuillets de matière de type chromosphérique froide (10^4K) et dense (10^{-13} g cm^{-3}) en suspension dans la couronne solaire, 100 fois plus chaude(10^6K) et plus ténue (10^{-15} g cm^{-3}). Les filaments sont parcourus par un courant électrique $\vec{j}$ et suspendus contre la gravité $\vec{g}$ par des champs magnétiques (force de Lorentz $\vec{j} \wedge \vec{B}$) dont les lignes de force sont ancrées dans la photosphère de part et d'autre d'une ligne d'inversion de polarité (Figure II-1). Des "pieds" relient le corps de la protubérance à la chromosphère. Ces "pieds", qui peuvent être des régions d'effondrement du champ magnétique (Milne et al, 1979), ou des régions d'instabilité de l'interface protubérance couronne (Nakagawa et Malville, 1969), sont actuellement les régions les plus mal comprises des protubérances (Figure II-3). Une organisation de la matière filamenteuse en fins filets verticaux a été décelée par Dunn (1960) et est peut être dûe à une instabilité de "tearing mode". La structure fine en arches magnétiques froides individuelles regroupées en bouquets à l'emplacement des "pieds" (Figure II-4) reste actuellement difficile à interpréter ("tearing modes" encore ?). Enfin, de nombreux types de protubérances existent, selon leur liaison avec des régions actives : les filaments de plage, par exemple, sont plus petits, plus bas, mais aussi plus actifs que les filaments quiescents. Leur densité et leur champ magnétique sont aussi plus forts (figure II-2).

Une revue des propriétés de base des protubérances (morphologie, observations et modèles) peut être trouvée dans Tandberg-Hanssen (1974), et, de façon plus spécialisée, dans Jensen et al, (1979).

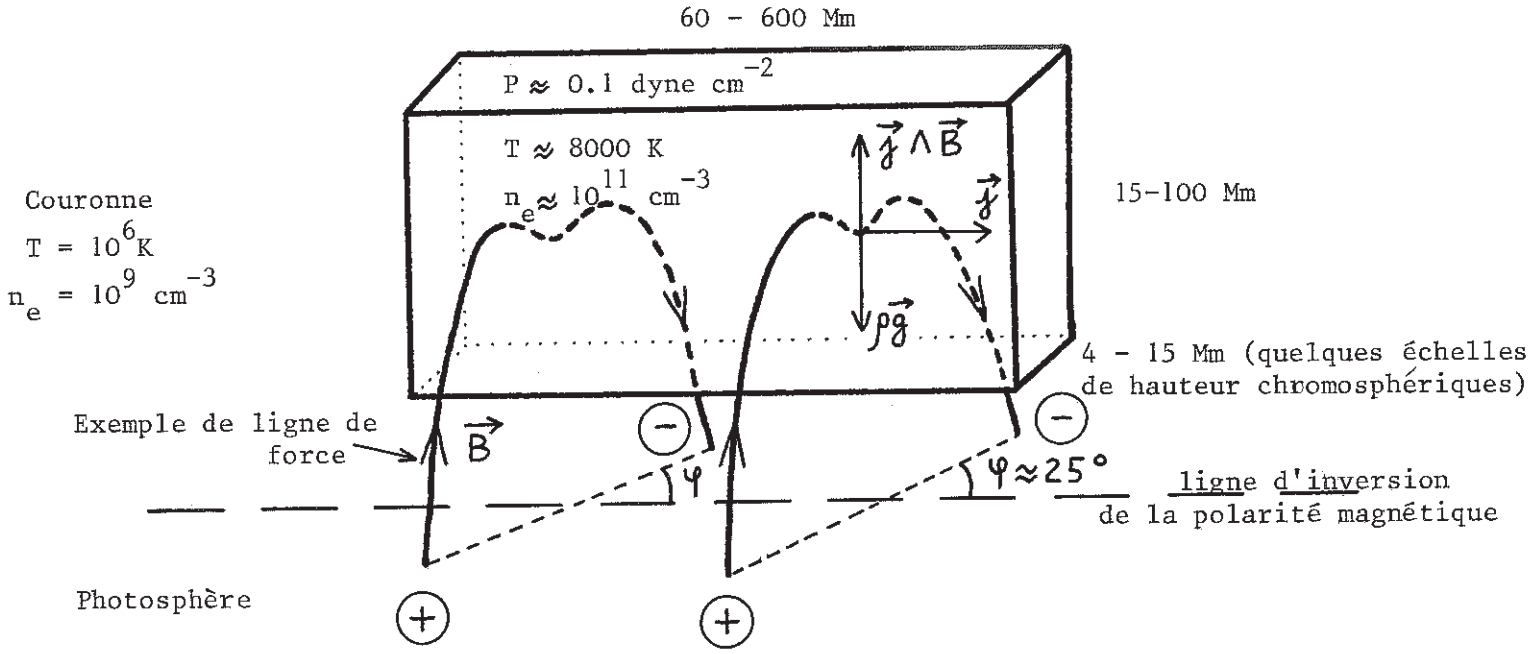

FIGURE II-1

Représentation très schématique d'une protubérance quiescente

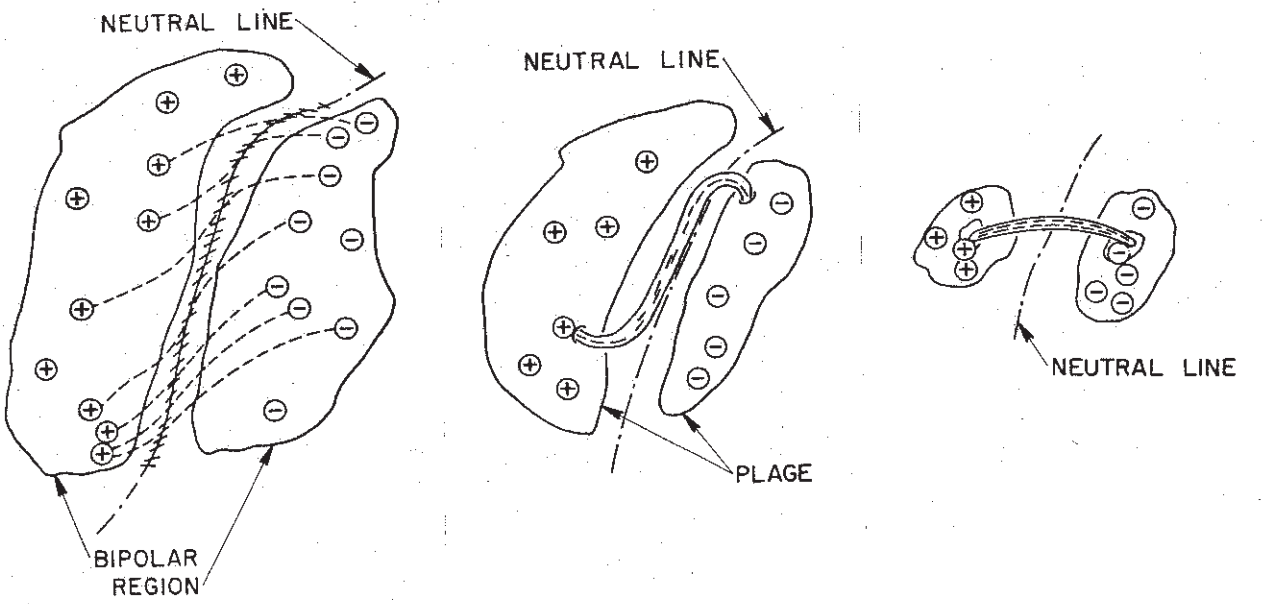

Filament quiescent | filament de plage | filament en boucle

FIGURE II-2

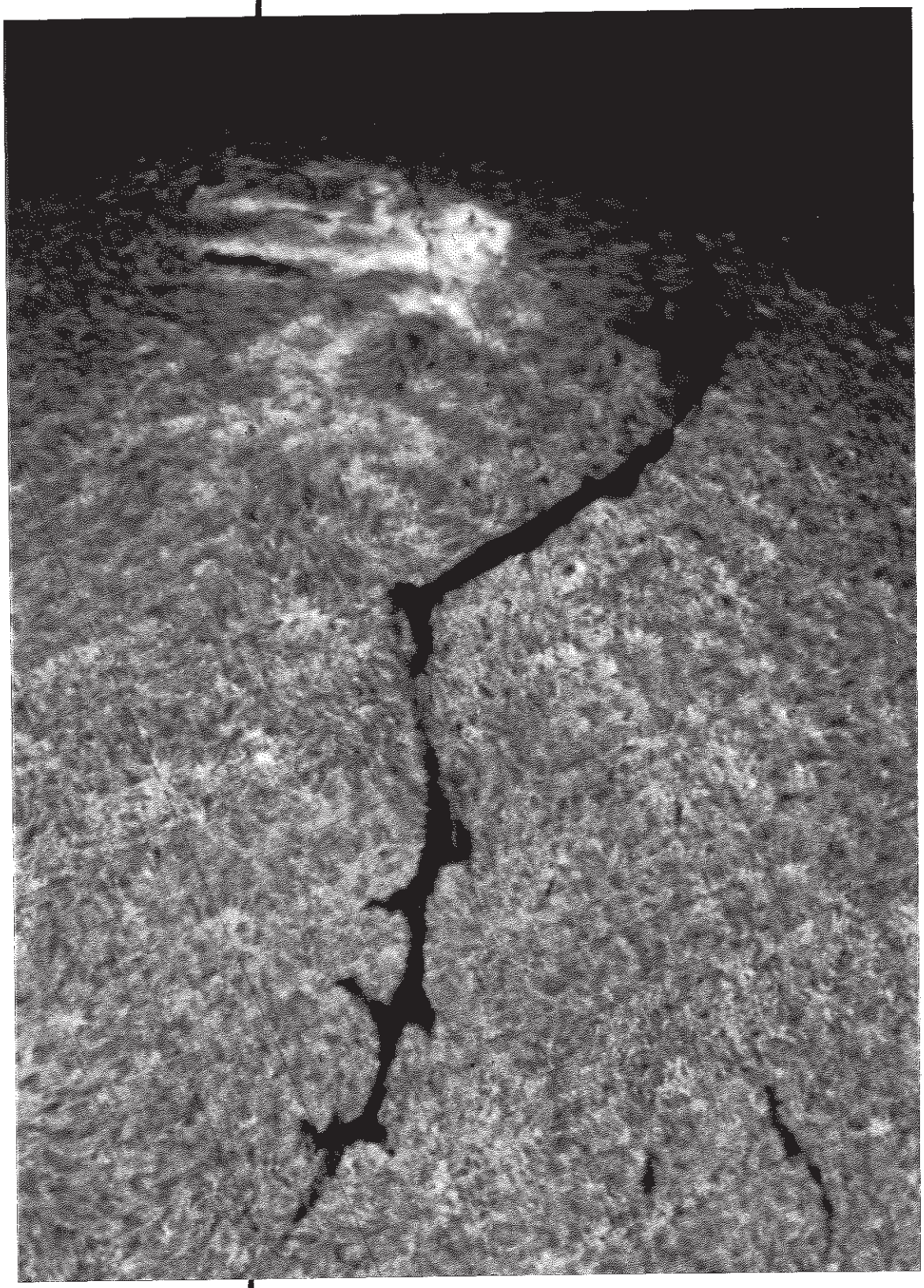

FIGURE II-3

FILAMENT VU SUR LE DISQUE EN Hα

REMARQUER LES "PIEDS"

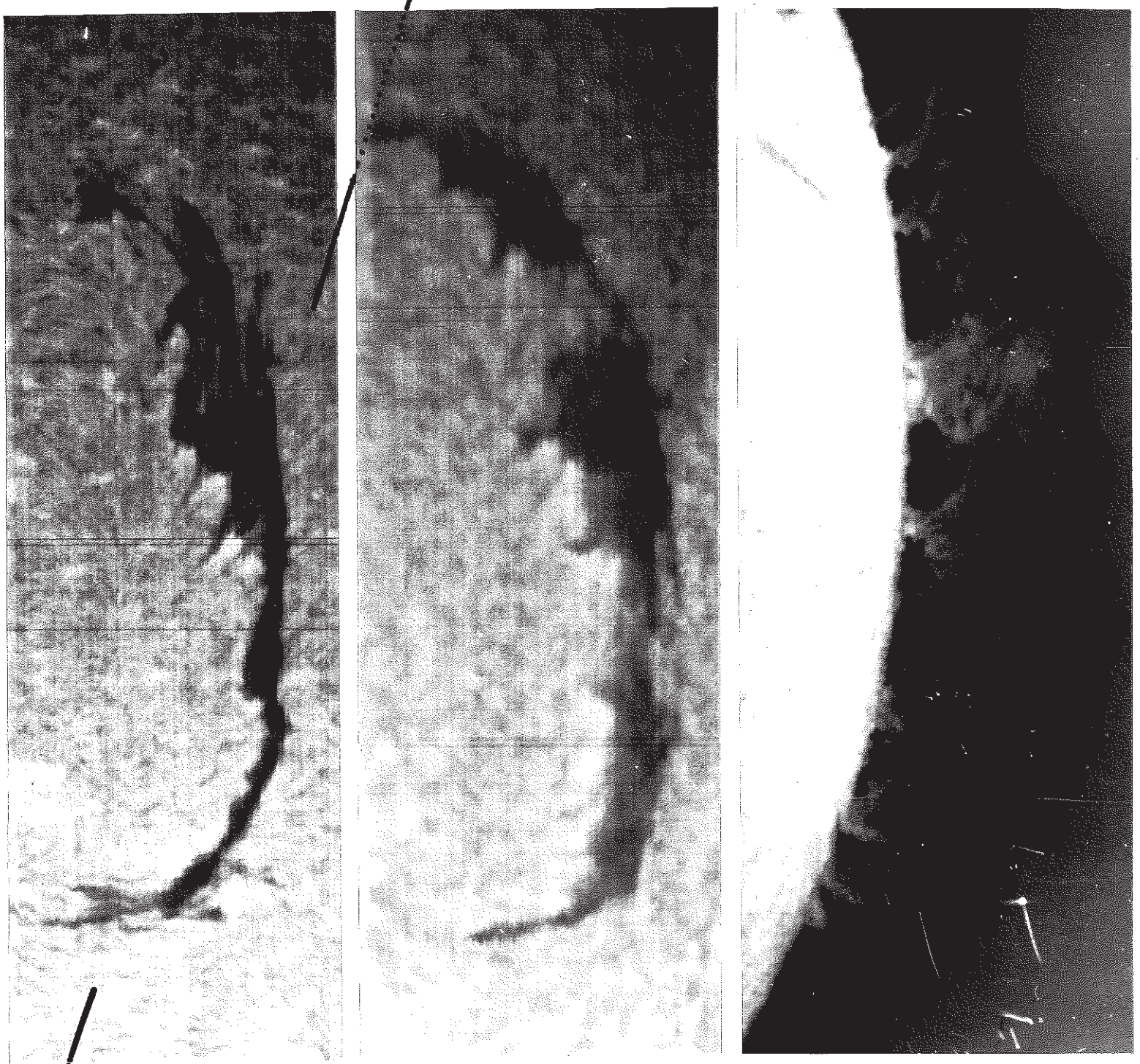

Passage au méridien central

bord Ouest

FIGURE II-4

Observations centre bord d'une protubérance en Hα

Remarquer : sur le disque, l'excès de brillance sous le filament (effet de serre ?) et les "pieds" le reliant à la chromosphère.
au limbe, la structure fine : protubérance en "viaduc" composée d'arches (magnétiques ?) froides individuelles regroupées en "bouquets" à l'emplacement des "pieds".

a - Le support magnétique des protubérances-modèles.

La géométrie des lignes magnétiques supportant les protubérances est un sujet controversé. Deux grandes classes de modèles ont été introduites par Kippenhahn et Schlüter (KS, 1957), et par Kuperus et Raadu (KR, 1973). Ces deux classes se distinguent principalement par une différence d'orientation entre les champs magnétiques protubérantiels et photosphériques. Leurs directions sont confondues dans les modèles de types KS, et opposées dans les géométries de type KR (Figure II-5). Les observations du champ magnétique (et aussi du champ des vitesses) ont pour but, entre autres, d'effectuer une discrimination entre ces divers modèles.

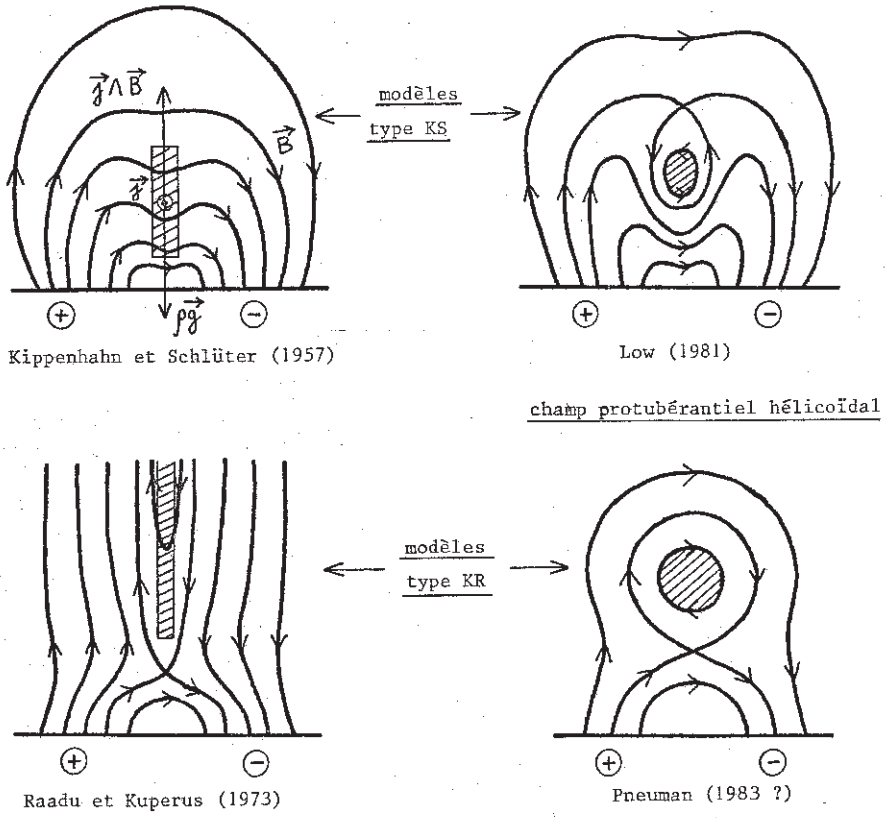

FIGURE II-5

Modèles de support magnétique : une composante normale du champ au plan du dessin peut être ajoutée. La matière froide du filament est hachurée. Elle est supportée par la composante du champ magnétique transversale à la protubérance.

b - Champs magnétiques-observations

De nombreux progrès ont été accomplis depuis les mesures Zeeman de Rust (1967) grâce à l'effet Hanlé. Rappelons que, sur les magnétographes classiques, l'analyse Zeeman se fait en polarisation circulaire et aboutit à la détermination de la projection $B_{//}$ du champ magnétique sur la ligne de visée. L'effet Hanlé permet, à partir de l'analyse de la polarisation linéaire, d'accéder aux 3 composantes du champ (Bommier et Sahal-Bréchot, 1979). Les mesures Hanlé du champ magnétique sont dues à J.L. Leroy, au Pic du Midi. En ce qui concerne les protubérances de la ceinture polaire, qui sont les plus calmes, les principales conclusions sont les suivantes (Leroy et al, 1982 et Leroy, 1982) :

1 - $2G \leqslant \|\vec{B}\| \leqslant 20\ G$ valeur moyenne : 8G

2 - gradient vertical positif $\frac{d\|\vec{B}\|}{dz} = 0.5\ G/10\ Mm$ (z : altitude)

3- Le champ magnétique $\vec{B}$ semble être horizontal dans les protubérances.

4- L'angle φ entre le vecteur $\vec{B}$ et le grand axe du filament est, en moyenne, de 25° (forte dispersion).

5- Dans 2/3 des cas, les mesures sont compatibles avec un modèle de type KR, et, dans 1/3 des cas, avec un modèle de type KS. Ce résultat est probablement le plus important en temps que contrainte sur les modèles.

6- Enfin, la direction de la composante du champ parallèle à l'axe du filament subit, à l'image du champ photosphérique, un renversement périodique en liaison avec le cycle d'activité solaire.

La conclusion 2 a été théoriquement prédite par Anzer (1969). Le "shear" φ (conclusion 4) peut jouer un rôle très important lors de la formation des protubérances (voir chapitre IV-1) et de leur disparition (chapitre III-1), dû à son influence sur la conduction thermique.

La conclusion 1 implique que le β du plasma protubérantiel est inférieur à 0.1. La structure est donc dominée par les forces magnétiques.

Remarquons enfin que les mesures de Leroy ne sont pas incompatibles avec une structure hélicoïdale du champ à axe horizontal, mais, par contre, le sont avec des hélices verticales, ce qui est en conflit avec les observations de structures fines (Dunn, 1960).

c - Champ des vitesses-observations.

Le champ des vitesses macroscopiques est obtenu par l'effet Doppler sur les raies. Seule la composante parallèle à la ligne de visée est observée. La vitesse de turbulence peut-être obtenue, sur certaines raies, par des mesures de largeur à mi-hauteur. Les mouvements ont été étudiés dans les protubérances, la zone de transition et la couronne environnantes, ainsi que en dessous, dans la photosphère. Le nombre de Reynolds magnétique $Rm = 10^{-3} V(km\ s^{-1})\ L(km)\ T(K)^{3/2}$ étant partout $\gg 1$, les lignes de champ magnétique sont gelées dans le plasma. Par suite, les écoulements se font parallèlement aux lignes de force, et la topologie des lignes fluides peut fournir des indications sur celle des lignes magnétiques.

- Mouvements photosphériques.

Leur observation sur le disque est due à Martres et al (1976, 1981). Les mouvements suggérés sont non horizontaux, de l'ordre de 0.25 km s^{-1}. Les lignes d'inversion de vitesses (radiales) semblent orthogonales à l'axe du filament.

- Mouvements dans les filaments (déduits des raies chromosphériques).

. Perpendiculaires à la ligne de visée (au limbe) :

Dunn (1960), Engvold (1976) et Maltby (1976) ont cru voir des mouvements verticaux descendants (1 km/s) à l'intérieur de structures fines ($< 0.5''$) de courte durée de vie ($<$ 5mn). Priest et Smith (1979) ont suggéré que de tels

mouvements pouvaient être le résultat d'une instabilité thermique au sommet d'arcades coronales. Uchida (1980) expliqua ces mouvements à l'aide d'un mécanisme de siphon. Heyvaerts et Mercier (1977) proposèrent un modèle global de circulation de courants électriques dans lequel la dissipation Joule sous la photosphère induisait une descente de la matière protubérantielle. Ces mouvements peuvent aussi résulter d'une diffusion du plasma au travers des lignes de force due à une instabilité d'interchange (Rayleigh-Taylor).

. Parallèles à la ligne de visée (décalages Doppler)

Au limbe, des mouvements horizontaux sur les bords des protubérances ainsi que des éjections de matière (80 km s^{-1}) ont été observés par Engvold et al (1978), ainsi que Engvold et Malville (1977). De telles éjections, dont la vitesse est comparable à la vitesse d'Alfvèn, peuvent provenir d'une nappe de courant ("current sheet") active (phase de reconnections).

Sur le disque, des mouvements descendants et verticaux ont été détectés par Kutoba (1980). Par contre, Martres et al (1981) y ont décelé, en Hα au DPSM de la tour solaire de Meudon, et à l'héliographe à 3 longueurs d'onde, de lents mouvements montants ($>$ 1 km/s), de longue durée de vie (plusieurs heures à plusieurs jours), avec une statistique bien meilleure (champ à 2 dimensions) que Kubota (champ à 1 dimension). Aucun modèle n'a encore été proposé pour expliquer de tels mouvements. La contradiction avec les observations au limbe d'Engvold (1976) n'est peut être qu'apparente, car ses résultats, non déduits de décalages Doppler, peuvent résulter des fluctuations de tout autre paramètre (ionisation par exemple). Des perturbations rapides de courte durée de vie ($\approx$ 10 mn, $\mp$ 5 km s^{-1}) ont été aussi rapportées en Hα par Mein (1977) et Martres et al (1981), sur les bords des filaments, suggérant une organisation en boucles de vitesses. Les modèles dynamiques de siphon de Pickel'ner (1971) et Ribes et Unno (1980) peuvent interpréter de telles circulations de matière.

- Mouvements dans la zone de transition et dans la couronne autour des protubérances (dans les raies EUV à partir d'observations sur orbite)

Dans la zone de transition, Lites (1976) détecta des mouvements montants (6-10 km s^{-1}) appuyant ainsi les conclusions de Martres et al (1981). Vial et al (1979), à partir d'observations au limbe, trouvèrent des vitesses inférieures à 30 km s^{-1}, et suggérèrent des boucles de vitesse, en accord avec Mein (1977). (Voir aussi Vial, 1981).

d - Conclusion

Notre vision magnétohydrodynamique des protubérances est donc encore très fragmentaire, tant au point de vue observationnel que théorique. La volonté d'obtenir des contraintes observationnelles précises sur les modèles, alliée à la disponibilité d'un instrument puissant et parfaitement adapté à l'étude statistique et quantitative du champ des vitesses dans les protubérances (le DPSM de la tour solaire de Meudon), nous ont conduit à l'étude approfondie des pages suivantes (II-2). Les résultats nous permettront l'élaboration d'un nouveau modèle de filament quiescent (IV-2), interprétant le plus fidèlement possible à la fois les observations de Leroy du champ magnétique et nos observations de vitesses.

II - 2 - CONTRIBUTION À LA DETERMINATION DU CHAMP DES VITESSES : MOUVEMENTS STATIONNAIRES ET OSCILLATIONS.

Article 1, communication 1 et article 2.

Cette étude est une suite logique (et un approfondissement) aux travaux entrepris par Mein (1977), et Martres et al (1981). Les données Hα proviennent du DPSM de la tour solaire de Meudon, et les données C IV du spectropolarimètre UV embarqué sur le satellite SMM (Solar Maximum Mission) de la NASA.

Article 1

Nous effectuons pour la première fois, une analyse de Fourier des vitesses mesurées dans et sous un filament respectivement en Hα ± 0.3 Å et Hα ±0.6 Å, ainsi qu'une analyse statistique des mouvements stationnaires. Les mouvements montants au travers des protubérances sont confirmés. Les oscillations chromosphériques sont presque indétectables dans le filament, suggérant une réflexion en dessous, et réduites dans les régions environnantes.

Communication 1

Une étude comparitive des vitesses en Hα ± 0.3 Å (filament)et C IV (zone de transition) est entreprise à partir d'observations coordonnées. Une bonne corrélation est obtenue entre les mouvements stationnaires dans les deux raies. Par contre, l'analyse de Fourier conduit à des résultats opposés : des oscillations sont présentes en C IV à l'emplacement du filament Hα. Ce résultat suggère que les régions C IV observées correspondent surtout à la zone de transition chromosphère couronne sous la protubérance.

Article 2

Une étude statistique du champ des vitesses (Hα ±0.3 Å) est entreprise à partir d'observations centre-bord. Deux analyses différentes sont effectuées selon la durée de vie des

mouvements :

- les mouvements de courte durée de vie (10 mn) sont interprétés en termes de boucles de vitesses et confrontés au modèle de Ribes et Unno (1980).

- les mouvements de longue durée de vie (plusieurs jours), par reconstitution du champ des vitesses à 3 dimensions, aboutissent pour la première fois à un modèle de circulation globale : montée de matière dans la protubérance et alimentation sur les bords. Ce résultat sera modélisé au chapitre IV-2.

Astron. Astrophys. 102, 124–128 (1981)

ASTRONOMY AND ASTROPHYSICS

ARTICLE 1

Dynamics in the Filaments

I. Oscillations in a Quiescent Filament

J.M. Malherbe, B. Schmieder, and P. Mein

DASOP, Observatoire de Meudon, F-92190 Meudon, France

Received February 9, accepted May 7, 1981

Summary. A time sequence of a quiescent filament has been obtained with the MSDP spectrograph operating on the Meudon Solar Tower, the duration was 720 s, the time step 30 s.

The Fourier analysis of the radial velocities measured in the Hα line shows that the steady velocities are principally upward in the filament, the chromospheric oscillations are almost undetectable inside the filament and reduced around it. Steady dynamical structures are most consistent with the theoretical model of filaments proposed by Unno and Ribes.

Key words: filaments – solar chromosphere – oscillations

Introduction

Recent studies on the mechanisms of heating of the solar corona have pointed out that a homogeneous stratified model did not allow to explain the heating (Mein and Schmieder, 1981). Other works take into account the inhomogeneities in the atmosphere and try to answer some questions relative to the transport of the energy by MHD waves and the heating by dissipation of the energy through magnetic structures (Webb and Roberts, 1980; Roberts, 1981).

The observations of quiescent filaments which are structures located inside the corona can be useful to understand these phenomena. Do oscillatory motions of the chromosphere exist in the filament, and how are they disturbed at the edges of the filament?

Oscillations in the filaments on the disk or in the prominences at the limb have been already detected but they were principally horizontal and observed as a consequence of major flares (Kleczek and Kuperus, 1969; Hyder, 1966). Chromospheric oscillations are different and generally vertical. Only a few filaments have been studied in order to record Doppler shifts (Maltby, 1979; review of Maltby, 1978).

Some theoretical models have been proposed to describe quiescent filaments in static equilibrium (Anzer's review, 1978) and thermic equilibrium, where wave heating balances energy loss by thermal conduction and radiative cooling (Milne et al., 1979). Models have also been proposed to explain the formation of prominences (see for example Chiuderi and Van Hoven, 1979), and MHD and thermic instabilities like flares and disparitions brusques (Raadu and Kuperus, 1973). Other authors try to explain stationary motions in quiescent filaments (Unno and Ribes, 1980; Heyvaerts and Mercier, 1977). Precise pictures of motions inside the filament and good determination of the physical parameters are required to define accurate theoretical models.

The technique of the 9 channel MSDP spectrograph operating on the Meudon observatory solar tower (multichannel subtractive double pass, Mein, 1977) is very adaptable to such detailed observations of time dependent chromospheric structures (Martres et al., 1981) because line profiles can be obtained in two dimensional fields with good temporal and spatial resolution.

We present in this paper the study of a quiescent filament observed with this technique during 720 s with a 30 s time step. The field of view ($6' \times 1'$) allows to study the dynamics of about 50 oscillations cells, which increases the freedom degree comparatively to the one slit spectrograph techniques.

Steady flows and oscillatory motions have been investigated by Fourier transforms.

Observations

The observed quiescent filament was located at N36 020 on 17 July 79. We got also some pictures the day after. If we use a system of coordinates XYZ (Z being normal to the solar surface, X parallel to the direction of the filament, Y perpendicular to X) the radial velocity is equal to:

$$Vr = -0.412\ V_X - 0.424\ V_Y + 0.806 V_Z.$$

The dopplershifts are not exactly equal to radial velocities.

Data Processing

The used method for data reduction was previously exposed (Mein, 1977). At each point of the field (x, y, being the cartesian coordinates) and each time t_i, Hα line was reconstituted, the variation of the intensity and the dopplershifts $I_i(x,y,t_i)$, $V_i(x,y,t_i)$ were calculated for some wavelengths $\Delta\lambda$ in the line.

To refer each frame to the neighbouring ones we use a new method based on the maximum of the correlation function of the intensity gradient ∇I which gives more precise results.

Fourier Analysis

The Fourier analysis allows to calculate the energy of the oscillations $V^2(x,y,P)$ for periods P between $2 \cdot \Delta t$ (time step) and

Send offprint requests to: B. Schmieder

∞. This quantity has been apodized by a function of the sequence duration T.

The power spectrum was calculated and normalized by the band width ($\Delta\nu = 0.026$ MHz in the case of a 720 s sequence). The results are represented on histograms V/I for $P = \infty$ or Vp/I for $P \neq \infty$. I and V, Vp are averaged function over T and represent respectively intensity fluctuations $\Delta I/I$, and Dopplershifts.

Relations between these quantities are defined by the mean functions:

$$\overline{Vp}^2(I) = \frac{1}{m}\sum_j jV_j^2(I) \quad \text{and} \quad \overline{V}(I) = \frac{1}{m}\sum jV_j(I)$$

with m total number of points x, y having an intensity equal to I, j number of points x, y having a velocity equal to V_j with an intensity equal to I.

Results

Analyses of the quiescent filament observed on July 17th have been performed for two different $\Delta\lambda$($\Delta\lambda = 0{,}3$ Å, $\Delta\lambda = 0.6$ Å) corresponding to two different altitudes.

Figure 1a and b represent maps of intensity $I(x, y)$ for $\Delta\lambda = +0.3$ Å and averaged over the time (720 s). The dark region (I^-) corresponding to the filament appears on Fig. 1b and region of weak positive intensity (I^+) on Fig. 1a. These two regions are clearly located in the distribution function of the intensity (Fig. 2a) left and right part of the diagram. At $\Delta\lambda = 0.6$ Å the distribution function (Fig. 2a) is practically symmetric. The filament is no longer visible except in some points (Fig. 3a and b).

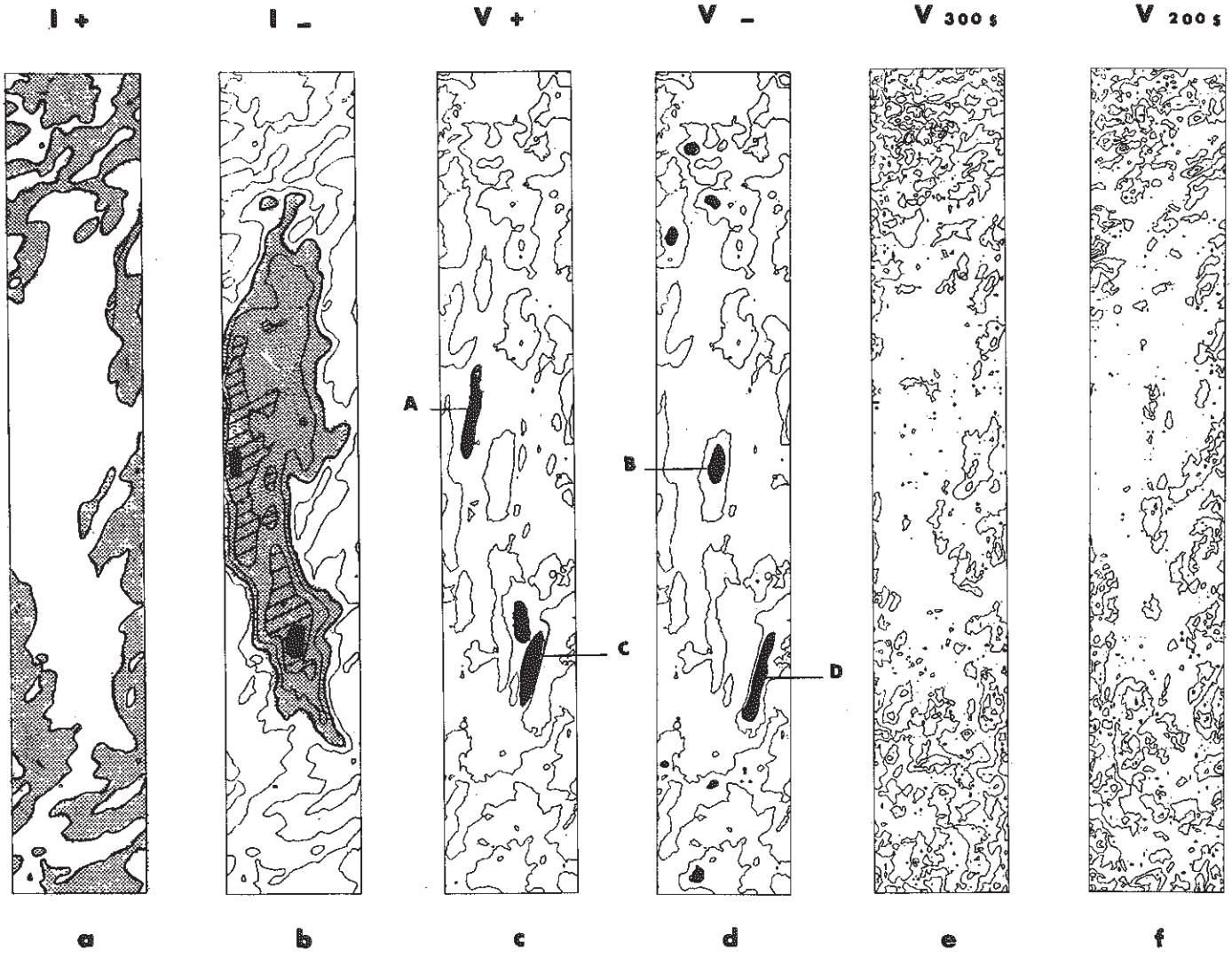

Fig. 1.

Maps

Hα ± 0.3 Å

- Hα intensity fluctuations
  - **a** bright regions I^+
  - **b** absorbing regions I^-
- Dopplershifts
  - **c** red shift V^+
  - **d** blue shift V^-
- Oscillation amplitude Vp
  - **e** period 300 s
  - **f** period 200 s

On all the maps, the zero isophote is represented. The step for I map is 10%, for V map 1 km s^{-1}, for Vp 0.14 km s^{-1}

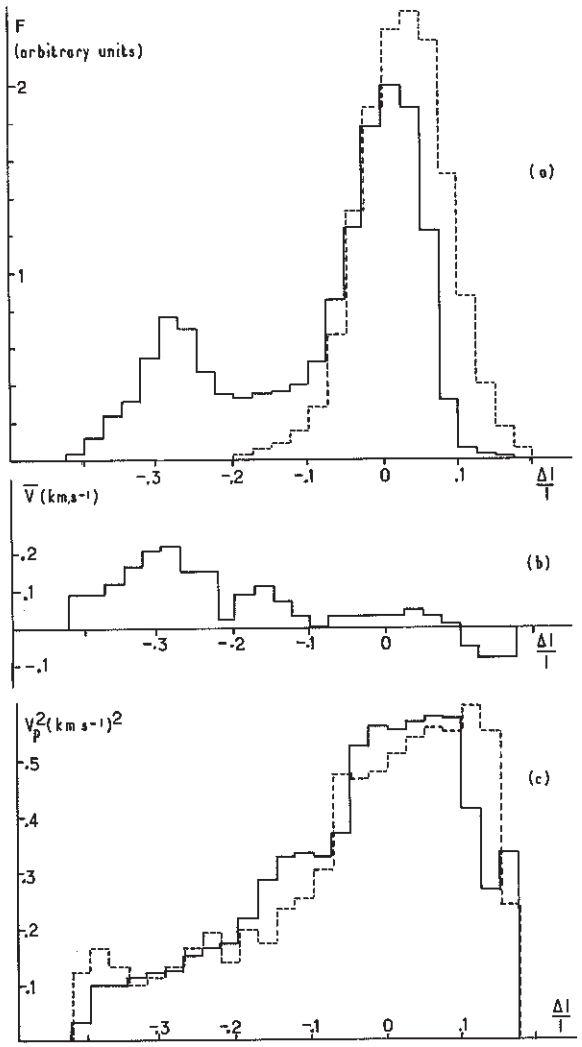

figure 2

Fig. 2. **a** Distribution function of the Hα intensity fluctuations at $\Delta\lambda=0.3$Å (continuous line) and at $\Delta\lambda=0.6$Å (dashed line). **b** Mean value of the steady velocities versus Intensity fluctuations (Hα ± 0.3Å). **c** Variation of the mean function $\overline{V}p^2$ versus Intensity fluctuation for the period 300 s (continuous line) and 200 s (dashed line)

The study of the dynamics of the filament can be separated into two parts:
the study of the "steady flow": stationary velocity field
the study of oscillations.

1. Steady Velocity Field

The stationary velocity field $\overline{V}$ is represented on Fig. 1 c and d ($V+$ corresponds to upward velocity, $V-$ to downward velocity). We remark that the inversion line of the velocities is parallel to the filament axis. It confirms some results obtained previously (Mein, 1977).

a) The superposition of the maps of V and I (Fig. 1 a–d) points out that *inside the dark features* corresponding to the filament the velocities are principally upward as it was previously observed on other quiescent filaments (Martres et al., 1981). The velocity values are stable and smaller than 1.5 km s^{-1}. Figure 4 shows an histogram of stationary velocity amplitude V versus intensity I averaged over 720 s. Intensities are referred to the mean value (whole field of view). Dark features of the filament are located on the left of the diagram and correspond to the highest amplitudes V. The gravity center of negative intensity points has a positive velocity, which confirms the behaviour of upward velocity.

b) Two *particular regions* noted A and C located in the filament have higher upward velocity reaching 3 km s^{-1} (Fig. 1 c and d). These regions can be associated to regions located at the edge of the filament, B and D, where velocities are downward (~ -2.5 km s^{-1}), Archs between A and B, C and D probably exist as suggest the velocity anti-correlations. These points are also visible in lower region as we have mentioned above. It seems that they correspond to vertical fibers which connect the filament with underlying layers. The following days, these connection fibers seem to disappear. All the velocities are weak and slowly upward.

c) The *quiet chromosphere* velocity field is represented by the right part of the histogram V/I (Fig. 4). We remark its symmetry versus the origin. Upward and downward velocities are present. The mean value of these velocities is near zero (Fig. 2 b).

2. Oscillations

Long periods cannot be discriminated from real steady flows but 300 s or 200 s can easily be separated.

The results can be summarized in the following way:

a) Oscillations appear to be weak *inside the filament*. Maps of velocity field for 300 s and 200 s oscillations (Fig. 1 e and f) do not show any velocity of amplitude >0.15 kms in the region corresponding to the filament.

This behaviour is confirmed by the unsymmetrical shape of the function (Fig. 2 c) of oscillation amplitude Vp^2 versus I (mean intensity referred to the whole field of view). Dark regions ($I<0$) correspond to the smallest amplitudes.

b) *Outside the filament*, oscillations are detected (Fig. 1 e and f). Figure 2 c shows the variation of the mean function Vp^2 versus the mean intensity I. The oscillation amplitude around the filament hardly reaches the value of 0.75 km s^{-1}. This is a relatively weak value for the oscillation of the quiet chromosphere measured in the Hα line (Mein and Mein, 1976).

The comparison between the maps of 300 s and 200 s oscillations shows that no correlation exists between dark or bright cells and oscillation cells in the quiet chromosphere. The oscillation cells seem to be located principally in mean intensity zones. We do not notice any correlation between oscillation cells and stationary velocity cells.

c) Figure 3 e represents the oscillation velocities observed at Hα ± 0.6. We remark that oscillations seem to avoid the regions located *under the filament*. Though, at the altitude corresponding to this wavelength the filament is no longer visible (Fig. 2 a) as we have denoted above. Oscillation amplitudes are smaller than at higher levels by a factor 1.6, in the other parts of the field. This is coherent with the decrease of density with height.

d) Figure 5 shows the power spectrum of oscillations inside the filament and outside, in the quiet chromosphere. The oscillation energy outside the filament is more important than inside. The power spectrum relative to the quiet chromosphere presents a sharp maximum around the period 240 s but this relative to the filament, a very flat one.

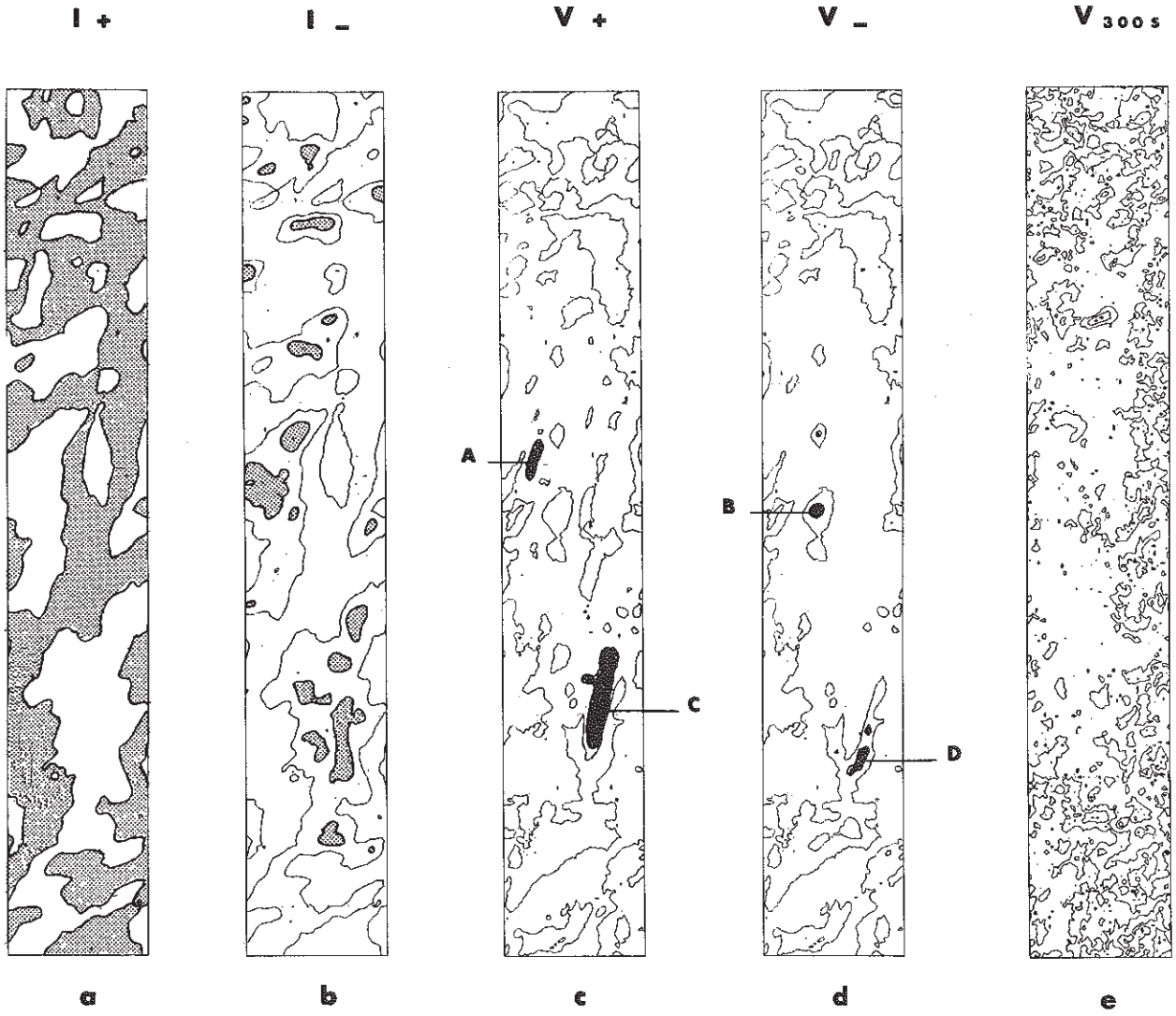

Fig. 3.

Maps		
Hα ± 0.6 Å	H intensity fluctuations	**a** bright regions I^+
		b absorbing regions I^-
	Dopplershifts	**c** red shift V^+
		d blue shift V^-
	Oscillations amplitude Vp	**e** period 300 s

On all the maps, the zero isophote is represented. The step for I map is 10%, for V map 1 km s^{-1}, for Vp 0.14 km s^{-1}

Discussion and Conclusion

We conclude that *outside the filament*, the amplitude of the oscillations is weaker than it could be observed in quiet chromosphere. As far as the oscillations are concerned, it seems that the filament structure is larger than the absorbing feature. This confirms a suggestion already done in a study on fast perturbations (Martres et al., 1981). So it seems that dark Hα features are only a part of the filament. *Inside the filament*, an upward steady flow is observed, the velocity being smaller than 1.5 km s^{-1} and oscillations are in practice undetectable. This last result is consistent with efficient reflection of acoustic waves at the top of the chromosphere. Chromospheric oscillations in lower layers could not be visible because of the high opacity of filamentary material.

As we have said before, material oscillations in quiescent filaments have not yet been much investigated. Very few theoretical works exist on this subject. Most of the models which take into account the wave heating in their energy balance are static and they are not easily relevant with observations.

Steady flow motions had been explained by some authors (Heyvaerts and Mercier, 1977) as current circulations in the filament connected with the subphotospheric layers. But their models had no spatial structure and investigated only motions concerning the whole configuration. The dynamical model of

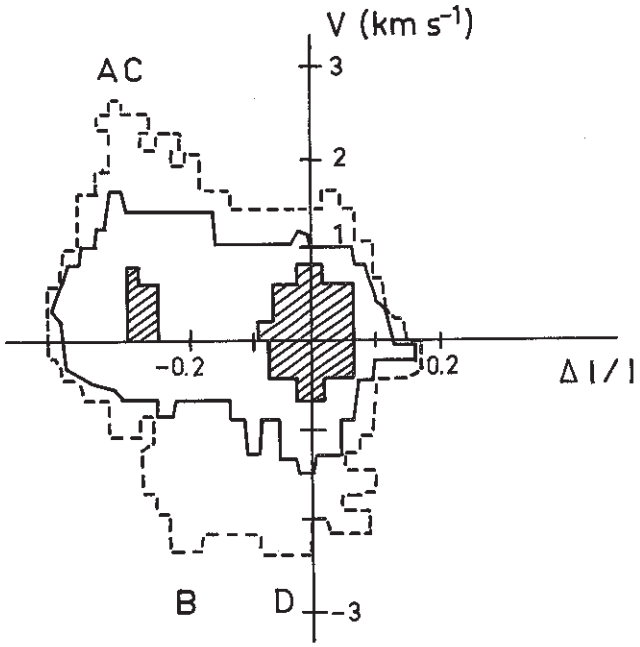

Fig. 4. Histogram of steady velocity V versus average intensity I (H$\alpha \pm 0.30$ Å)

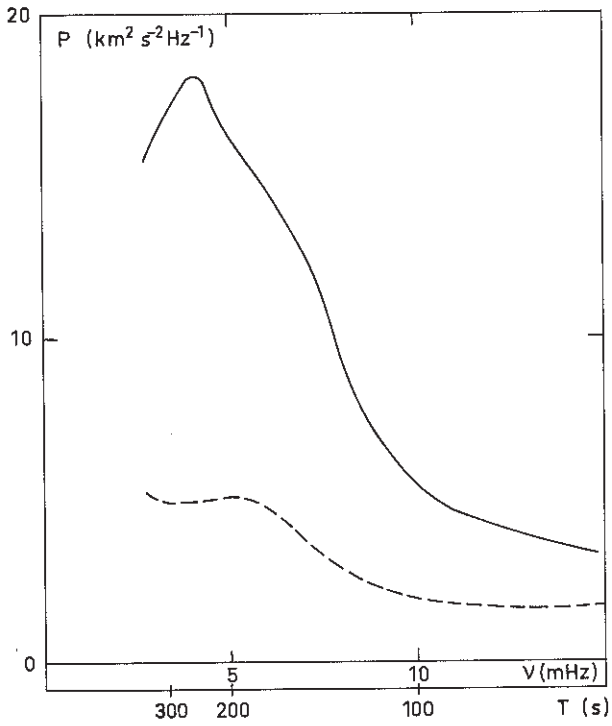

Fig. 5. Power spectrum of oscillations inside filament (dashed line) outside the filament (continuous line) (H$\alpha \pm 0.30$ Å)

Unno and Ribes (1980) with detailed spatial magnetic structures, allows to interprete our observations and seems to be in good agreement with them. The fast and upward stationary motions observed at the edges of dark features (feet of the filament), could occur in magnetic flux tubes supporting the filament. This model does not describe the slow and upward stationary motions observed through the whole absorbing features, but does not appear inconsistent with them. We can assume an upward steady flow rising through the filament from the chromosphere into the corona. This flow could cross the magnetic flux tubes supporting the filament near the transition zone level, where the magnetic induction and velocities are found to be nearly zero.

Hence, more detailed observations are needed and a deeper discussion could be the subject of another paper.

Another point of view concerning the filament observations, is the existence of fine scale features already observed by Hirayama, 1964; Maltby, 1976). If they are confirmed, the theoretical models may be modified including the effects of the radiative transfer inside the filament. In our observations, no threads could be identified in the velocity field, perhaps because of the limited spatial resolution. Radiative transfer calculation in the Hα line could be also required, especially in bright regions, to interpret with certitude the sign of the Doppler shifts, which could be reversed, as suggested by Martres et al. (1981), if source function increases with height.

Acknowledgements. The observations have been obtained at the Meudon Solar Tower by C. Coutard, R. Hellier, A. Miguel. The processing data was performed with the microphotometer of INAG (CDCA) and with the computer of CNRS at Orsay (CIRCE).

References

Anzer, U.: 1978, *Coll.* IAU n° 44, 322
Chiuderi, C., Van Hoven, G.: 1979, *Astron. J.* **232,** L69
Hirayama, T.: 1964, *Publ. Astron. Soc. Japan* **16,** 104
Heyvaerts, J., Mercier, C.: 1977, *Astron. Astrophys.* **61,** 685
Hyder, C.L.: 1966, *Z. Astrophys.* **63,** 78
Kleczek, J., Kuperus, M.: 1969, *Solar Phys.* **6,** 72
Maltby, P.: 1976, *Solar Phys.* **46,** 149
Maltby, P.: 1978, *Coll.* IAU n° 44, 332
Martres, M.J., Mein, P., Schmieder, B., Soru-Escaut, I.: 1981, *Solar Phys.* **69,** 301
Mein, N., Mein, P.: 1976, *Solar Phys.* **49,** 231
Mein, P.: 1977, *Solar Phys.* **54,** 45
Mein, N., Schmieder, B.: 1981, *Astron. Astrophys.* **97,** 310
Milne, A.M., Priest, E.R., Roberts, B.: 1979, *Astron. J.* **232,** 304
Raadu, M.A., Kuperus, M.: 1973, *Solar Phys.* **28,** 77
Roberts, R.: 1981, *Solar Phys.* (in press)
Unno, W., Ribes, E.: 1980, *Astron. Astrophys.* **91,** 129
Webb, A.R., Roberts, B.: 1980, *Solar Phys.* **68,** 87

COMMUNICATION 1

présentée au "Solar Maximum Mission" (SMM) workshop
Janvier 1983
Goddard Space Flight Center - Greenbelt - USA

DYNAMICS OF SOLAR FILAMENTS :

MASS MOTIONS AND OSCILLATIONS IN Hα AND C IV

J.M. MALHERBE, B. SCHMIEDER, P. MEIN

Observatoire de Meudon, DASOP (LA 326),
92190 MEUDON - F R A N C E

A B S T R A C T

Time sequences of a filament have been obtained in the course of SMY coordinated observing program with the MSDP spectrograph operating in Hα at the Meudon Solar Tower, and with the UVSP in CIV aboard the SMM satellite.

In both lines, the statistical analysis of radial velocities shows that the steady velocities are mainly upward in the filament. The Fourier analysis of velocity oscillations leads to opposite results in both lines : chromospheric oscillations are almost undetectable inside the Hα filament, while oscillations are present, at the Hα filament location, in CIV. This result suggests that the observed CIV regions correspond to the chromosphere-corona transition zone below the prominence.

I - INTRODUCTION

Solar prominences are thin sheets of chromospheric-like material suspended in the low corona by magnetic fields. Main properties can be found in Tandberg-Hanssen (1974) and Jensen et al (1979). Basic theoretical models of solar filaments were presented by Kippenhahn and Schlüter (1957) and Kuperus and Raadu (1973). These models describe the magnetostatics of support and present quite different properties : the Kippenhahn-Schlüter (KS) prominence has the same magnetic polarity as the neighbouring photosphere, while the Kuperus-Raadu (KR) structure exhibits a polarity reversal below the filament.

Other more sophisticated models, belonging to these two classes, were proposed : Anzer and Tandberg-Hanssen (1970), then Lerche and Low (1980) and Low (1981) modified KS model to produce helical structures. This model was also revisited by Low (1982) to explain fine structures reported by Dunn (1960) and generalized by Milne et al (1979) to take into account energy balance.

But recent observations revealed that filaments are always associated with velocity fields. The most extensive results concerning Hα motions in disk filaments are due to Mein (1977), Martres et al (1981) and Malherbe et al (1981, 1983). It was shown that upward motions (> 1 km s^{-1}) occur through prominences; velocity loops slightly inclined on the filament long axis were also suggested. Malherbe et al (1983) pointed out that steady flow models were required to explain the physics of quiescent prominences.

Siphon flow models were proposed by Pickel'ner (1971), Uchida (1980) and Ribes and Unno (1980); Priest and Smith (1979) suggested that motions could be the result of a thermal instability at the top of magnetic loops.

The most recent observations of magnetic fields, due to Leroy et al (1982), indicated that, at least in the polar regions, the prominence support seems to be of KR type in 2/3 of observed cases, and of KS type in only 1/3 of cases. To account for these new magnetic measurements and the dynamical properties of filaments reported by Malherbe et al (1983), a quasi-static reconnection model of KR type was proposed by Malherbe and Priest (1983).

Thus, the study of velocity fields in quiescent prominences is an important component for the understanding of the filament structure. An analysis of steady flows and oscillations in Hα was performed by Malherbe et al (1981). But the study of coronal formations around prominences requires observations in EUV lines. Such lines are very adapted to detect prominence activity (Mouradian et al, 1980). The dynamics in the transition region around prominences is not yet well known (Lites, 1976; Engvold et al, 1983). Thus, we present here new results from coordinated ground based observations in Hα (MSDP, Meudon) and space observations in CIV (UVSP aboard SMM). The observations and the data processing are exposed in section II. We compare in section III the steady velocity fields in Hα and CIV. A good correlation is found between the velocity structures in both lines.

Oscillations are investigated in section IV by the means of Fourier Transform. Quite different results are obtained in Hα and CIV. Interpretations and new constraints on theoretical models are given in the discussion.

II - OBSERVATIONS AND DATA PROCESSING

We obtained a set of observations of a filament in the course of a coordinated SMY program during 45mn on October 2, 1980. Our observations yield, with good accuracy intensity fluctuations, and radial velocities of material in Hα and CIV.

The filament was located in Active Region 2701 (22 N - 23 E).

II-1 - Observational techniques

Hα observations were obtained with the Multichannel Subtractive Double Pass (MSDP) spectrograph (Mein, 1977) operating at the Meudon Solar Tower, from 12:54 UT to 13:36 UT. MSDP technique allows observations of a 2D field of view (8' x 1') simultaneously in 9 channels distant of 0.3 Å in Hα line, with good temporal (30s) and spatial (1") resolutions. Thus, such an instrument is very adaptable to detailed observations of time dependant chromospheric structures. The method of data reduction was previously exposed in details by Mein (1977). Let us recall only that intensities and Dopplershifts are deduced by a computer code simulating a lambdameter technique from the 9 point reconstitution of Hα profiles at $\mp\Delta\lambda$ of the line core. CIV observations were obtained at the same time with the Ultraviolet Spectrometer and Polarimeter (UVSP) aboard the Solar Maximum Mission (SMM) satellite.

Our observations consisted in one large 2D Dopplergram of (4' x 4') followed by a time sequence of 2D Dopplergrams of (1' x 1'). The temporal and spatial resolutions were respectively of 30s and 3". In the standard observing mode, intensities and Dopplershifts are derived from measurements of 2 channels in CIV line, distant of 0.3 Å (Woodgate et al, 1982). But such a technique (called Single Dopplergram Determination or SDD) is limited to the detection of velocities smaller than 30 km s^{-1}. Our observing mode consisted in using coupled Dopplergrams alternatively displaced towards the red and the blue wing (Double Dopplergram Determination or DDD). This method was previously exposed by Simon et al (1982). We shall recall only that the DDD mode would be equivalent to a single one, if 4 channels were present, and allows a more precise determination of velocities, up to 80km s^{-1}, with the same temporal resolution (30s), than the classical 2 channel SDD method.

II-2 - Statistical and Fourier analysis

Thus, at each time t, and at each point of the fields (x, y being cartesian coordinates), maps of intensity fluctuations I (x,y,t) and radial velocities V(x,y,t) were computed for the two lines (Hα $\mp$ 0.3Å and CIV).

We present in this paper the study of Hα and CIV time sequences, respectively 840s and 2640s long. The time step was 60s in Hα (14 pictures of 8'x1' with 1" resolution) and 30s in CIV (88 pictures of 1'x1' with 3" resolution).

To refer each frame to the neighbouring ones, we used a method based on the detection of the correlation function maximum calculated on the spatial intensity gradients, which give more precise results.

The main difficulty lay in the superposition of Hα and CIV maps. Mein et al (1982) and Schmieder et al (1982) showed that the best fit between Hα and CIV levels was obtained when CIV velocities were multiplied by CIV intensities to the power 0.5 (to take into account density fluctuations) and compared to Hα velocities. We used this method of mass flux correlation to refer, at the same time, the large CIV field (4'x4') to the Hα one (8'x1').

Statistical results were obtained over the sequence duration T : maps of mean intensities $\bar{I}$ and velocities $\bar{V}$ were computed, as well as maps of standard deviations σ_I, σ_V of these quantities (section III). The energy of oscillations was investigated, after apodization of the time sequences, by Fourier Transform. At each point (x,y) of the field, the power spectrum V^2_p of velocity oscillations was computed for frequencies between 2/T and 1/2 Δ t (Δ t being the time step). Oscillatory maps were obtained at central frequencies equal to k/T (k integer), the band width being 1/T (section IV). 2D histograms between physical quantities $\bar{I}$, $\bar{V}$, σ_I, σ_V and V^2_p were calculated, integrated and averaged over spatial structures of the fields. Evidence of relationships between these parameters was found and is presented in sections III and IV.

III - STEADY VELOCITY FIELD

Figure 1 shows maps of intensities $\overline{I}$ and Dopplershifts $\overline{V}$ averaged over the sequence duration (840s in Hα, 2640s in CIV). The filament is clearly visible in Hα intensities but it is not visible in CIV ones. On the contrary, a good correlation is found between Hα and CIV velocity maps (see also Schmieder et al, 1982; Mein et al, 1982). Blueshifts are present at the filament location in both lines, in agreement with Martres et al (1981), Malherbe et al (1981, 1983) and Lites (1976). Redshifts are also observed in the faculae.

III-1 - Statistical Relationships

Figure 2 shows the distribution function of velocities and the average intensity $\langle \overline{I} \rangle$ versus velocity. $\langle \overline{I} \rangle$ was calculated using the formula

$$\langle \overline{I} \rangle = \sum_i ni(\overline{V})\, \overline{I}_i \Big/ \sum_i ni(\overline{V})$$

where $ni(\overline{V})$ is the number of points of velocity $\overline{V}$ having an intensity equal to $\overline{I}_i$.

The regions corresponding to the filament and the faculae are respectively located, in both lines, in the domains of positive and negative velocities. Thus, a good correlation between upflows and dark regions (filament), and downflows and bright regions (faculae) is confirmed in Hα (Malherbe et al, 1981). A relation between downflows and bright regions seems also to hold in CIV, in agreement with Simon et al (1982), but a relation between upflows (filament) and dark regions is not clear, because the filament appears in CIV in bright regions as well as in dark ones. Such a relationship is clarified by results in figure 3.

Intensities and velocities were averaged along Y direction, locally parallel to the filament long axis, and plotted versus X direction. The origin of X axis is located at point O (see figure 1). A small enhancement of CIV brightness corresponds to the dark Hα filament (fig. 3). The filament seems to lie along a velocity inversion line in Hα as well as in CIV. Typical average velocities are 1km s^{-1} (Hα) and 3km s^{-1} (CIV) in the prominence.

III-2 - Evolution of particular points

Maps of standard deviations of CIV velocity, intensity, and velocity multiplied by intensity to the power 0.5 were computed (Figure 4). The location of the Hα filament appears well in figure 4c. Then a temporal evolution of velocities in the filament body is suggested (fig. 4a) and a temporal evolution of intensities occurs at point A (fig. 4b and 1), as shown in fig. 5a. Point A is located between two parts of the Hα filament, which disconnected and reconnected from time to time. The signature of this instability may be seen in Hα at points B and C (fig. 1),*. The variations of point A (CIV) and points B and C (Hα) are not in phase, suggesting different altitudes of observation (loop ?) and maybe a heating process.

Outside the filament and regions around point A, the velocity and intensity variations seem to be very quiet in CIV.

III-3 - Statistical results

Table 1 summarizes statistical results for the filament only, all regions outside the filament and all regions together. A better correlation is found between Hα and CIV velocity fluxes when the CIV velocity is multiplied by the intensity to the power 0.5, to account for density fluctuations. If the velocity variations can be interpreted in terms of oscillations, the ratio $\langle \sigma^2 \rangle / \langle \bar{V}^2 \rangle$ may be a measure of the oscillatory power. It increases from 0.23 to 0.38 in Hα from the filament to the faculae, while it decreases from 8.23 to 0.68 in CIV. Thus, very large amplitude oscillations are expected in the CIV filament, if present, while very small ones outside. This conclusion is reversed in Hα , but with amplitudes generally smaller (effect of density). Oscillations are studied in the next section.

IV - VELOCITY OSCILLATIONS

The mean standard deviation of velocities, plotted versus the velocity in figure 6, exhibits opposite behaviour in Hα and CIV. Then, oscillations, if present, will be located in Hα redshift regions (quiet sun and faculae), and in CIV blueshift regions (filament). Such a result is suggested by figure 7, where the mean power spectrum is

* where dark material appeared in C as it disappeared in B.

reported versus the velocity (Hα and CIV) or intensity (Hα), at 2 frequencies : 280s (Hα) or 307s (CIV), and 210s (Hα) or 184s (CIV). Figure 7a is in agreement with previous results (Malherbe et al, 1981); the Hα filament appears in dark regions ($\overline{\Delta I/I} < 0$) with a power spectrum smaller than in quiet or bright ones. In Fig. 7b, it appears in blueshifts, where the power spectrum is smaller than in redshifts. Such a conclusion is reversed in CIV (Fig. 7c).

The power spectrum integrated over different regions is displayed in figure 8 versus frequency. If no oscillations are detected in the Hα filament (figure 8a), two peaks are present in CIV : oscillationsof 5 and 3 mn. The comparison between different regions (inside the filament and outside) leads to opposite conclusions in CIV and Hα (figs. 8b and c). Results of fig. 8c are in agreement with Malherbe et al (1981).

V - DISCUSSION AND CONCLUSION

The oscillatory behaviour of corresponding Hα and CIV regions seems to be opposite. Oscillations are not detected in the Hα filament, while chromospheric oscillations are present outside it (in the faculae and quiet regions). On the contrary, downward velocity regions (faculae) do not seem to oscillate in CIV, while oscillations are detected in upward velocity regions, corresponding to the Hα filament location.

The absence of oscillations in CIV downflows may be not too surprising, if such cells are the signature of coronal material motions flowing down in flux tubes.

The presence of oscillations in CIV at the location of the Hα filament may be natural, if the observed region in CIV corresponds to the transition region below the Hα filament. But new computations are required to clarify this last point. If the filament is visible in Hα $\mp$0.3 Å, lower regions may be studied in Hα $\mp$0.6 Å. We propose to compare the power spectrum at Hα $\mp$ 0.6 Å to the CIV power spectrum in regions corresponding to the Hα $\mp$ 0.3 Å filament. We suggest also to study the individual behaviour of CIV oscillatory cells, in order to obtain a more precise CIV power spectrum. At last, studying a time sequence of CIV quiet regions, if possible, should be also of interest for the understanding of the transition layers below or around prominences.

REFERENCES

Anzer, U., Tandberg-Hanssen, E. : 1970, Solar Phys., 11, 61

Dunn, R.B. : 1960, Thesis, Harvard University

Engvold, O., Reichmann, Tandberg-Hanssen, E. : 1983, in preparation.

Jensen, E., Maltby, P., Orrall, F.Q. : 1979, Physics of Solar Prominences, IAU Coll. n° 44.

Kippenhahn, R., Schlüter, A. : 1957, Z. Astrophys., 43, 36.

Lerche, I., Low? B.C. : 1980, Astrophys. J., 238, 1088.

Leroy, J.L., Bommier, V., Sahal-Brechot, S. : 1983, Solar Phys. in press

Lites, B. : 1976, Astrophys. J. Letters, 210, L111

Low, B.C. : 1981, Astrophys. J., 246, 538.

Low, B.C. : 1982, Solar Phys., 75, 119.

Malherbe, J.M., Schmieder, B., Mein, P. : 1981, Astron. Astrophys. 102, 124.

Malherbe, J.M., Schmieder, B., Ribes, E., Mein, P. : 1983, Astron. Astrophys., in press.

Malherbe, J.M., Priest, E.R. : 1983, Astron. Astrophys., in press.

Martres, M.J., Mein, P., Schmieder, B., Soru-Escaut, I. : 1981, Solar Phys. 69, 301.

Mein, P. : 1977, Solar Phys., 54, 45.

Mein, P., Simon, G., Vial, J.C., Shine, R.A. : 1982, Astron. Astrophys. 111, 136.

Milne, A.M., Priest, E.R., Roberts, B. : 1979, Astrophys. J., 232, 304.

Mouradian, Z., Martres, M.J., Soru-Escaut, I. : 1980, Japan-France sem. on Solar Phys., 195, Moriyama and Henoux eds.

Pickel'ner, S.B. : 1971, Solar Phys. 17, 44.

Priest, E.R., Smith, E.A. : 1979, Solar Phys., 64, 267.

Raadu, M.A., Kuperus, M. : 1973, Solar Phys. 28, 77.

Ribes, E., Unno, W. : 1980, Astron. Astrophys. 91, 129.

Schmieder, B., Vial, J.C., Mein, P., Tandberg-Hanssen, E. : 1982, proceedings of the 24th Cospar, in press.

Simon, G., Mein, P., Vial, J.C., Shine, R.A., Woodgate, B.E. : 1982, Astron. Astrophys. 115, 367.

Tandberg-Hanssen, E. : 1974, Solar Prominences, D. Reidel Pub. Co., Dordrecht, Holland.

Uchida, Y. : 1980, Japan-France sem. on Solar Physics, 169, Moriyama and Henoux, eds.

Woodgate, B.E., Tandberg-Hanssen, E., Bruner, E.C., Beckers, J.M., Brandt, J.C., Henze, W., Hyder, C.L., Kalet, M.W., Kenny, P.J., Knox, E.D., Michalitsanios, A.G., Rehse, R., Shine, R.A., Tinsley, H.D. : 1980, Solar Physics, 65, 73.

$\langle\ \rangle$ = spatial average; $\overline{\ }$ = temporal average; + = positive values only; − = negative values only.

spectral line	mean velocity km/s $\langle\overline{V}\rangle$	mean blueshift km/s $\langle\overline{V_+}\rangle$	mean redshift km/s $\langle\overline{V_-}\rangle$	ratio between up and down fluxes $\lvert F_+/F_- \rvert$	standard deviation Km/s $\langle\sigma_V\rangle$	$\langle\overline{V^2}\rangle$	mean quadratic velocity $(km/s)^2$ $\langle\overline{V^2}\rangle$	mean variance $(Km/s)^2$ $\langle\sigma^2\rangle$	mesure of oscillatory power $\langle\sigma^2\rangle/\langle\overline{V}^2\rangle$	region
Hα $\overline{+}$0.3Å	0.92	1.24	-0.53	10.41	0.53	1.52	1.87	0.35	0.23	filament
CIV	1.13	3.0	-2.7	2.29	9.46	13.86	128.3	114.4	8.23	only
CIV ($V\sqrt{I}$)				5.21						
Hα $\overline{+}$0.3Å	-0.4	0.47	-0.81	0.26	0.49	0.80	1.10	0.30	0.38	all regions except filament
CIV	-5.24	2.39	-6.71	0.07	4.9	53.0	89.0	36.0	0.68	
CIV ($V\sqrt{I}$)				0.10						
Hα $\overline{+}$0.3Å	-0.16	0.76	-0.74	0.65	0.5	0.93	1.24	0.31	0.33	all regions
CIV	-4.1	2.67	-6.4	0.14	5.7	46.0	96.0	50.0	1.09	
CIV ($V\sqrt{I}$)				0.18						

TABLE 1

FIGURE CAPTIONS

Figure 1 : Maps of Hα $\mp$ 0.3 Å and CIV intensities $\overline{I}$ and radial velocities $\overline{V}$

The common field of view (about 1' x 1') between Hα and CIV observations is indicated by the square. The location of the Hα filament is reported on the CIV intensity map.

Figure 2 : The relationship between intensities $\overline{I}$ and velocities $\overline{V}$ in Hα $\mp$ 0.3 Å (a) and CIV (b).

- in abscissae : the velocity $\overline{V}$
- in dashed line : the distribution function of velocities over the field of view.
- in continuous line : the mean value of intensity $\langle \overline{I} \rangle$

Figure 3 : Mean cross section of Hα $\mp$ 0.3 Å and CIV intensities and velocities.

- In abscissae : the direction (X) of cross section. The origin of X axis is located at point 0 (see figure 1).

(a) : mean value of intensities $\overline{I}$
(b) : mean value of velocities $\overline{V}$

The direction (Y) of averaging is reported in figure 1.

Figure 4 : Maps of CIV standard deviations.

(a) radial velocity
(b) intensity
(c) radial velocity multiplied by the intensity at the power 0.5 (mass flux).

The location of the Hα filament is reported in figure (4c).

Figure 5 : Temporal evolution of particular points in Hα $\mp$0.3Å and CIV.

(a) : evolution of CIV intensity and velocity of point A (see figures 1 and 4).
(b) : evolution of Hα $\mp$0.3.Å intensity and velocity of points B and C (see figure1).

Figure 6 : The relationship between the standard deviation of velocity and the velocity in Hα $\mp$0.3.Å (a) and CIV (b).

- in abscissae : the velocity $\overline{V}$
- in dashed line : the distribution function of velocity
- in continuous line : the mean standard deviation of velocity. $\langle \sigma^2 \rangle$

Figure 7 : The relationships between the power spectrum and the intensity (a) or the velocity (b and c) in Hα $\mp$0.3Å and CIV at fixed frequencies.

(a) : in abscissae : Hα intensity fluctuations $\overline{I}$
in dotted line : distribution function of Hα intensity
in dashed line : mean power spectrum at 210 S.
in continuous line : mean power spectrum at 280 s.

(b) and (c) : in abscissae : the velocity $\overline{V}$
in dashed line : mean power spectrum at 280s(Hα) or 307s(CIV).
in continuous line : mean power spectrum at 210s(Hα) or 184s(CIV)

Figure 8 : Power spectra of different regions in Hα $\mp$0.3Å and CIV

(a) : filament only - comparison Hα $\mp$0.3Å/CIV
(b) : CIV regions
(c) : Hα $\mp$0.3Å regions.

In abscissae : the frequency.

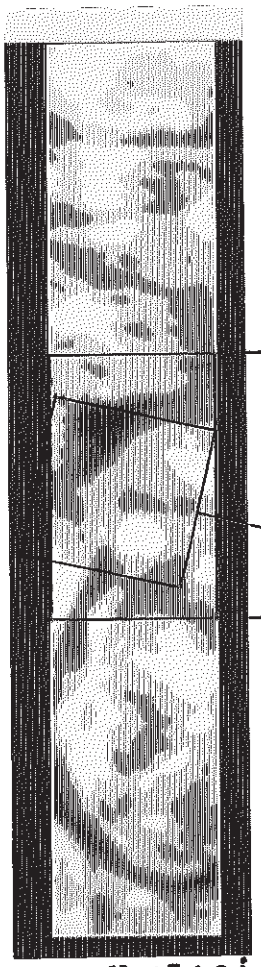

Hα ∓0.3Å
INTENSITY
(5.5' x 1')

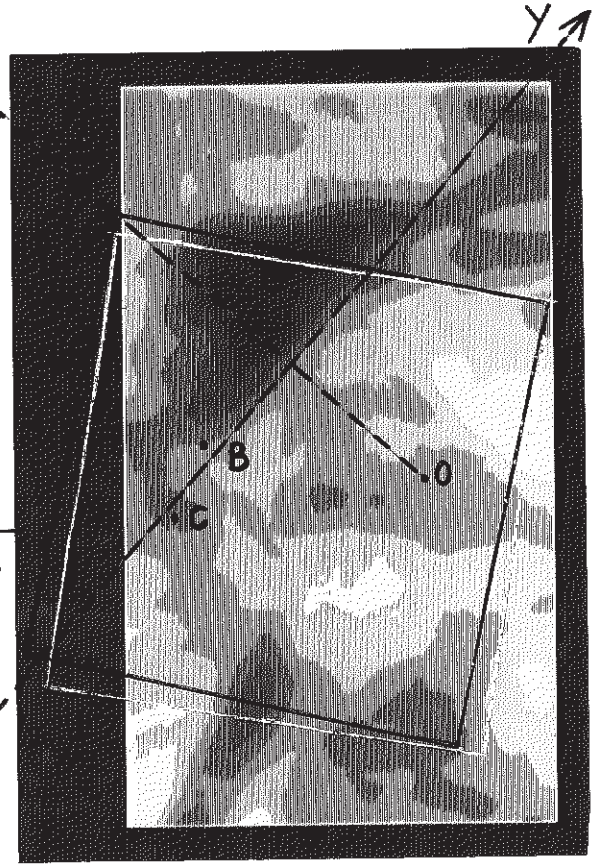

Hα INTENSITY

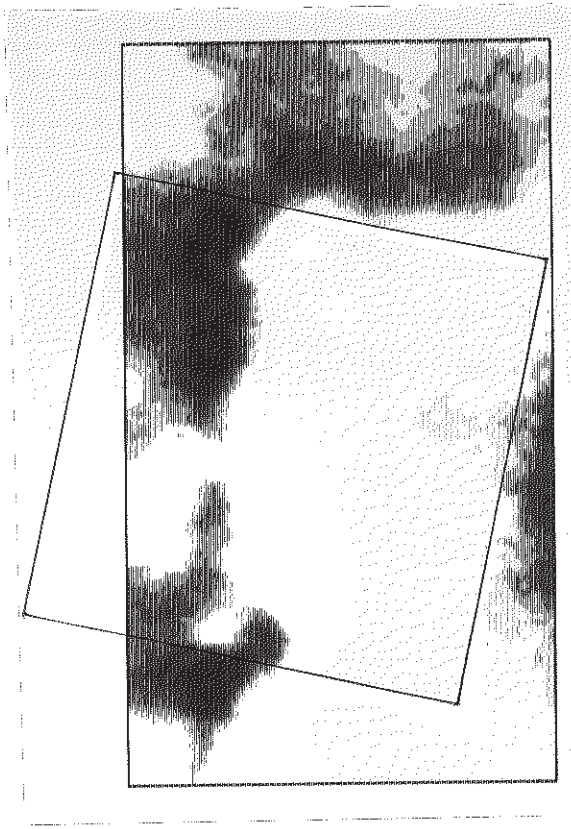

Hα BLUESHIFTS

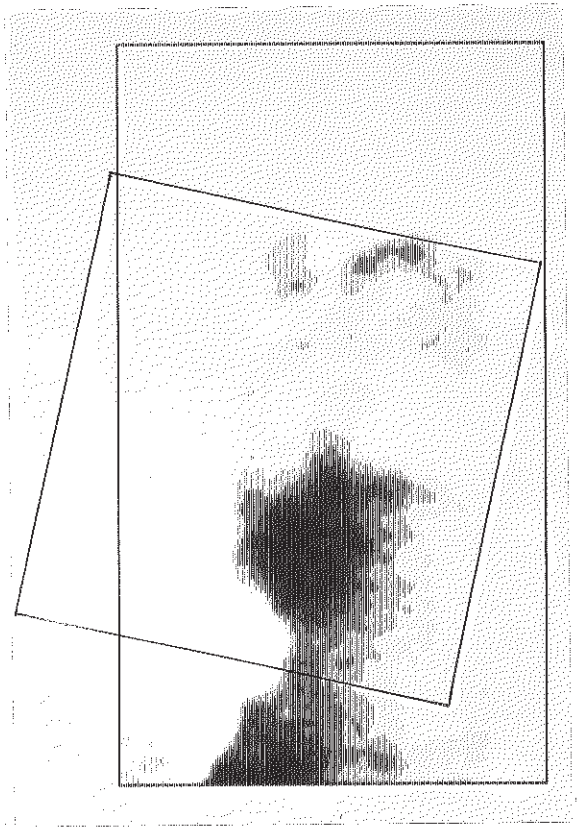

Hα REDSHIFTS

FIGURE 1

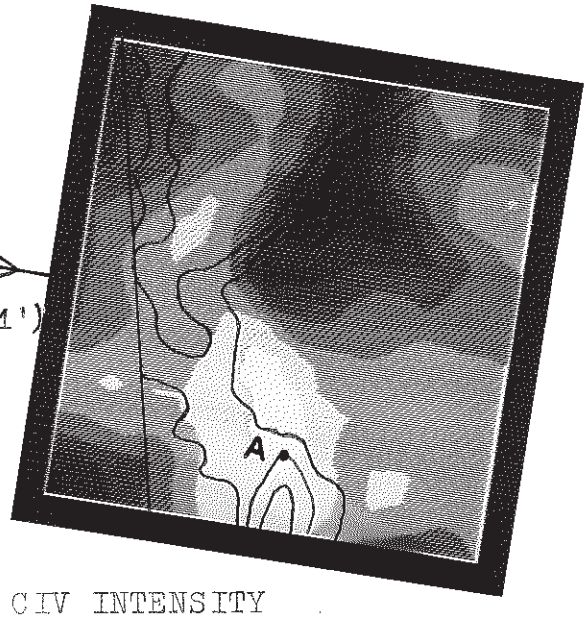

CIV INTENSITY

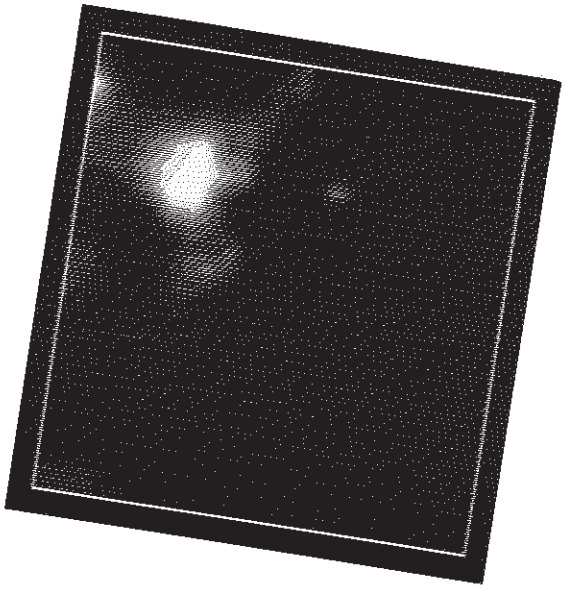

CIV BLUESHIFTS

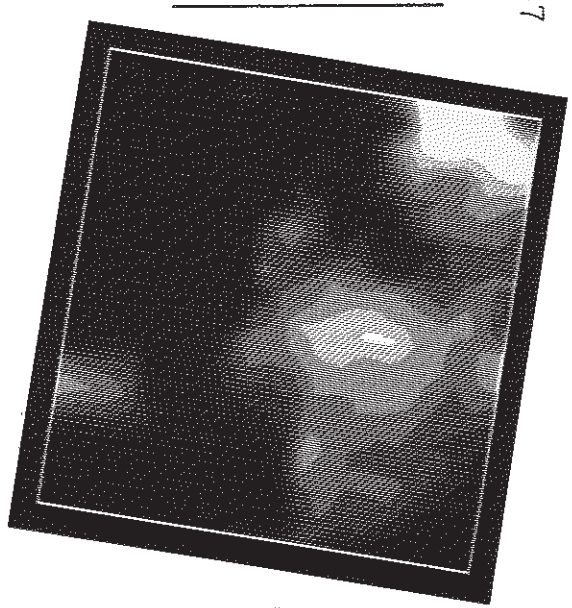

CIV REDSHIFTS

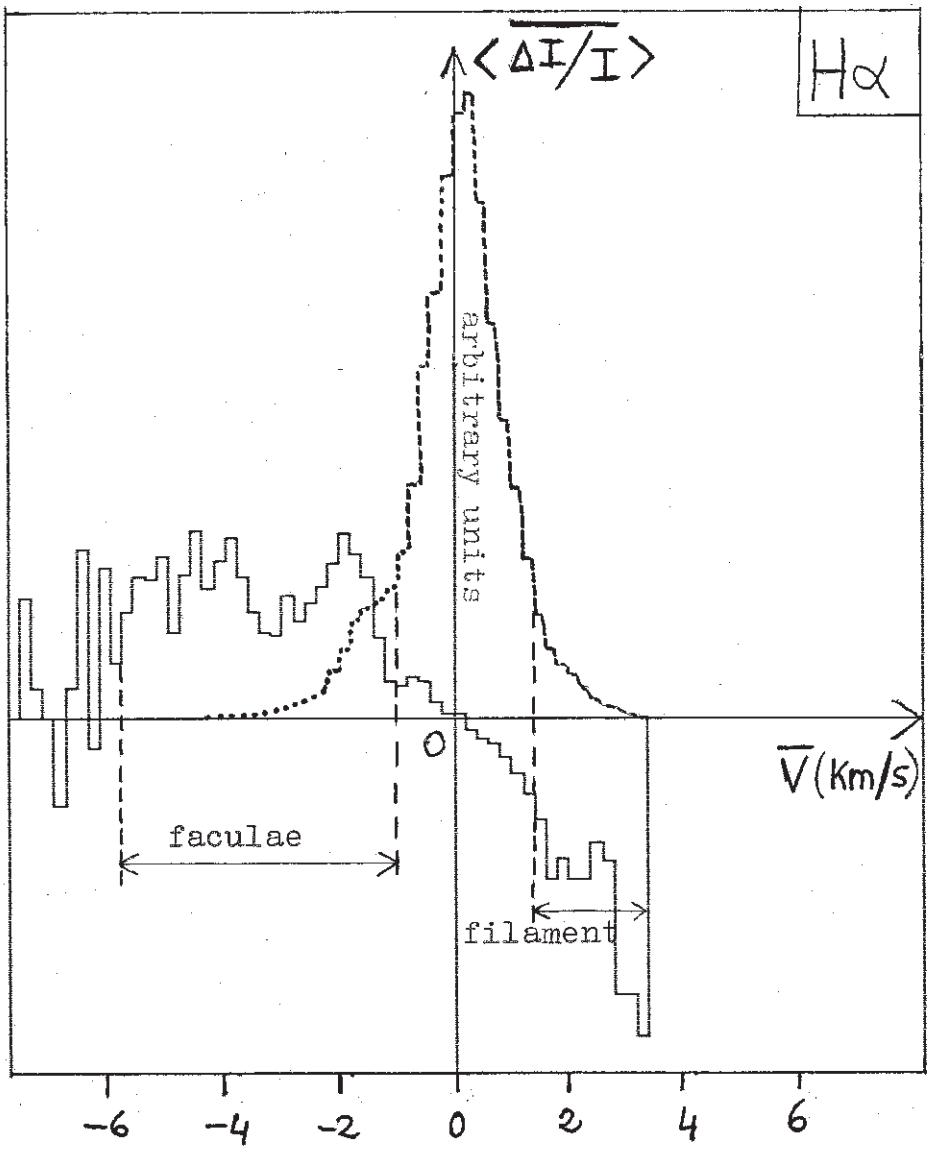
$\langle \overline{\Delta I/I} \rangle$
Hα
arbitrary units
0
$\overline{V}$(Km/s)
faculae
filament
-6
-4
-2
0
2
4
6

(a)

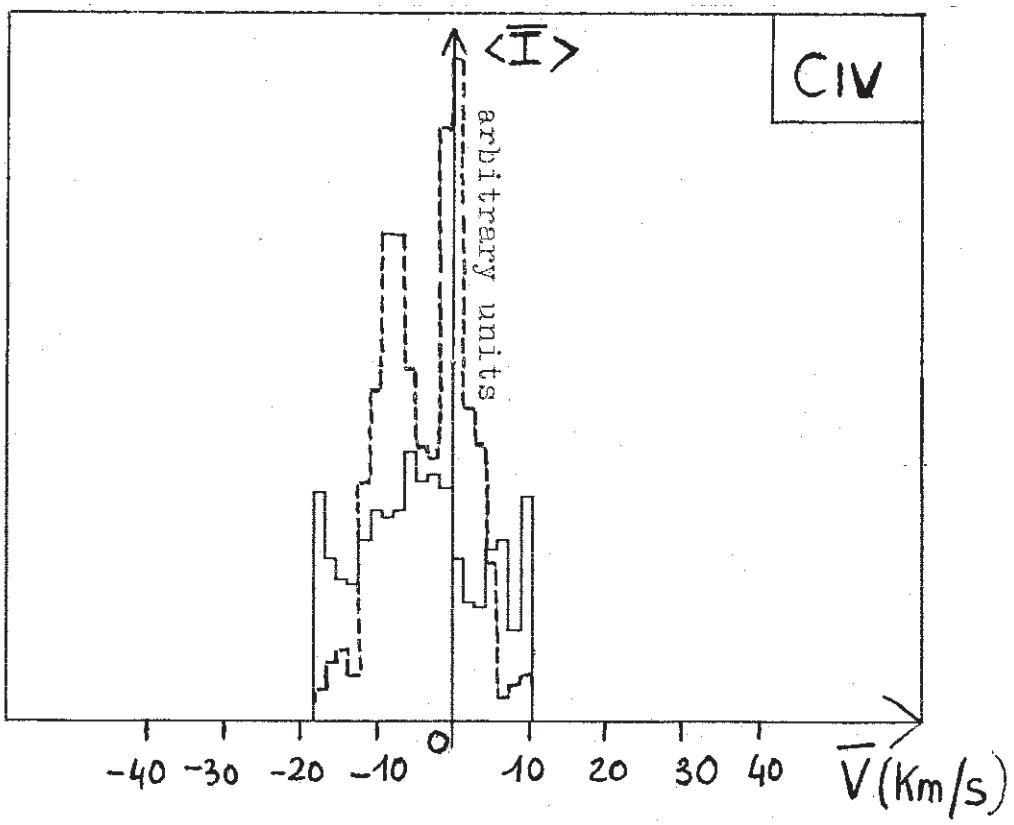
$\langle \overline{I} \rangle$
CIV
arbitrary units
0
-40
-30
-20
-10
10
20
30
40
$\overline{V}$(Km/s)

(b)

FIGURE 2

FIGURE 3

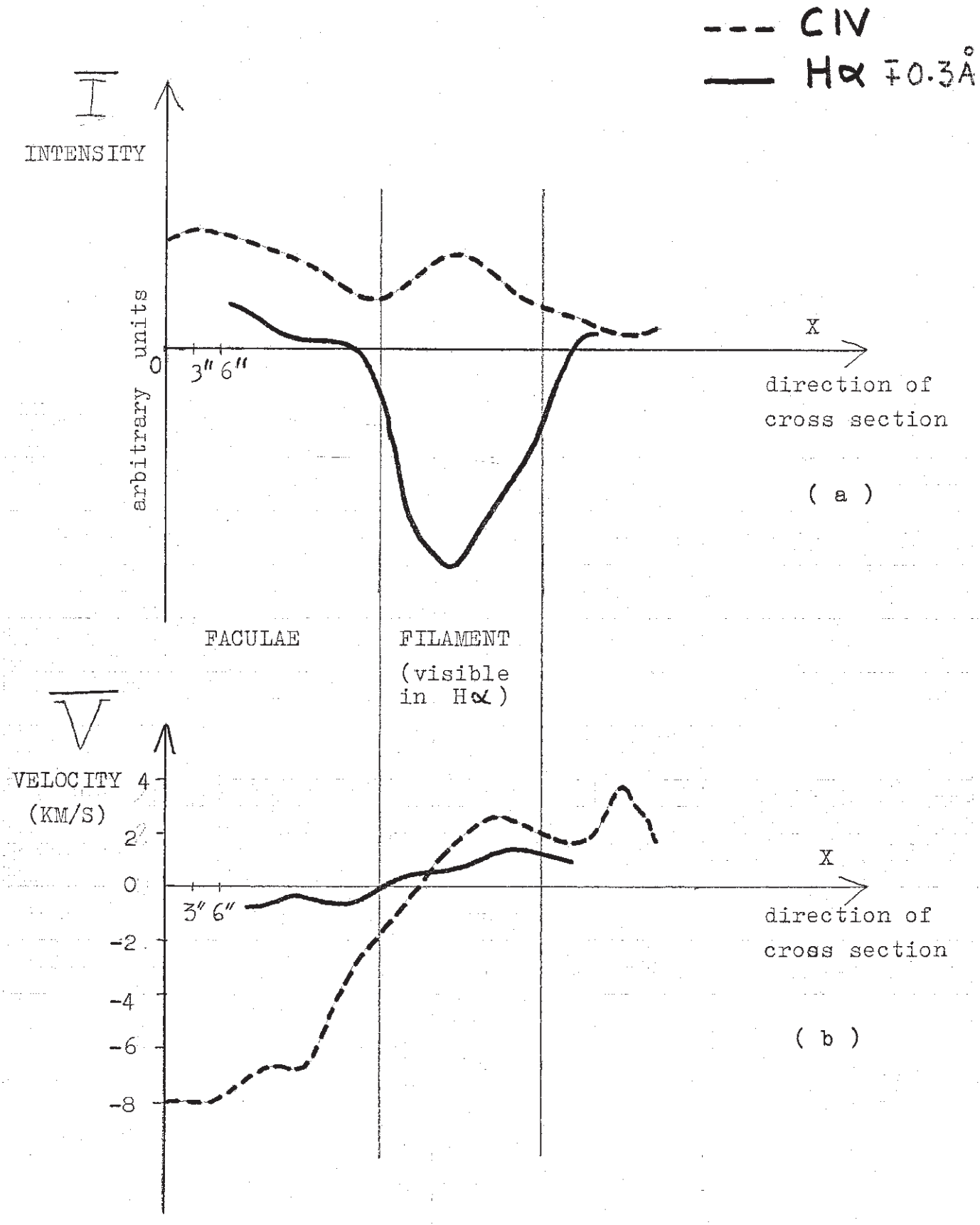
--- CIV
— Hα ∓0.3Å
I
INTENSITY
arbitrary units
0
3" 6"
X
direction of cross section
(a)
FACULAE
FILAMENT
(visible in Hα)
V
VELOCITY (KM/S)
4
2
0
-2
-4
-6
-8
3" 6"
X
direction of cross section
(b)

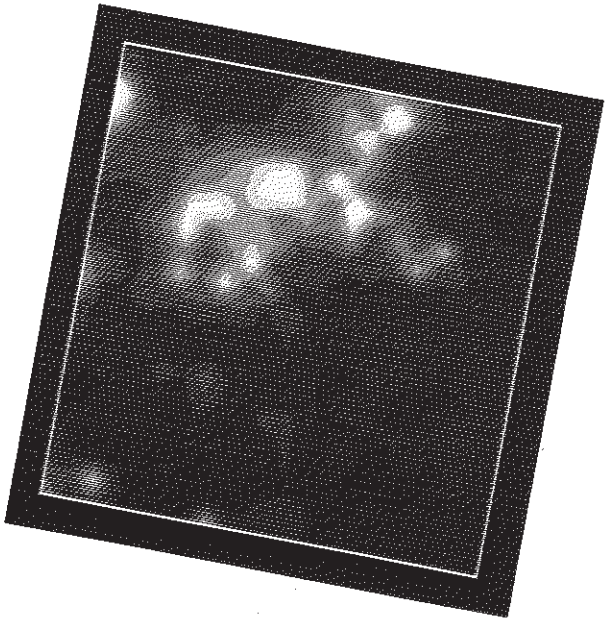

$\sigma(V)$

(a)

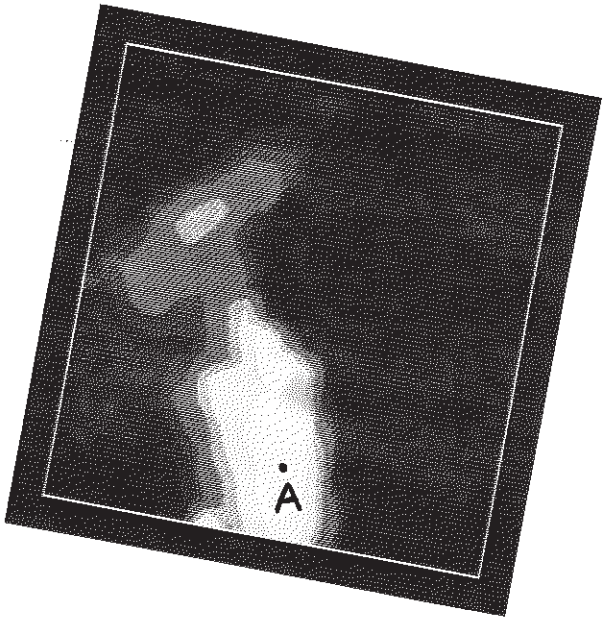

$\sigma(I)$

(b)

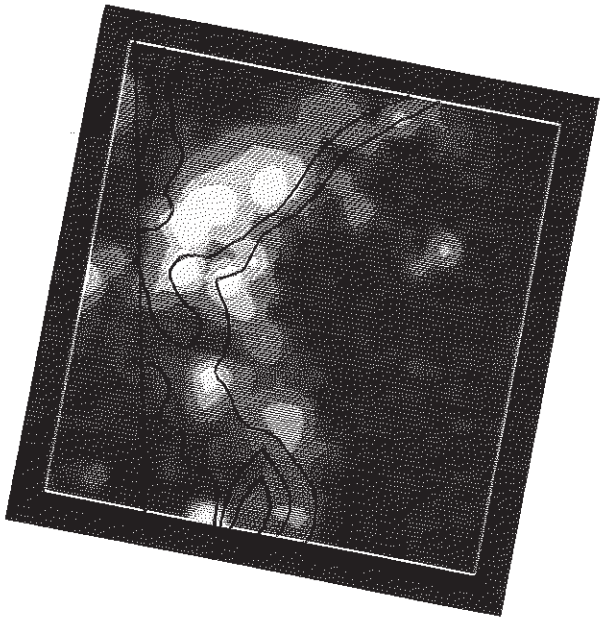

$\sigma(V\sqrt{I})$

(c)

FIGURE 4

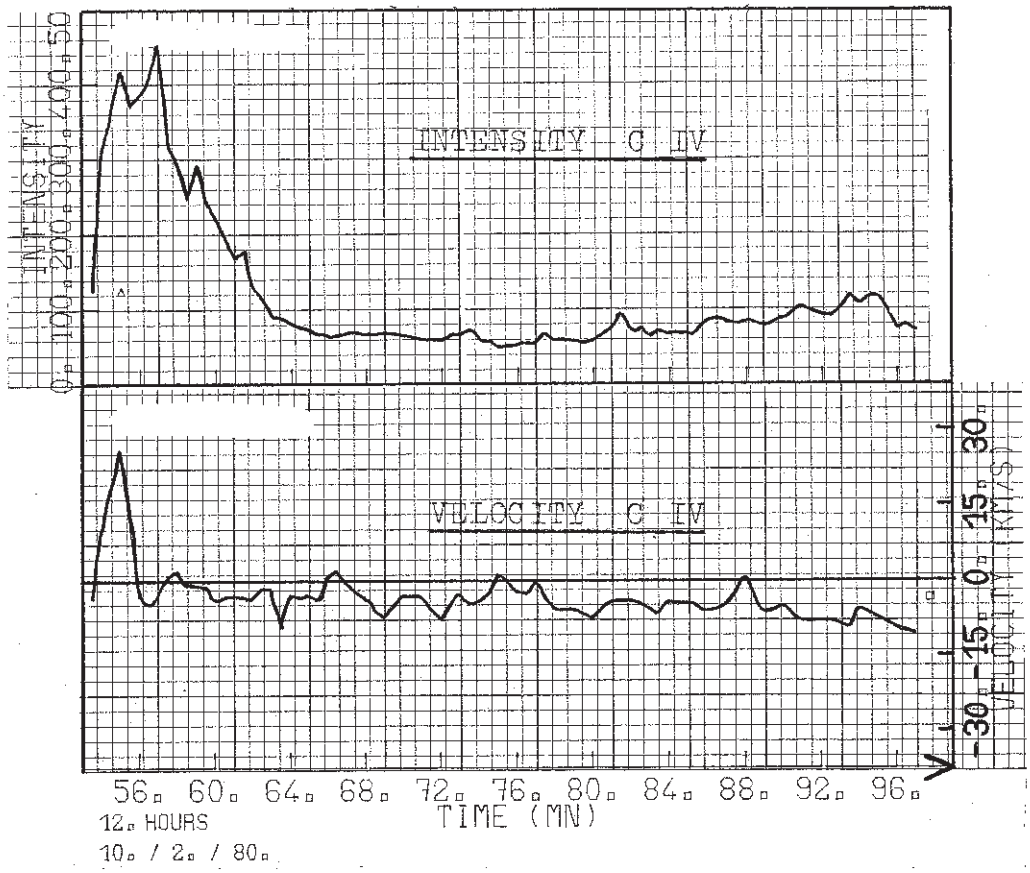

(a) TEMPORAL EVOLUTION IN C IV OF POINT(A)

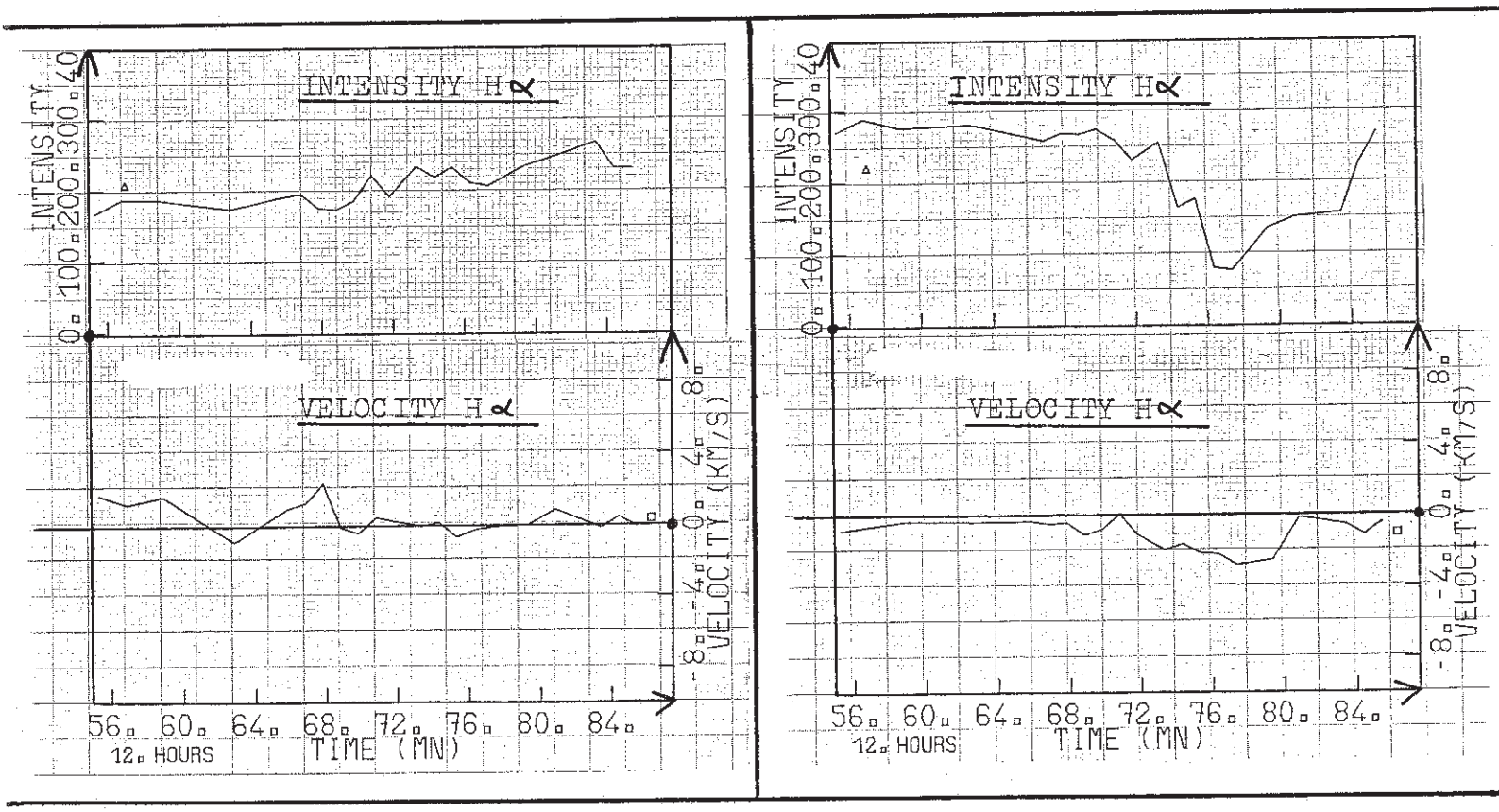

POINT (B) POINT (C)

(b) TEMPORAL EVOLUTION IN Hα ∓0.3 Å

FIGURE 5

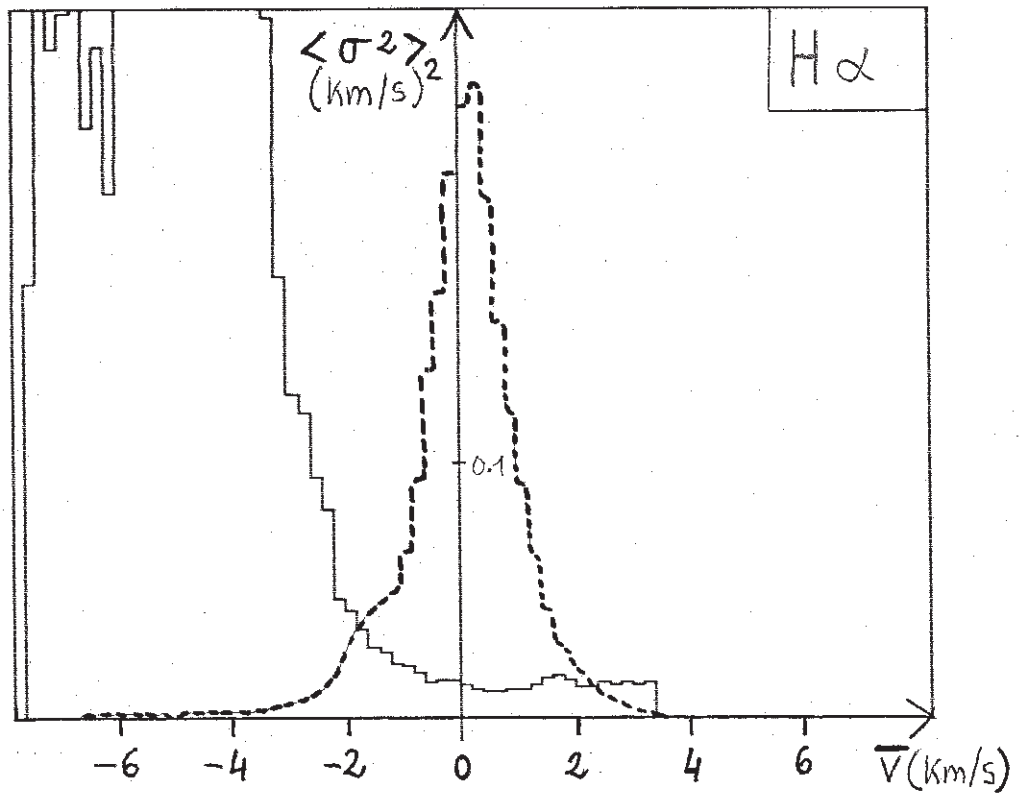
$\langle \sigma^2 \rangle^2$
(Km/s)^2
Hα
0.1
-6
-4
-2
0
2
4
6
$\overline{V}$(Km/s)

(a)

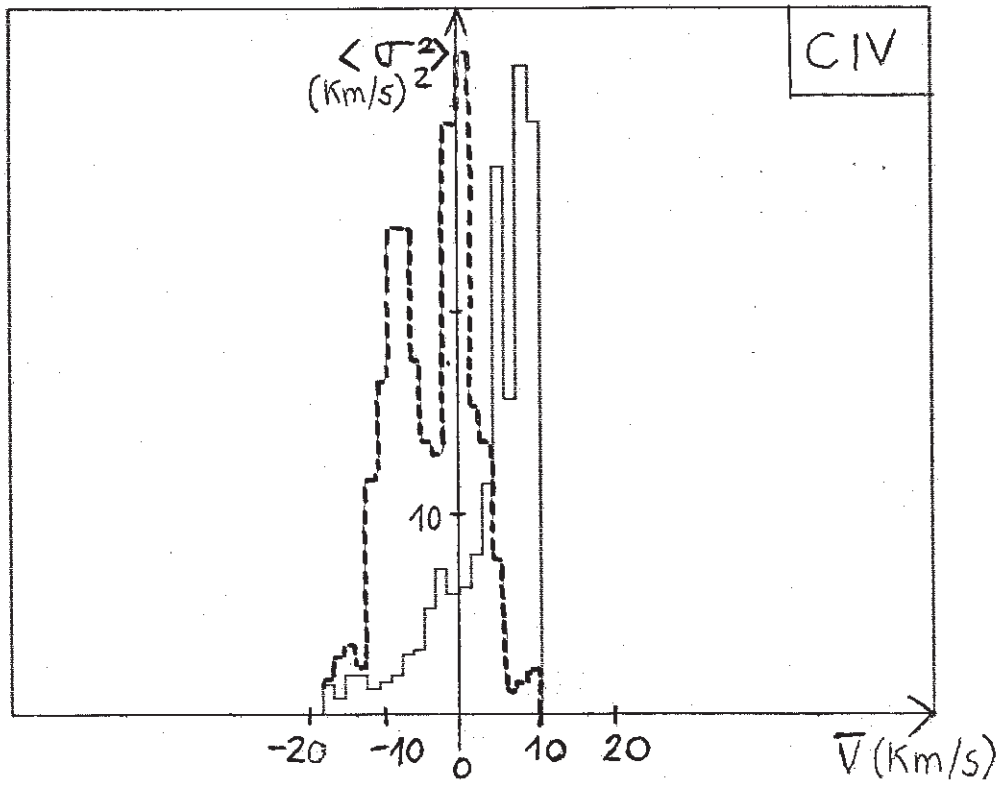
$\langle \sigma^2 \rangle$
(Km/s)^2
CIV
10
-20
-10
0
10
20
$\overline{V}$ (Km/s)

(b)

FIGURE 6

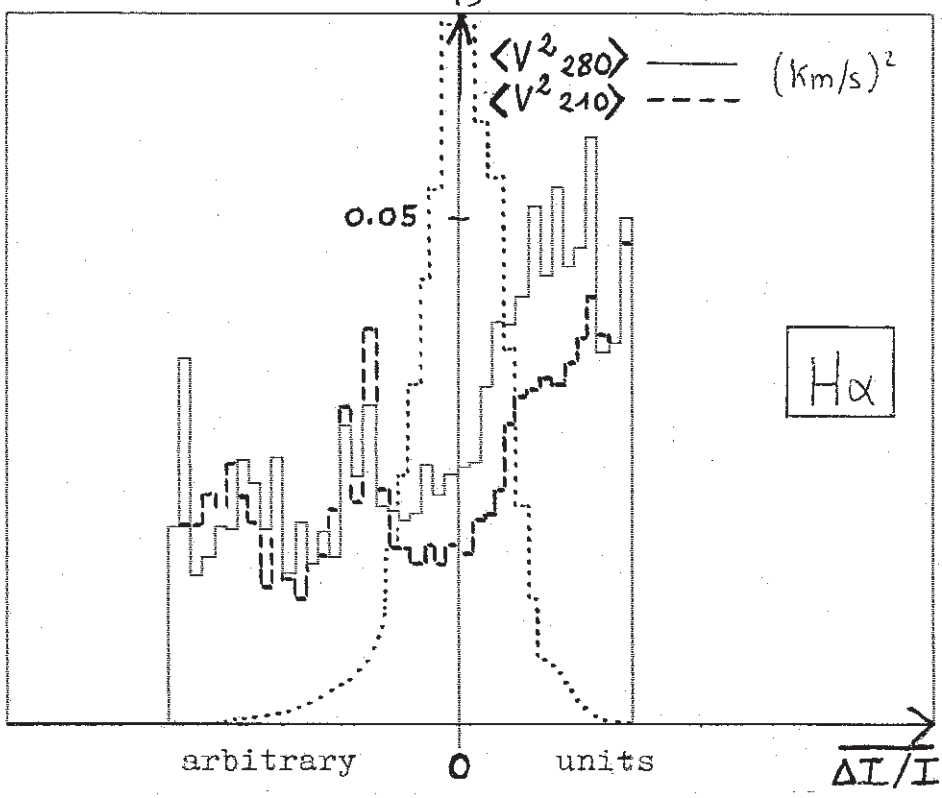
⟨V² 280⟩
⟨V² 210⟩
(Km/s)²
0.05
Hα
arbitrary
0
units
ΔI/I

(a)

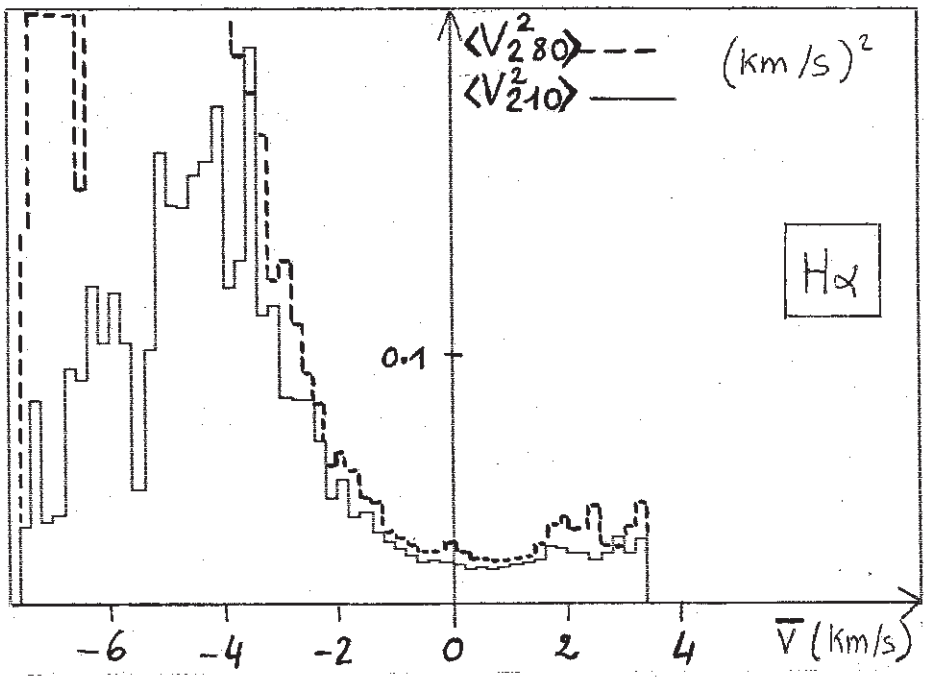
⟨V²280⟩
⟨V²210⟩
(km/s)²
Hα
0.1
-6
-4
-2
0
2
4
V̄ (Km/s)

(b)

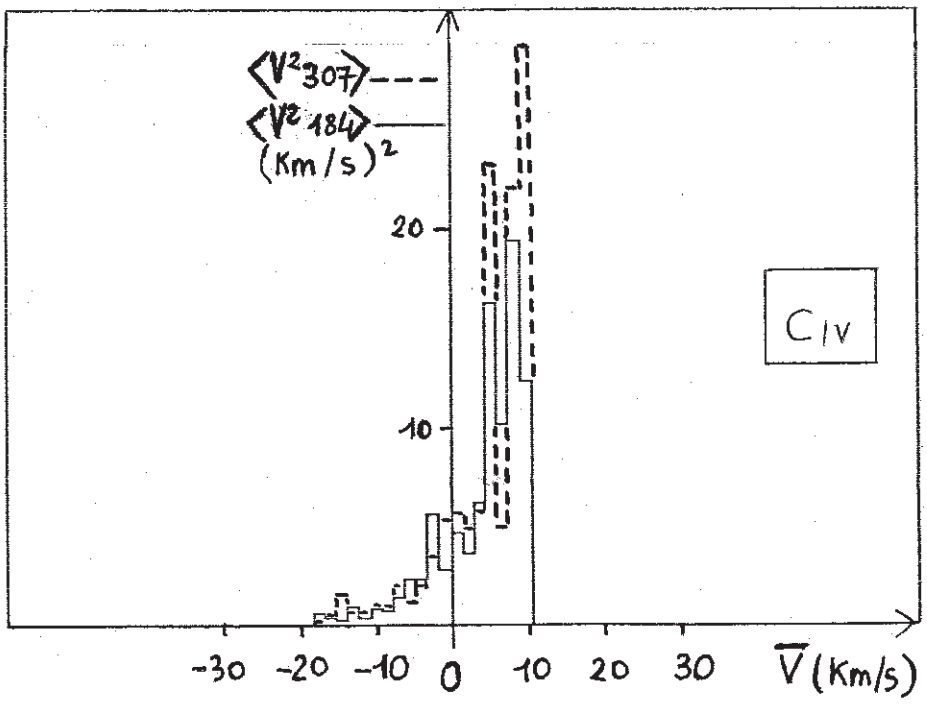
⟨V²307⟩
⟨V²184⟩
(Km/s)²
20
10
CIV
-30
-20
-10
0
10
20
30
V̄ (Km/s)

(c)

FIGURE 7

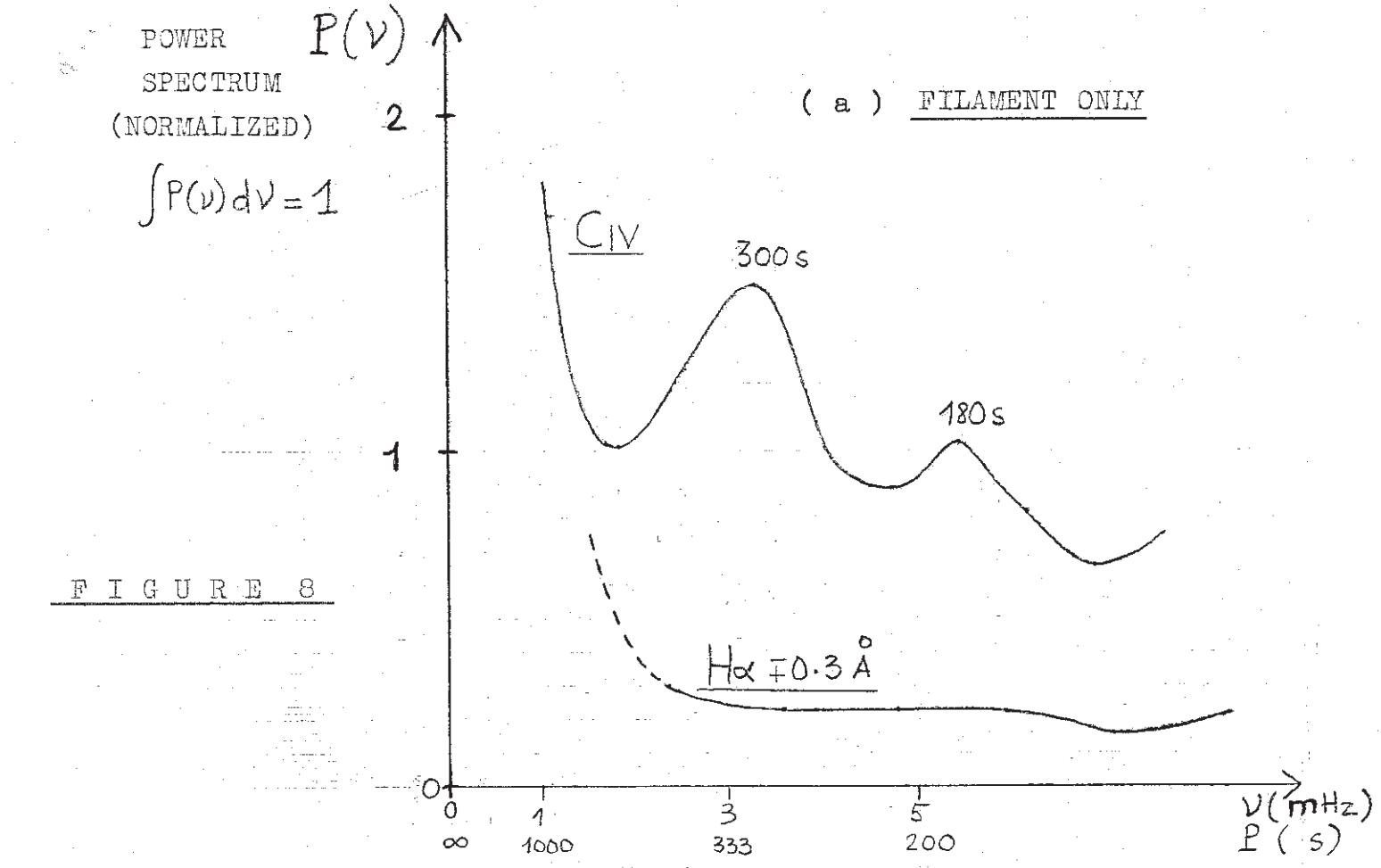
POWER SPECTRUM (NORMALIZED)
P(ν)
∫P(ν)dν = 1
(a) FILAMENT ONLY
C IV
300 s
180 s
Hα ∓0.3 Å
2
1
0
0 1 3 5
∞ 1000 333 200
ν(mHz)
P (s)

FIGURE 8

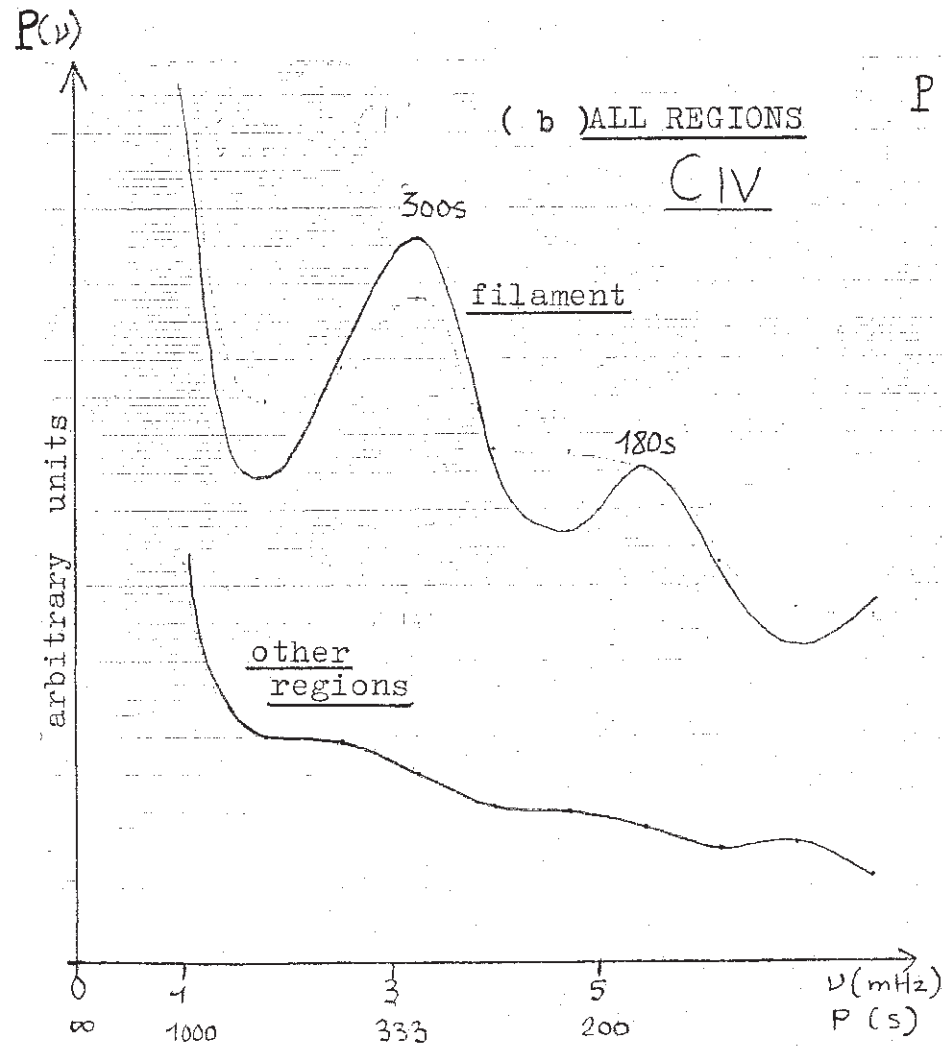
P(ν)
(b) ALL REGIONS
C IV
300s
filament
180s
other regions
arbitrary units
0 1 3 5
∞ 1000 333 200
ν(mHz)
P (s)

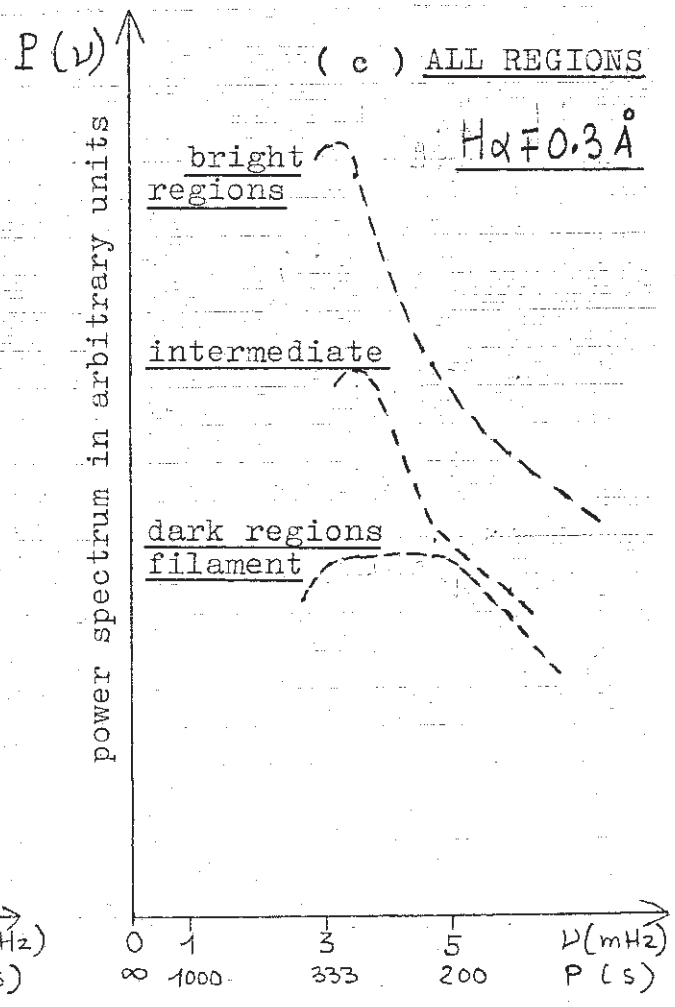
P(ν)
(c) ALL REGIONS
Hα ∓0.3 Å
bright regions
intermediate
dark regions
filament
power spectrum in arbitrary units
0 1 3 5
∞ 1000 333 200
ν(mHz)
P (s)

III - INSTABILITES DANS LES PROTUBERANCES

"LES DISPARITIONS BRUSQUES"

"DANS LES CRISES VIOLENTES, CES FLAMMES PRÉSENTENT DES VOLUMES SI EXTRAORDINAIRES, DES MOUVEMENTS SI RAPIDES, DES INTENSITÉS SI VARIABLES QUE L'OBSERVATEUR EST PLONGÉ DANS LA PLUS PROFONDE ADMIRATION ET, EN MÊME TEMPS, DANS LE PLUS PROFOND EMBARRAS..."

SECCHI, 1875, "LE SOLEIL"

III - 1 - ETAT DES OBSERVATIONS ET DES MODÈLES

La plupart des protubérances sont le siège, au cours de leur vie, d'une disparition brusque (DB) ou d'une éruption. Ces phénomènes peuvent être répartis schématiquement en deux classes, selon qu'ils sont accompagnés d'une restructuration catastrophique du champ magnétique (éruptions et certaines DB) ou non (majorité des DB). Ainsi beaucoup de filaments réapparaissent au même endroit après une DB.

a - Les disparitions brusques-observations

Quelques indices d'instabilité ont été découverts :

- un filament dont la distance entre les pieds est très différente de sa hauteur semble être instable (Martres, 1982), en accord avec le modèle de Nakagawa et Malville (1969).

- les DB sont souvent précédées par des évènements avant coureurs : augmentation de densité optique en Hα (Martres, 1956), due probablement à une instabilité thermique ; vrillage des pieds de boucles magnétiques (Xiaoma et al, 1982) pouvant conduire à une instabilité de "kink" ; torsion de la protubérance entière, d'où élongation des lignes de force et augmentation du "shear" (Moore et Labonte, 1980), pouvant mener à une déstabilisation par perte d'équilibre thermique ; apparition d'arches chaudes (10^5K à 10^6K) au dessus du filament (Schmahl et al, 1982) suggérant un chauffage dû à la dissipation d'ondes MHD.

Ces perturbations peuvent être consécutives à une éruption au voisinage, ou même assez loin, de la protubérance. Une onde de choc hydromagnétique (Moreton, 1960, 1965) se propageant dans la chromosphère et la couronne à une vitesse de l'ordre de 1000 km s^{-1}, peut être engendrée dans la phase de flash et "secouer", sur son passage, le filament, qui peut se mettre à osciller autour d'une position d'équilibre stable, ou bien se déstabiliser, disparaître et, souvent réapparaître ensuite.

Inversement, les DB peuvent précéder ou accompagner une éruption, pouvant se produire sur le sîte même de la disparition (Bruzek, 1951, 1957). De tels phénomènes peuvent être dûs à l'émergence de flux magnétique (Slonim,1980) formant un "current sheet" avec le champ préexistant, suivie par une instabilité résistive de "tearing modes" pouvant déclencher, dans sa phase non linéaire, un processus de reconnections magnétiques stationnaires, hautement dynamique. Une autre possibilité est la perte d'équilibre thermique du filament, déclenchant un mécanisme de chauffage du plasma (Webb and Jackson, 1981). Ces deux types d'instabilité peuvent correspondre aux deux types de DB observés par Mouradian et al (1980) :

DB1 et DB2 selon que la restructuration du champ magnétique est complète (DB1) ou non (DB2). Dans ce cas (DB2), Mouradian et al (1980) suggérèrent un mécanisme de chauffage provoquant l'ionisation du plasma : la réapparition d'un filament, après une DB, a été observée au même endroit dans des raies EUV, avant sa réapparition en Hα. Un tel résultat a été aussi obtenu par Kahler et al (1979).

b - les mécanismes de déstabilisation-théorie

Très schématiquement, plusieurs mécanismes peuvent être proposés :
- bifurcations entre équilibres multiples
- instabilités magnétiques consécutives à une perte d'équilibre magnétostatique
- instabilités magnétiques dûes à l'émergence de nouveau flux
- instabilités magnétiques consécutives à une perte d'équilibre thermique.

Une revue complète est faite dans Priest (1981) et Priest (1982). Les mécanismes d'activation que nous allons expliciter ici ont surtout été élaborés pour comprendre les protubérances éruptives. Néanmoins, les mécanismes gouvernant les DB pourraient bien être les mêmes, compte tenu de leur association étroite aux éruptions ; en ce sens, la DB peut éventuellement incarner un stade "avorté" de protubérance éruptive, la différence principale résidant dans l'énergie

magnétique mise en jeu.

bifurcations entre équilibres multiples à conditions aux limites identiques.

Lorsque plusieurs équilibres, pour des conditions aux limites identiques, existent, des bifurcations sont possibles entre eux (Low, 1977 ; Heyvaerts et al, 1980). Cependant, un tel mécanisme, qui conduit généralement à une modification complète de la géométrie magnétique, semble improbable pour les DB, après lesquelles les filaments sont vus souvent réapparaître.

instabilités magnétiques consécutives à une perte d'équilibre magnétostatique.

Le passage d'une onde de Moreton peut provoquer des mouvements d'oscillations globales du filament. A l'aide d'équations du type oscillateur harmonique ($\ddot{x} + p\dot{x} + qx = 0$), dont ils calculèrent les coefficients, Hyder (1966), et Kleczek et Kuperus (1969), ont proposé, respectivement, un modèle d'oscillations verticales et horizontales. Hyder (1966) suggera qu'une DB pouvait se produire lorsque le déplacement initial du filament était dirigé vers la couronne, le mouvement étant amplifié par la décroissance de densité avec l'altitude. Kuperus et Raadu (1974) étudièrent la stabilité d'une protubérance supportée par le champ magnétique induit par son image sous la photosphère, et montrèrent qu'une perte de masse ou une augmentation du courant avaient un effet déstabilisant pouvant expliquer une DB. Par suite, Van Tend et Kuperus (1978) ajoutèrent au champ une composante horizontale variable avec l'altitude, pour simuler le champ des régions actives, et montrèrent l'existence d'une intensité critique au delà de laquelle tout équilibre devenait impossible.

Récemment Hood et Priest (1980) étudièrent la stabilité magnétique d'un filament cyclindrique, d'altitude d au dessus de la photosphère, parcouru par un champ hélicoïdal et suspendu dans une arcade coronale, la structure de l'ensemble étant tordue ("twist" d'angle φ) uniformément (Figure III-1).

Ils trouvèrent, malgré l'effet stabilisant de l'ancrage ("line tying") des lignes de force dans la photosphère, que l'équilibre était instable aux perturbations dont le nombre d'onde est représenté figure III-1.

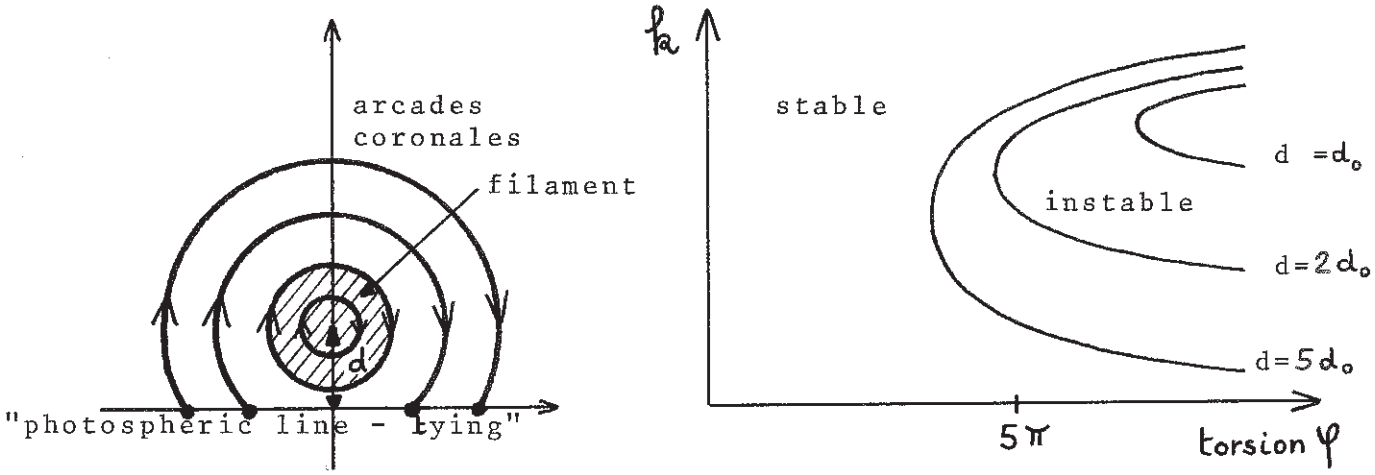

FIGURE III-1

Ainsi une instabilité peut survenir au dela d'une torsion ou d'une altitude critiques.

Instabilités de "kink", "tearing mode" et émergence de flux magnétique

De nombreux auteurs ont étudié la stabilité de filaments en forme de boucle dont les deux pieds sont ancrés ("line-tied") dans la photosphère, et ont montré qu'une telle structure est sujette à l'instabilité de "kink" lorsque la torsion excède 2.5 π (Hood et Priest, 1981a), de façon analogue à la Figure III-1.

Sur les surfaces singulières, définies par

$$\vec{\nabla} \wedge (\vec{V} \wedge \vec{B}) = \vec{0}$$

dans l'équation d'induction

$$\partial \vec{B} / \partial t = \vec{\nabla} \wedge (\vec{V} \wedge \vec{B}) + \vec{\nabla}^2 \vec{B} / \mu\sigma \quad ,$$

le rôle de la résistivité domine celui de la convection et une instabilité de "kink" résistif ou "tearing mode" peut survenir. C'est en particulier le cas des filaments en "current sheet" plans (modèle de Kuperus et Raadu par exemple) ou cylindriques. Le "tearing mode" est une instabilité de grande longueur d'onde provoquant le déchirement et la reconnection des lignes de force du champ magnétique, formant ainsi une nouvelle configuration. Les temps de croissance (linéaires) de cette instabilité sont :

$\tau_p = \tau_D^{1/2} \tau_A^{1/2}$ ("tearing plan")

ou $\tau_c = \tau_D^{1/3} \tau_A^{2/3}$ ("tearing cylindrique")

avec $\tau_D = \mu\sigma \ell^2$ (temps résistif)

et $\tau_A = \ell (\mu\rho)^{1/2} / B$ (temps hydrodynamique d'Alfvèn).

B est le champ magnétique (10G), ρ la densité (10^{-13} g cm^{-3}), ℓ une dimension caractéristique (10^4km) et $\sigma = 8\ 10^{-4} \times T^{3/2}$ ($T = 10^4$K) la conductivité du plasma. Dans un filament, ($\tau_D \approx 10^{11}$S et $\tau_A \approx 10^2$S), on obtient $\tau_p = 3\ 10^6$s et $\tau_c = 10^5$s, temps trop longs vis à vis des temps caractéristiques (10^3s) d'instabilités observés.

Ces temps peuvent être réduits si le plasma est turbulent (diminution de la conductivité par un facteur $\gg 1000$) ou si l'instabilité se développe sur de petites échelles (10^2km). C'est l' "emerging flux model" d'Heyvaerts et al (1977), dans lequel le tearing mode déclenche un processus stationnaire de reconnections magnétiques dans le "current sheet" formé entre le champ émergent et préexistant.

Instabilités magnétiques consécutives à une perte d'équilibre thermique.

Milne et al (1979), généralisant le modèle de Kippenhahn-Schlüter (1957) en y introduisant une équation d'énergie, mirent en évidence un "shear" critique des arcades magnétiques, au delà duquel l'équilibre cesse d'exister : le déclin de la conduction thermique vers les régions froides impliquant une diminution des pertes radiatives totales, la protubérance peut s'échauffer et disparaître.

Hood et Priest (1979 et 1981b) ont résolu l'équation d'énergie le long d'une ligne de champ d'une boucle froide. La température en son sommet est représentée en fonction du taux de chauffage h et de la pression p (supposée uniforme) sur la figure III-2. Il existe une valeur critique de h ou de p^{-1} au delà de laquelle tout équilibre froid est impossible (point catastrophe). La boucle s'échauffe alors vivement, cherchant un nouvel équilibre thermique, pouvant déclencher une éruption.

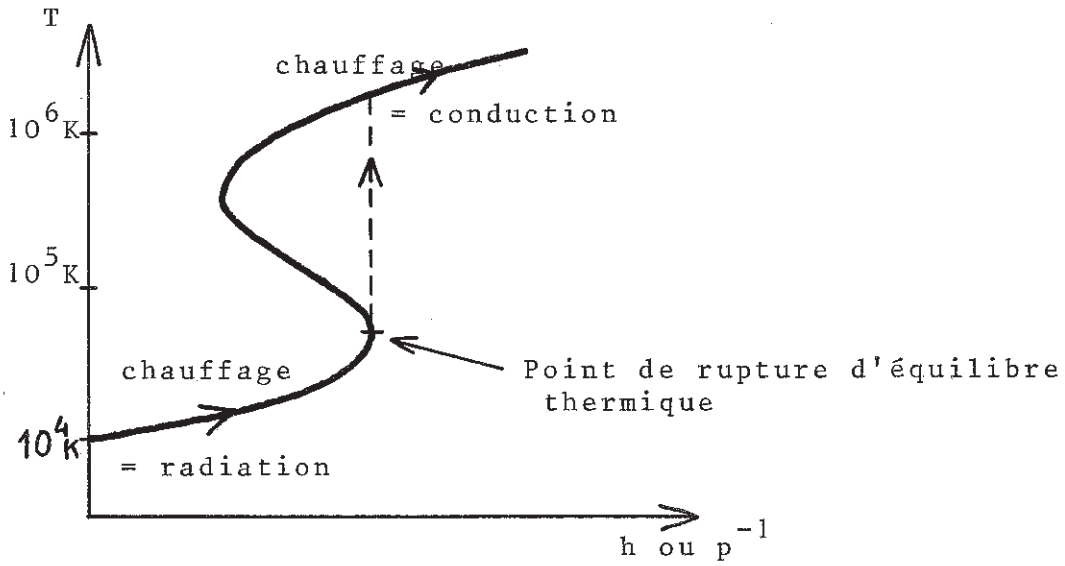

FIGURE III-2

c - Conclusion

L'activation des protubérances couvre un champ d'étude extrêmement vaste. Nous n'avons pas parlé des "surges", ni des transitoires coronaux ("transients") déclenchés par les filaments éruptifs, ni des "post flare loops" qui se forment après les éruptions de filaments en double filet ("two ribbon flares"). De nombreux mécanismes d'activation sont possibles, et seules des observations performantes peuvent apporter des éléments de discrimination entre les diverses théories. Le DPSM de la Tour Solaire de Meudon est particulièrement bien adapté à l'étude des structures à évolution rapide comme les DB , car il permet d'obtenir toutes les 5s, avec une bonne résolution spatiale (1"), les profils de la raie Hα de tous les points (28 000) d'un champ à 2 dimensions (8' x 1'), d'où l'on déduit cartes d'intensité et de vitesse Doppler. Une étude statistique de l'évolution de la thermodynamique (profils et intensités) et de la dynamique du milieu est alors possible et orientée vers l'élaboration de nouveaux modèles, ou la confrontation aux théories existantes.

III - 2 - CONTRIBUTION À L'ÉTUDE DES INSTABILITÉS : DEUX MÉCANISMES DE DISPARITIONS BRUSQUES.

Communications 2 et 3

Ce travail a été entrepris dans la voie tracée par Mouradian et al (1980). Deux mécanismes de "disparitions brusques", dynamique et thermique, sont mis en évidence et quantifiés.

Communication 2 : processus thermique

Dans ce type de DB, les mouvements Hα sont faibles ($\leqslant$ 10 km s^{-1}). Nous avons mis l'accent sur la comparaison entre les profils observés et des profils théoriques calculés par un programme de transfert. Pour ce faire, nous avons utilisé une atmosphère plan parrallèle du type VAL-3C. Nous y avons introduit une couche froide statique (filament) dans la couronne. Les calculs effectués pour différentes températures de filament, ont suggéré un mécanisme de chauffage.

Mais des mouvements sont en réalité toujours présents. Pour mieux comprendre la relation qui existe entre le décalage Doppler observé et la vitesse réelle dans l'atmosphère, nous pensons développer cette étude dans le futur en couplant la dynamique et le transfert.

Communication 3 : processus dynamique

Dans ce type de DB, des accélérations de matière Hα (0 $\longrightarrow$ 100 km s^{-1}) ont été détectés dans des boucles de champ magnétique appartenant probablement à la structure du filament, à l'aide d'une méthode originale d'interprétation des profils de raie ("cloud model", Beckers, 1968). Nous montrons que des mécanismes de siphon stationnaire sont incapables d'expliquer de telles observations.

Depuis la présentation de cette communication, nos travaux d'interprétation ont considérablement avancé. Carlqvist (1979) avait suggéré que de telles accélérations pourraient être produites par la formation, improbable ici, de doubles couches électrostatiques au sommet des boucles. Steinolfson et al (1979), suivis par Shibata et al (1982) avaient montré qu'un "pulse" de pression au pied des boucles pouvait être une explication. Nous avons testé ce mécanisme et aussi étudié la réponse d'une boucle à un "twist" soudain d'un de ses pieds ; ces deux processus ont les mêmes effets dynamiques et nous ont paru inadéquats pour expliquer notre observation. Nous avons montré (article en préparation avec M.A. Raadu) que l'éjection de plasmoïdes de champ "force free" dont le comportement est identique à celui d'un dipôle, est possible si la boucle qui canalise le mouvement s'ouvre vers l'extérieur. Nous avons pu calculer cette ouverture de façon à simuler parfaitement la dynamique de notre observation, mais la stabilité du mouvement reste à analyser.

RESUME DES COMMUNICATIONS 2 ET 3 :
Poster présenté au colloque UAI n° 102 - Août 1982 - ZURICH
"Solar and stellar magnetic fields : origins and coronal effects"

MHD INSTABILITIES IN SOLAR FILAMENTS : HEATING AND DYNAMICAL PROCESSES AS TWO MECHANISMS OF "DISPARITIONS BRUSQUES" (DB) .

J.M. MALHERBE[X], G. SIMON[X], N. MEIN[X], P. MEIN[X], B. SCHMIEDER[X]
J.C. VIAL[XX]

[X]Observatoire de Meudon, DASOP, 92190 MEUDON , FRANCE
[XX]LPSP-CNRS, 91370 VERRIERES LE BUISSON , FRANCE

A B S T R A C T :

Disappearances of filaments have been observed in Hα at Meudon with the Multichannel Subtractive Double Pass (MSDP) spectrograph operating on the Solar Tower. The analysis of MSDP data evidences two different cases of DB likely related to heating or dynamical processes. In both cases, the DB are associated with flares .

- In the first case (June 22, and September 3, 1980), the flare occurs both sides of the filament; the disappearance begins a few minutes before the Hα impulsive phase and the filament reappears during the post flare phase. The velocity field is always weak (< 10 km/s). Upward motions appear near the flare sites and reach a maximum value a few minutes before the flare outburst. At the flare time, shears or velocity loops can be suggested, and downflows are dominant. During the preflare phase, the Hα line core becomes brigther than the mean chromospheric one. A line broadening occurs in several points. Theoretical profiles using a VAL-3C model with a cold filament show that the disappearance can be interpreted as an enhancement of density or, more likely, as a heating of the plasma prior to the flare.
- In the second case (June 22, 1981), the flare occurs 4 hours after the beginning of the DB, far from the filament, which does not reappear later. Thin threads (thickness < 3 ") with high and upward radial velocities ($\geqslant 50$ km/s) are observed. These motions correspond likely to the rise of material along magnetic loops . The dynamics inside such a magnetic loop is investigated : a high speed flow reaching 100 km/s, supersonic and probably super-alfvènic, strongly accelerated , is evidenced. Flux tube deformations , likely due to the centrifugal forces exerted by the flow on magnetic lines , are suggested. The DB seems to be relevant to mass motions inside the magnetic structure of the filament and thus is related to a dynamical process .

We finally suggest that, in order to discriminate between the various kinds of "Disparitions Brusques" , the measure of mass fluxes seems to be a good criterion .

COMMUNICATION 2

présentée oralement au 24ème congrès du COSPAR
O T T A W A - Mai 1982
Symposium S M Y (Solar Maximum Year)

HEATING OF PREFLARE FILAMENTS

J.M. MALHERBE, G. SIMON, N. MEIN, P. MEIN, B. SCHMIEDER
Observatoire de Meudon, DASOP, 92190 MEUDON, FRANCE
and
J.C. VIAL
LPSP (CNRS), B.P. 10, 91370 Verrières le Buisson, FRANCE

ABSTRACT

Disappearances of preflare filaments have been observed on June 22, 1980 (S 07, E 13) (flare at 13.04 U.T.) and September 3, 1980 (flare at 7.52 U.T.). The analysis of MSDP data (Meudon) leads to the following conclusions :

- Disappearances begin a few minutes before the Hα impulsive phase.
- The filaments can be seen again after the flares.
- Upward motions start around 10 mn before the maximum flare intensity ; during the flare, upward motions occur in several points, without disturbing significantly preexisting downflows.

Velocity maps suggest shears or velocity loops.

The filament disappearance seems to be due to a heating mechanism beginning before the flare maximum.

I - INTRODUCTION

During the flare-build up study observing program in 1980, we observed two times the disappearance of a filament in connection with a flare. In both cases, the filament appears again at the same place after the flare.

The observations presented here were obtained in the Hα line with the Multichannel Subtractive double pass Spectrograph (MSDP) operating at the solar tower in Meudon Observatory [1].

The filament on June 22, 1980 was located in active region 2517. It has been also observed at the Heliophysical Observatory of Debrecen (Hungary), at the Wise Observatory of Tel-Aviv (Israel) and in radiowavelengths at Nançay (France).

The flare begins ar 13h04 U.T. and extends along the whole filament, but activity was high several hours before the flare. In particular, we may note type III radiobursts connected with high velocities in the western part of the filament at 9h47 U.T. and 10h08 U.T.

II - STUDY OF THE INTENSITY OF Hα LINE

We have calculated intensity fluctuations at 0.3 Å from the center of Hα in a field of 1' x 8' for 15 times between 12h44m50s and 13h06m30s U.T. We have also observations before and after the flare (9h37m6s ; 13h49m37s U.T.)

These observations can be characterized by two kinds of evolution (Fig. 1) :

- a long term variation in the body of the filament (P1, P2)
- a drastic one in the flare sites (P3).

Figure 2 shows isophote contours of intensity fluctuations.

For each pattern, we have indicated the integral over the cell of the intensity above the mean value. We can notice that :

- the filament appears as an absorbing feature at 9h38, vanishes between 13h01 and 13h03 U.T. and seems brighter than the mean intensity at 13h06 U.T.

- the brightness of the facula A is enhanced during the sequence up to the flare time.

- three peaks of intensity occur during the flare in the field of view.

- the facula B vanishes during that time.

We have also studied profiles of Hα line in some points of the body of the filament versus time. The core of the line becomes brighter than the mean chromosphere line core a few minutes before the flare. Two cases are present (Fig. 3) :

- case (A) P2 the line width remains constant
- case (b) P1 the line width increases

As a comparison, the evolution of Hα profiles is also shown at flare site.

Theoretical profiles (Fig. 4) using the VAL-3C model [2] with a cold filament overlying the transition zone show an enhancement of brightness in the line core when the temperature or the density of the filament increases and a line broadening only when the density becomes greater.

The "disappearance" of the filament can be interpreted as :

- a heating of the plasma prior to the flare (case a and b)
- an enhancement of the density (case b).

III - STUDY OF THE VELOCITY FIELD

The most striking character of the field is that the velocities are generally very low (less than 9 km/s) and are located in a few patterns. Figure 5 shows isovelocities + 3 km/s and - 3 km/s. For each cell the integral and the maximum value of the velocity are indicated. We can notice that :

- ascending velocities appear near the flare site prior to the flare (cell C).

- velocities structures, appearing during the flare (D), suggest shears or velocity loops.

Note that the integral of the velocity over each cell can be regarded as a measure of the mass flux. The upward flux (C) is maximum 3 minutes before the flare beginning and 13 minutes before the flare maximum (time from Hα flare patrol Boulder, fig. 6).

The total flux in high velocity cells is negative, indicating that downflows are dominant during the flare.

The filament begins to reappear at 13h20 U.T., as seen on the Israel movie. The last MSDP picture of the sequence at 13.48 U.T. shows no velocity greater than 2 km/s.

IV - SECOND EXAMPLE OF A FILAMENT HEATING

We have also observed a short disappearance of a filament on September 3, 1980 in AR 2646 (Fig. 7). It shows similar characteristics :

- low velocity cells
- enhancement of the central intensity of Hα

Heating and cooling mechanism can explain the disappearance and reappearance of the structure. No large instability appears during the flare.

V - CONCLUSION

Disappearance of filaments on June 22 and September 3, 1980, are characterized by low velocities starting a few minutes before the flare outburst. During the post flare phase, filaments reappear, suggesting a disappearance by heating mechanisms. In other cases (for example June 22, 1981 [3]) very

high velocities are present during the disappearance, and the filament does not reappear later. These events are more likely related to dynamical processes. In order to discriminate between various kinds of "disparitions brusques", mass fluxes seem to be a good criterion.

REFERENCES

[1]. Mein, P., Solar Phys. 49, 283 (1977)

[2]. Vernazza, J.E., Avrett, E.H., Loeser, R., Astrophys. J. suppl. serie 45, 635.

[3]. Malherbe, J.M. et al - this volume

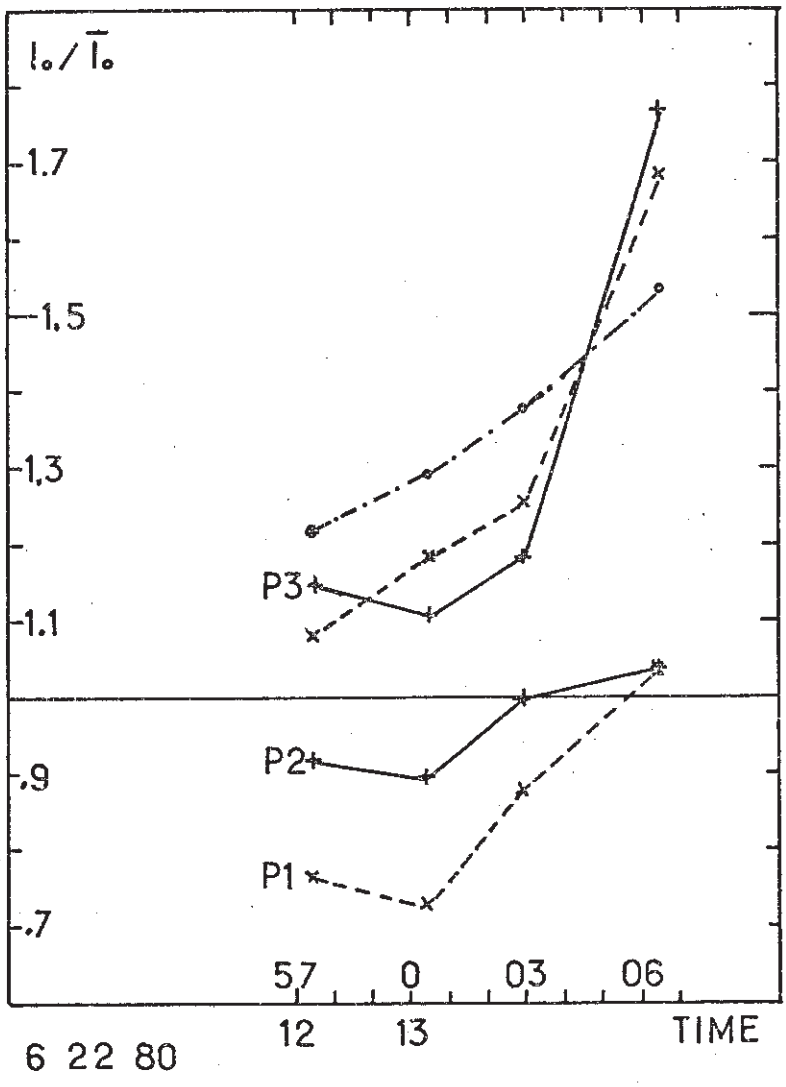

Fig. 1 Ratio of the central intensity of H_α line to the average central intensity, versus time for five points : P1 and P2 refer to the filament core, P3 to the flaring site, the last two points belong to the facula A (see Fig. 2).

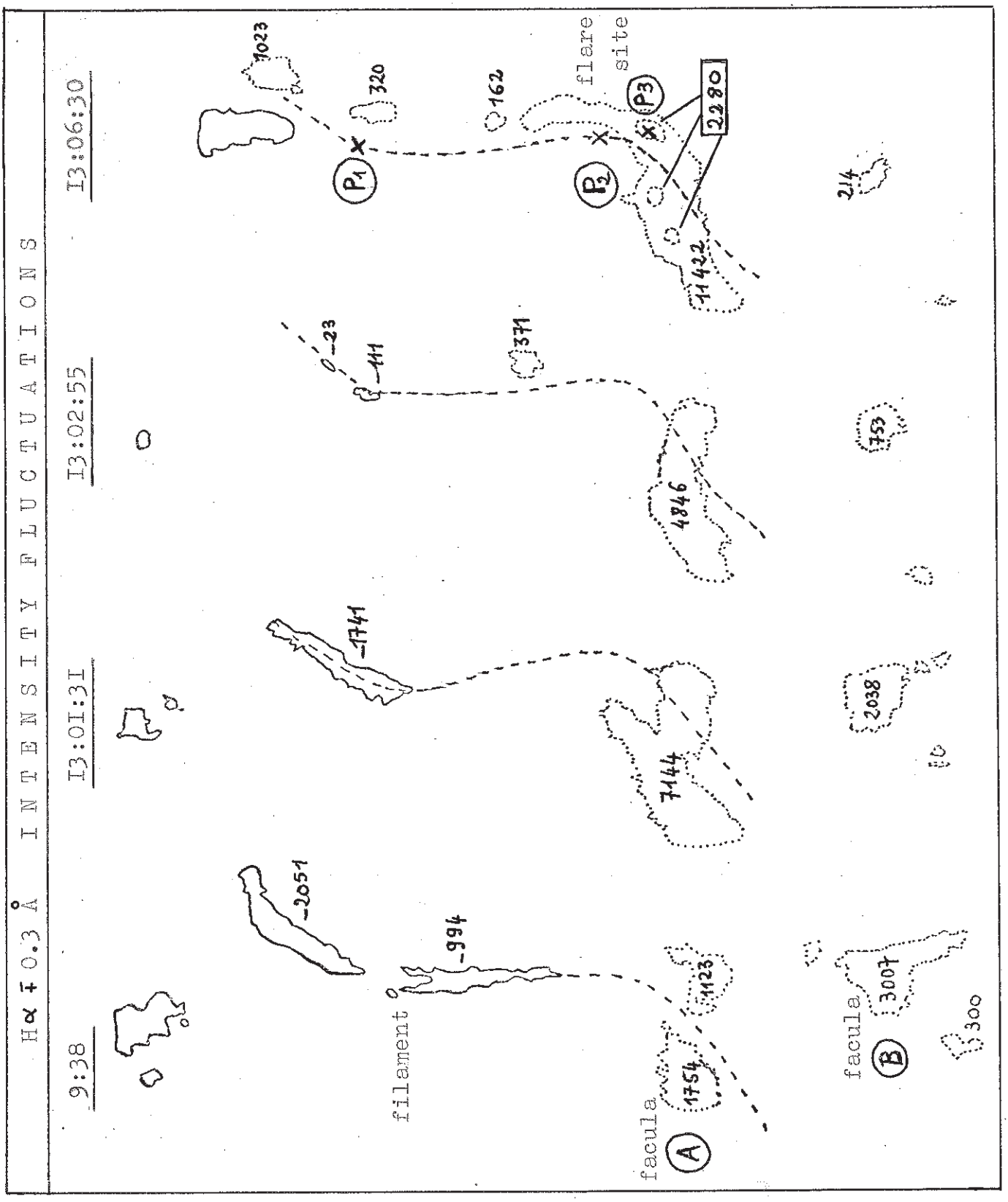

Fig. 2 Isophotes contours of intensity fluctuations

—— full line : absorbing feature (I less than 0.8 $\bar{I}$)

···· dotted line : bright feature (I greater than 1.2 $\bar{I}$ and 1.6 $\bar{I}$)

---- broken line : location of the filament.

We have indicated the value of the integral of the intensity over each cell in arbitrary unit.

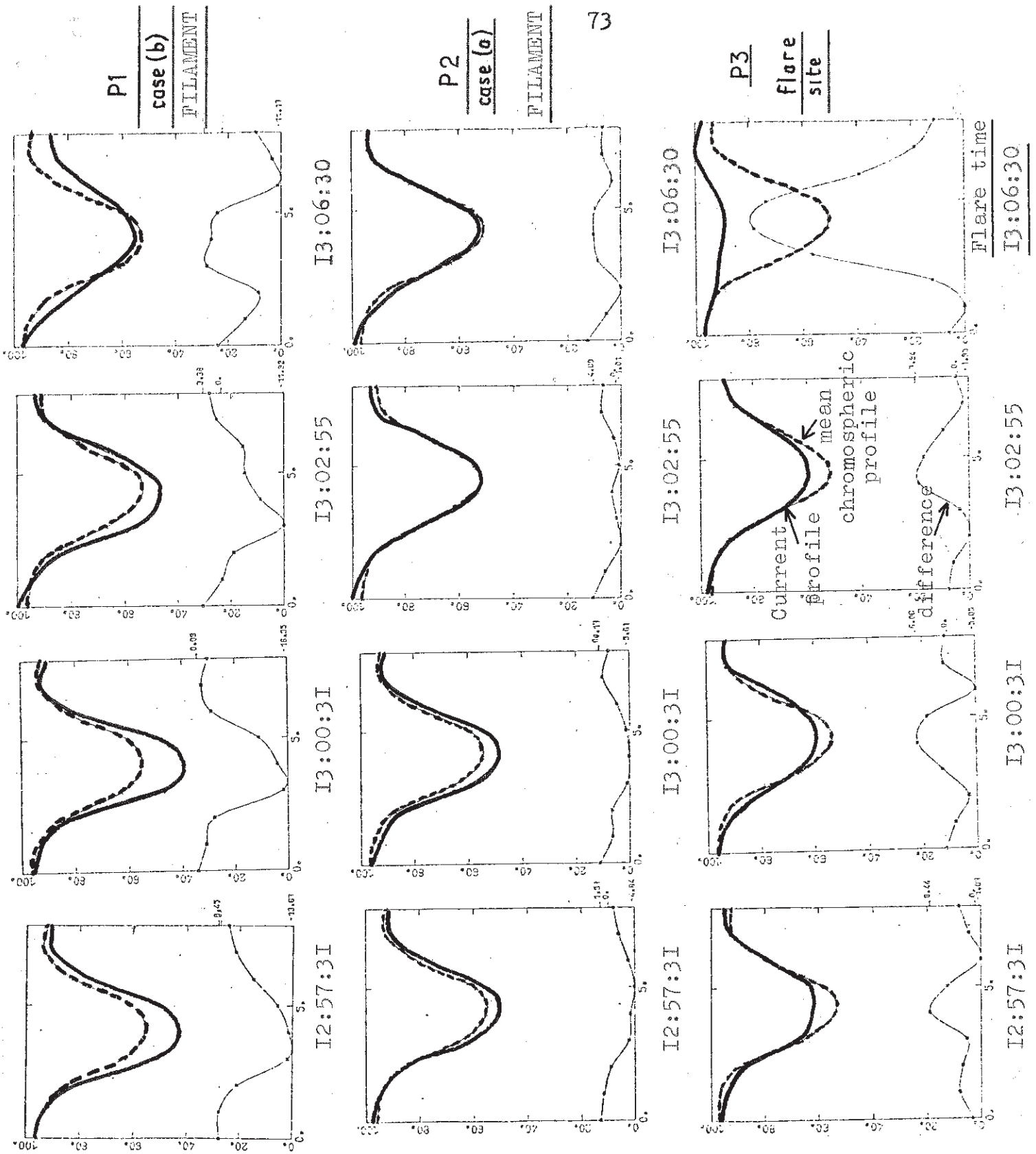

Fig. 3 Variation of the Hα profile for 2 points in the core of the filament (P1, P2) and for the flaring site (P3).

Time increases from left to right.

Broken lines show the average profile. Differences between each profile and the average values have also been plotted (arbitrary units).

Fig. 4 Theoretical profile of Hα in case of a filament lying above the chromosphere (height 3000 km - width 5000 km)

····· mean filament T_e = 8000 K, Ne

—— hot filament T_e = 10000 K, Ne

– – – dense filament N_e x 2.5 , Te = 8000 K.

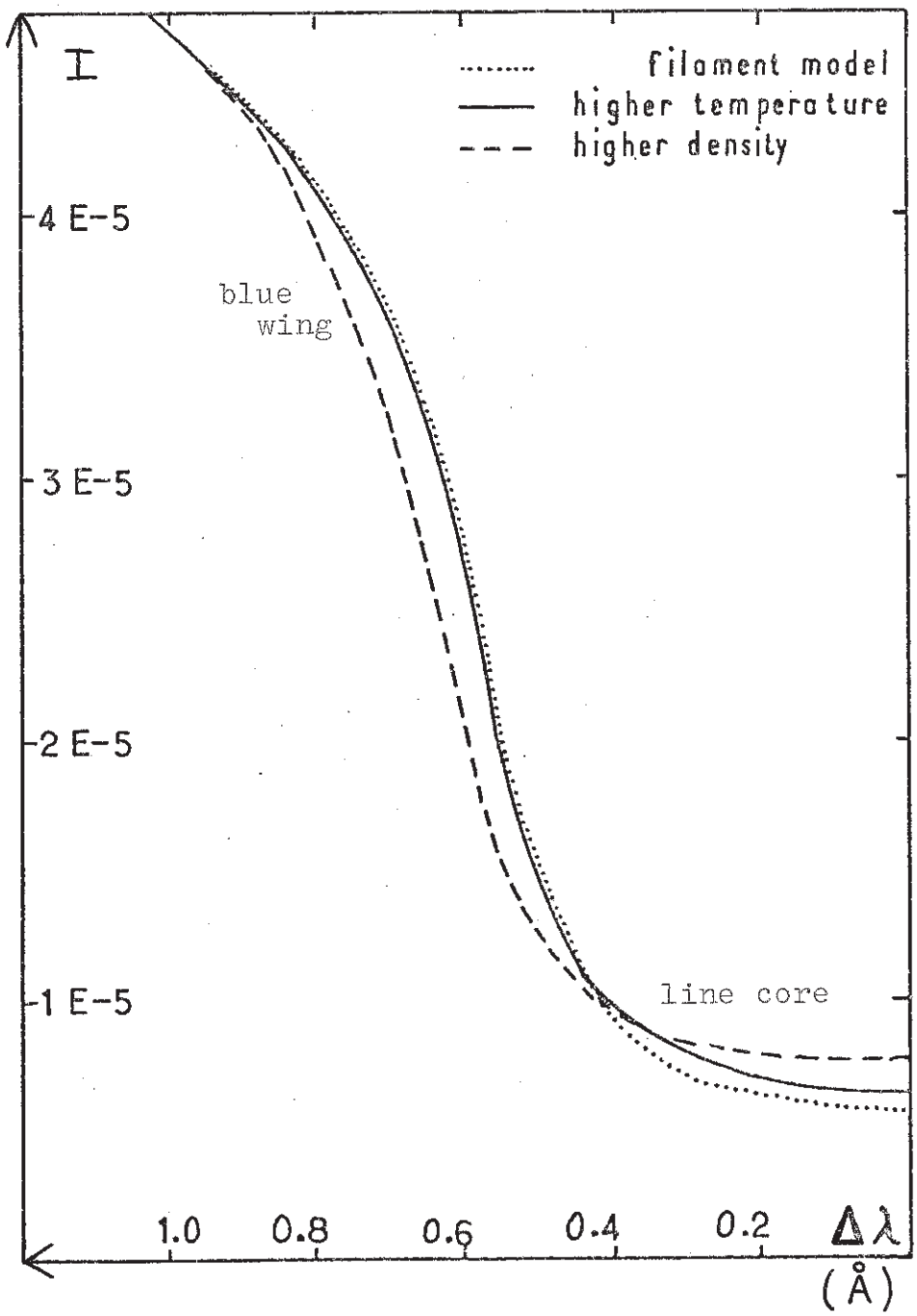

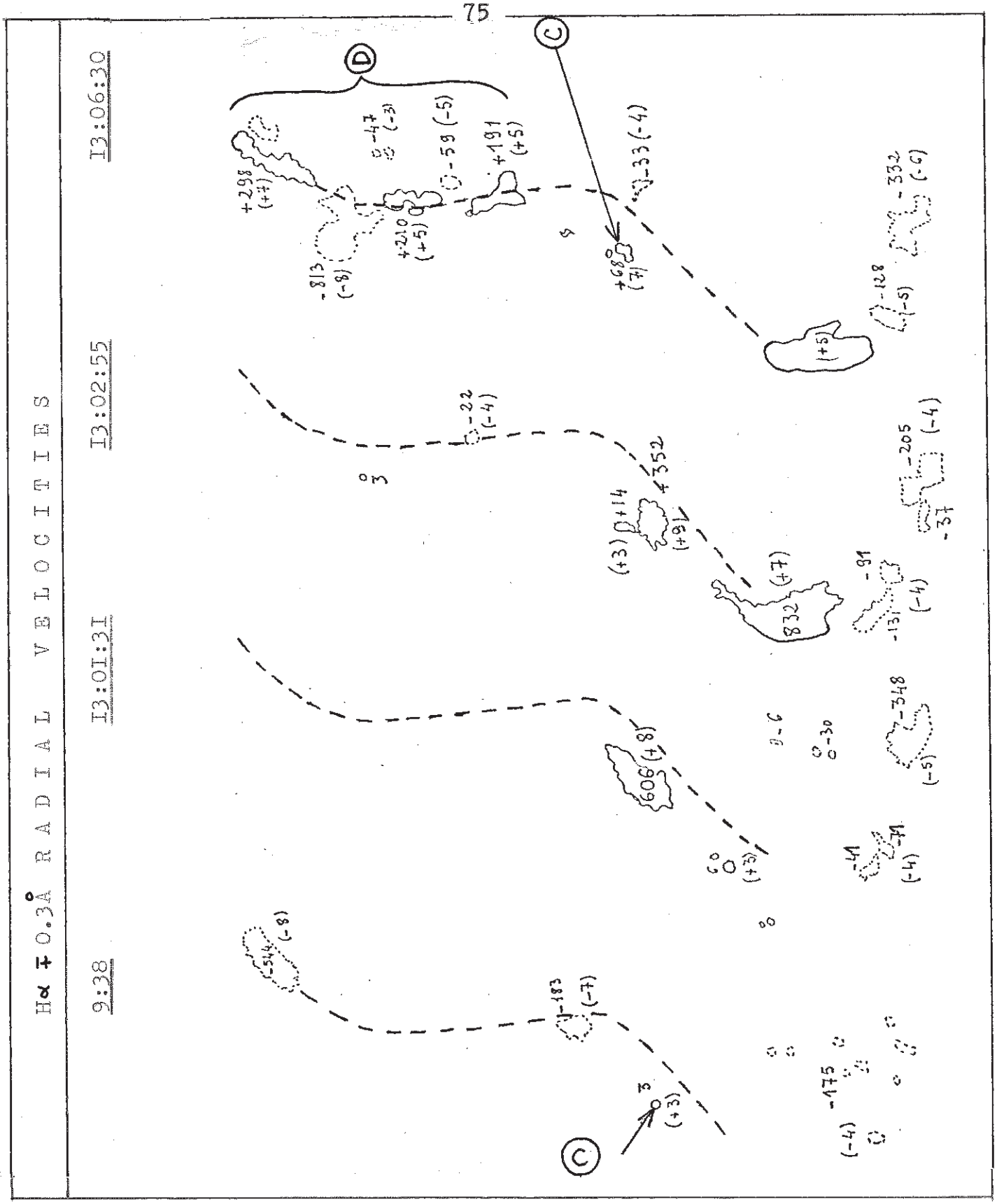

Fig. 5 Isovelocity contours

____ full line : upward velocity cells V > 3 km/s

.... dotted line : downward velocity cells V < - 3 km/s

---- broken line : location of the filament

We have indicated the value of the integral of the velocity in each cell in km x arc sec^2 x s^{-1}, and between brackets the maximum value of velocities in the cell in km/s.

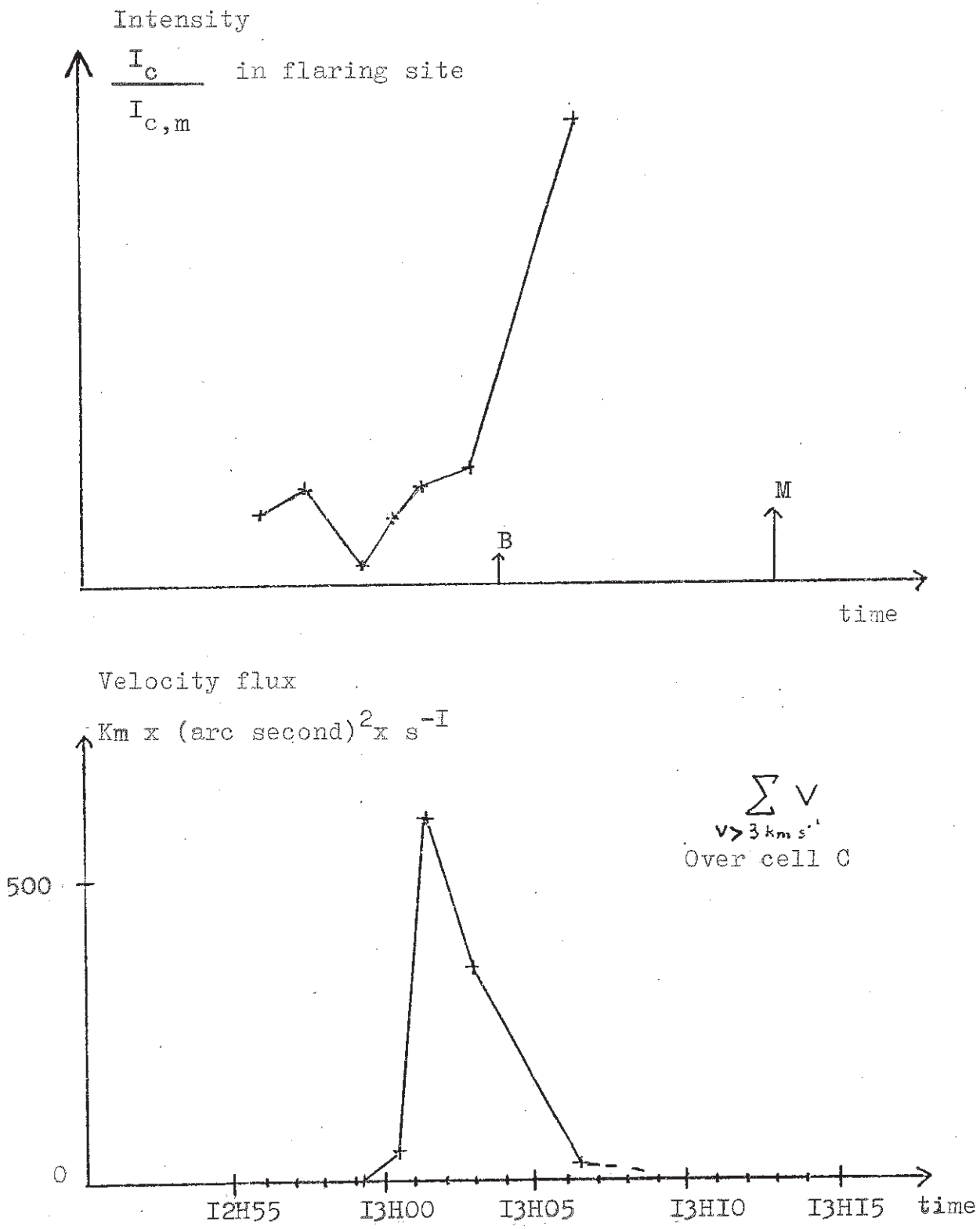

Fig. 6 Velocity "flux" versus time for the cell C.

In the upper part of the figure we have plotted the maximum intensity for the flare site. Arrow indicates the beginning (B) and the maximum (M) of the flare as indicated by Boulder.

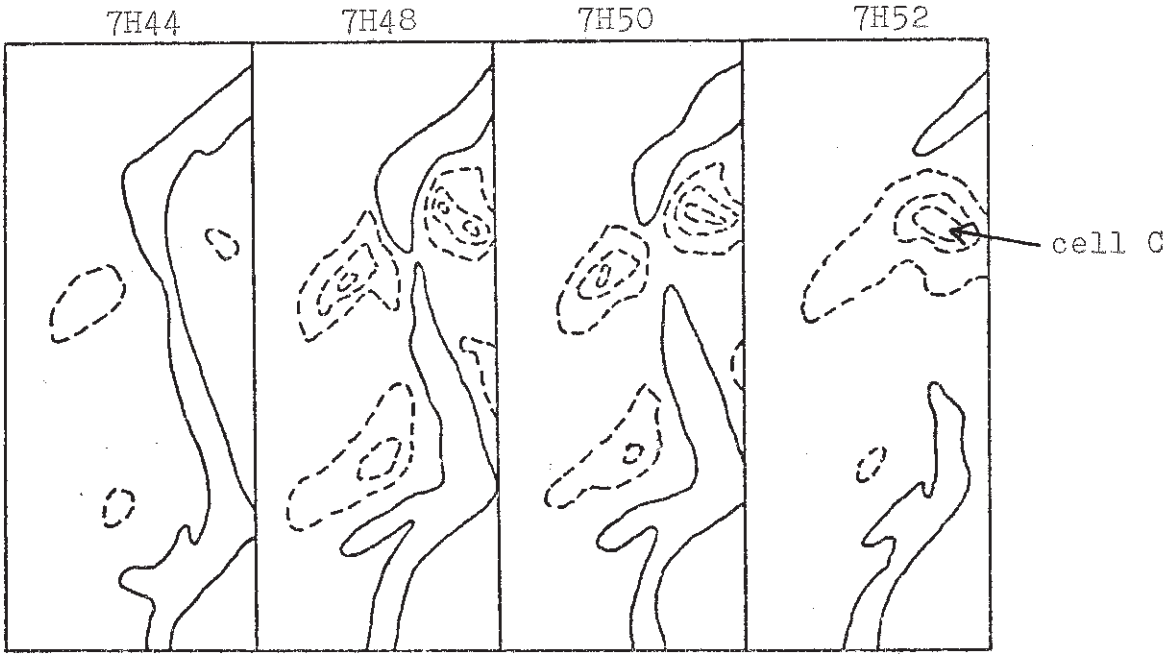

Hα $\mp$0.3 Å INTENSITY FLUCTUATIONS

——— dark regions

– – – bright regions

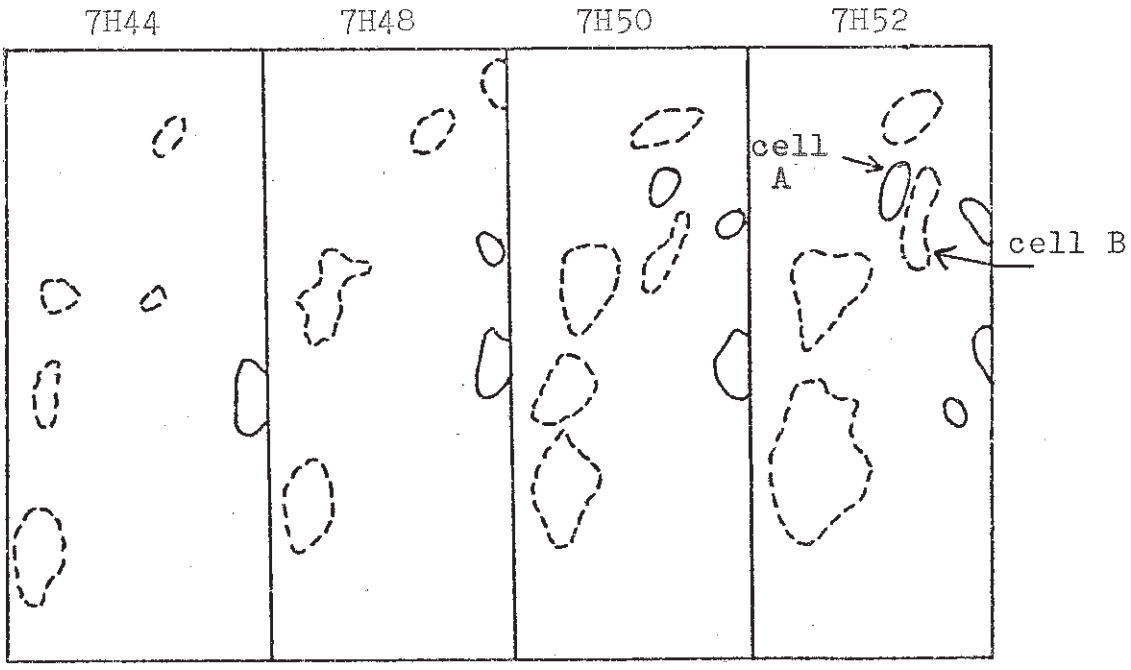

Hα $\mp$0.3 Å RADIAL VELOCITY FIELD

——— upward
– – – – downward
} motions (isocontours of $\mp$ 3 km/s)

fig. 7 : Disappearance of September 3, 1980.
Intensity and velocity contours show a similar behaviour as for June 22, 1980. A, B, and C point at the flare site.

COMMUNICATION 3

présentée oralement au 24ème congrès du COSPAR
O T T A W A - Mai 1982
Symposium S M Y (Solar Maximum Year)

MASS MOTIONS IN PREFLARE FILAMENTS

J.M. MALHERBE, P. MEIN, B. SCHMIEDER
Observatoire de Meudon, DASOP (LA326)
92190 MEUDON, FRANCE

ABSTRACT

The "disparition brusque" (DB) of a filament (N20, E35) has been observed above an active region with the Multichannel Subtractive Double Pass (MSDP) spectrograph operating on the Meudon Solar Tower, from 10h45 UT to 13h30 UT on June 22, 1981. A flare located South East of the filament occurs 4 hours after the beginning of the DB.

Velocity fields and intensity fluctuations are measured in the Hα line. The DB doesn't take place simultaneously in all parts of the filament : thin threads (thickness $< 3''$) with upward radial velocities reaching about 50km/s are successively observed inside the prominence from S to N regions. These motions correspond likely to the rise of material along magnetic loops closely related to the prominence structure. The dynamics inside such a magnetic loop is investigated : a high speed flow (supersonic, likely superalfvènic) strongly accelerated is evidenced and a deformation of the flux tube, probably due to the centrifugal forces exerted by the flow on the magnetic lines, is suggested.

These results are confronted to some theoretical works on dynamics inside magnetic loops, especially to siphon flow models. However, as in the case of the prominence support problem, better theoretical models are still needed.

I. MORPHOLOGICAL EVOLUTION OF THE ACTIVE REGION.

The observations were obtained on June 22, 1981 by :

- the Hα and K spectroheliograph
- the 3 wavelengths heliograph (Hα ∓ 0.75 Å) } operating at Meudon
- the MSDP spectrograph of the solar tower (Hα)
- the radioheliograph (169 MHz)
- the numerical multichannel radiospectrograph (152 to 468 MHz) } operating at Nançay

The location (N20, E35) of the studied filament was NW of the active region 3170 (N15, E45). This filament is a component (N) of a more extended one, which disconnected in two parts (N and S) on June 21. The N component disappears on June 22, between 10h45 and 13h30 UT, at first the western part, then the other one.

The S component disappears on June 23, and appears again on June 26. A flare, located in Active Region 3170 occurs on June 22, at 14h45 UT. The radio data show that type I storms and type III bursts occur in the S component of the filament during the DB of the N component.

II. MSDP OBSERVATIONS OF THE DB ON JUNE, 22.

Let us recall that the MSDP spectrograph allows to record a large solar area (2 dimensions of 8′ x 5′) with a good spatial resolution (1″) and temporal resolution (30s). The observations of the same region are simultaneously obtained in 9 wavelengths (9 channels) distant of 0.3 Å (spectral resolution 0.15 Å) in Hα , from which line profiles are computed. Intensity fluctuations and dopplershifts are derived from profiles by a code simulating a lambdameter technique and measured for a given line width $2\Delta\lambda$[1].

The figure 1 shows maps of intensity fluctuations and radial velocities in H$\alpha \pm$ 0.3 Å (line core) at 3 different times covering the DB of the N component of the prominence. During the disappearance, which begins in S regions, slow upward motions (lifetime $\geqslant$ 1h) are observed inside the filament ($\leqslant$ 6km/s), while slow downward motions (lifetime $\leqslant$ 5mn) occur at its edges. The assymetry in the wings of the profiles (more absorption in the blue wing than in the red wing) evidences thin threads (thickness $< 3''$) of high and upward radial velocities ($\geqslant$ 40km/s) . Such a structure is located on figure 1 at 11h55 UT.

III. DYNAMICS INSIDE A MAGNETIC LOOP DURING THE DB.

Thin threads of high velocities can be considered as motions along a magnetic loop in a plane parallel to the line of sight. These motions have been studied during 12 mn with a time step of 1 mn. Only one foot of the loop (upward motions), located at a filament bottom, is visible on MSDP observations ; the second one (downward motions) is visible on the 3λ heliograph observations ; simultaneously type III radio bursts are observed at the same location suggesting a large velocity loop with particle acceleration. This loop, parallel to the filament, seems to be closely related to its structure and support. Figure 2 shows an example of a line profile formed inside the loop derived by subtracting a mean profile from the observed profile. Maps of intensity ΔI and radial velocities VR have been computed from the line profiles of the loop and the results are summarized in figure 3 at three times (t_1, t_2, t_3). Two points of maximun absorption can be considered as fluid particles and followed in the plane of the solar disk by their motions along x direction (fig. 3).

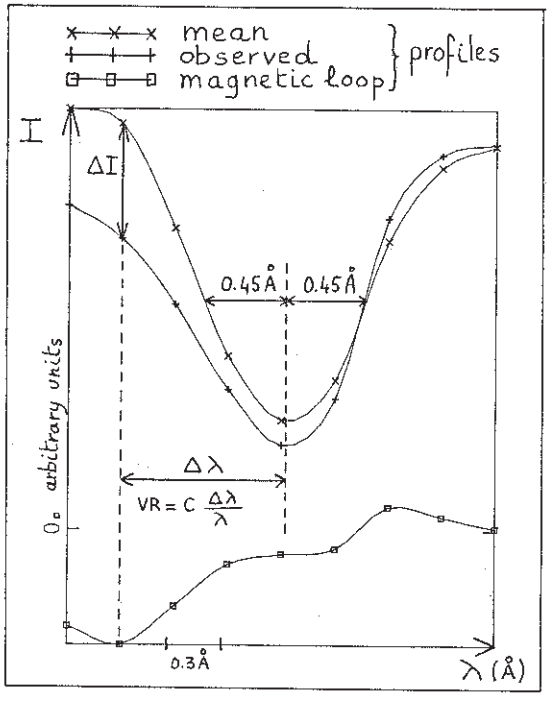

fig2. Hα line profiles

The knowledge of the velocity $\dot{x}$ and radial velocity VR of these 2 particles allow to calculate the velocity vector $\vec{V}$ = (VX,VZ) in the plane (XOZ) of the loop. This result has been plotted in figure 4 (A,B,C). Let us remark also the decreasing absorption of the filament (fig.3, right) at the location of the loop's foot versus time, which suggests a pumping of the filament material by the loop. The figure 4 (D) shows the trajectory of the two fluid particles. The top of the loop is higher than 25000 km ; velocities of 90 km/s (part.2) and 130 km/s (part.1) are reached, with strong acceleration for part.1 (at maximum 1.2 $g_\odot$). The temporal evolution of the radial velocity maximum (value and location along the loop) (fig.4 A,B) suggests that the flow is not stationary and that the loop is slowly growing, likely under the action of centrifugal forces exerted on the tube by the supersonic (and probably superalfvènic) flow. So the trajectory of part.2 could be the third one (fig.4).

IV. DISCUSSION.

Mass motions inside the several observed loops (as the previously studied one) seem to explain the DB. Mass flow inside such loops (lifetime $\sim$1h) appears to be sufficient to empty the filament. Many mechanisms can be investigated in order to explain the high speed flow in the loop and the deformation of the tube. Let us examine at first the siphon flow models :

- steady siphon flow mechanisms :

hydrodynamics inside a steady flux tube leads to $\frac{Po}{P} = \exp\left(\frac{Z}{H}\right) \exp\left(\frac{M^2-Mo^2}{2}\right)$

with :
- Po/P ratio of gas pressure between the bottom and the top of the loop
- Z/H " of the loop's height and the scale height $\approx$100
- M/Mo respectively Mach numbers at the top and bottom of the loop.

The first term is relevant to the prominence support, the second one to the flow. With our data $Po/P \sim 10^{43} \times 10^{21}$. We conclude that, although such steady models have been successfully used by NOCI [2] (in the corona with Z/H$\approx$1), or by Meyer and Schmidt [3]

(in the photosphere for Evershed effect with $Z/H \approx 1$), we must consider a time dependant mechanism, even if neglecting the problem of loop support. Pinch or torsionnal effects at the foot of the loop may account for the flow inside the tube.

- Flux tube deformations

We suggest a deformation due to centrifugal forces. Although the self consistent reaction of the loop magnetic field to the dynamics is an unsolved question, Anzer's method [4] to calculate the forces on a loop may be used, but the model of Kopp and Pneumann [5] is expected to be the most fruitful to estimate the flow with given geometry and evolution of magnetic lines.

Finally our results set two problems : the prominence structure as a cold Hα loop system and the acceleration process of material inside such loops.

References

1. Mein P., Solar Physics, 54, 45 (1977)
2. Noci G., Solar Physics, 69, 63 (1981)
3. Meyer F. and Schmidt H.U., Mitt. Astron. Ges., 25, 194 (1968)
4. Anzer U., Solar Physics, 57, 111 (1978)
5. Kopp R. and Pneumann G., Solar Physics, 50, 85 (1976)

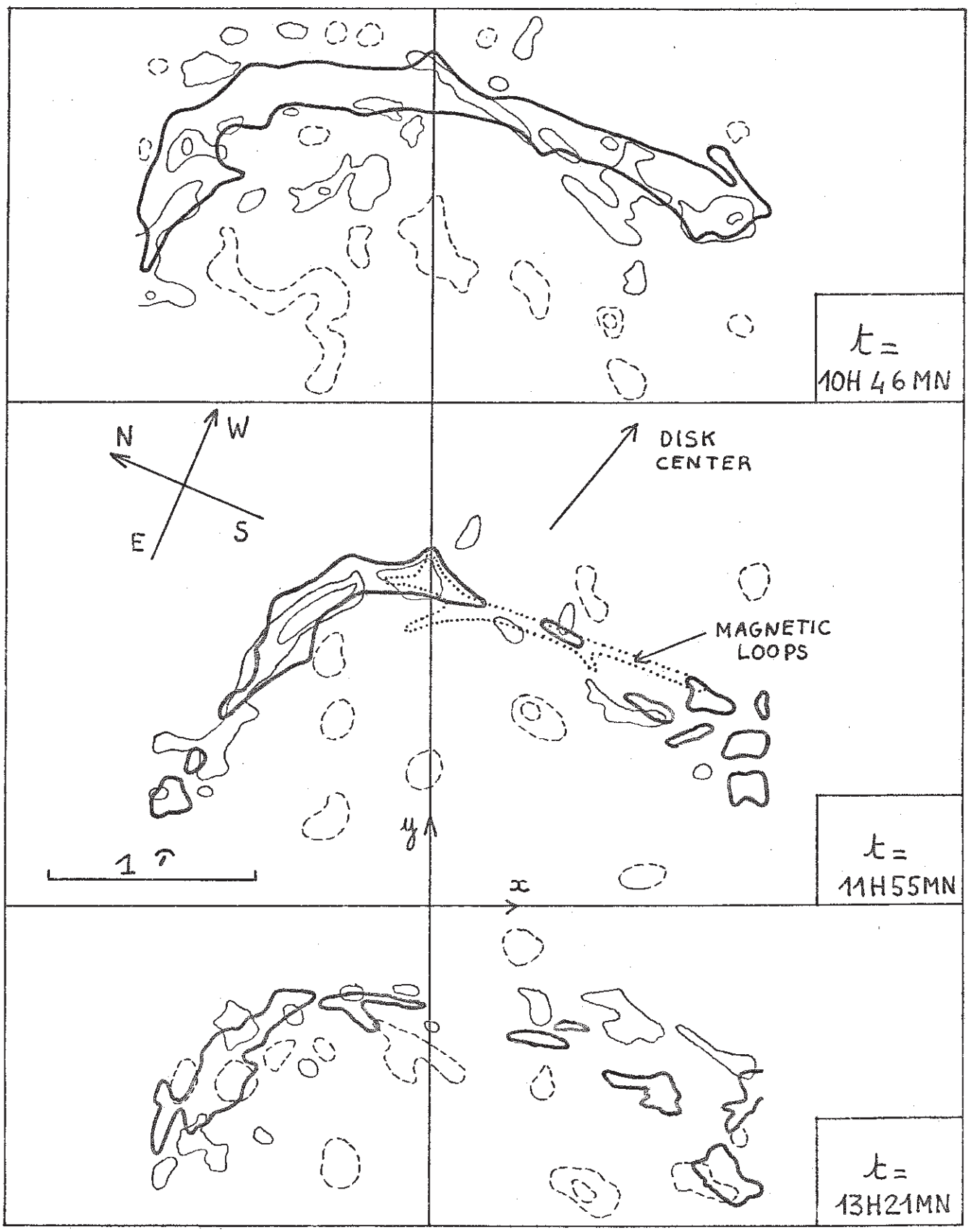

FIGURE 1 : MSDP OBSERVATIONS OF THE DB IN Hα ∓ 0.3 Å

Intensity fluctuations

upward
downward
} radial velocities (levels 1 and 4 km/s)

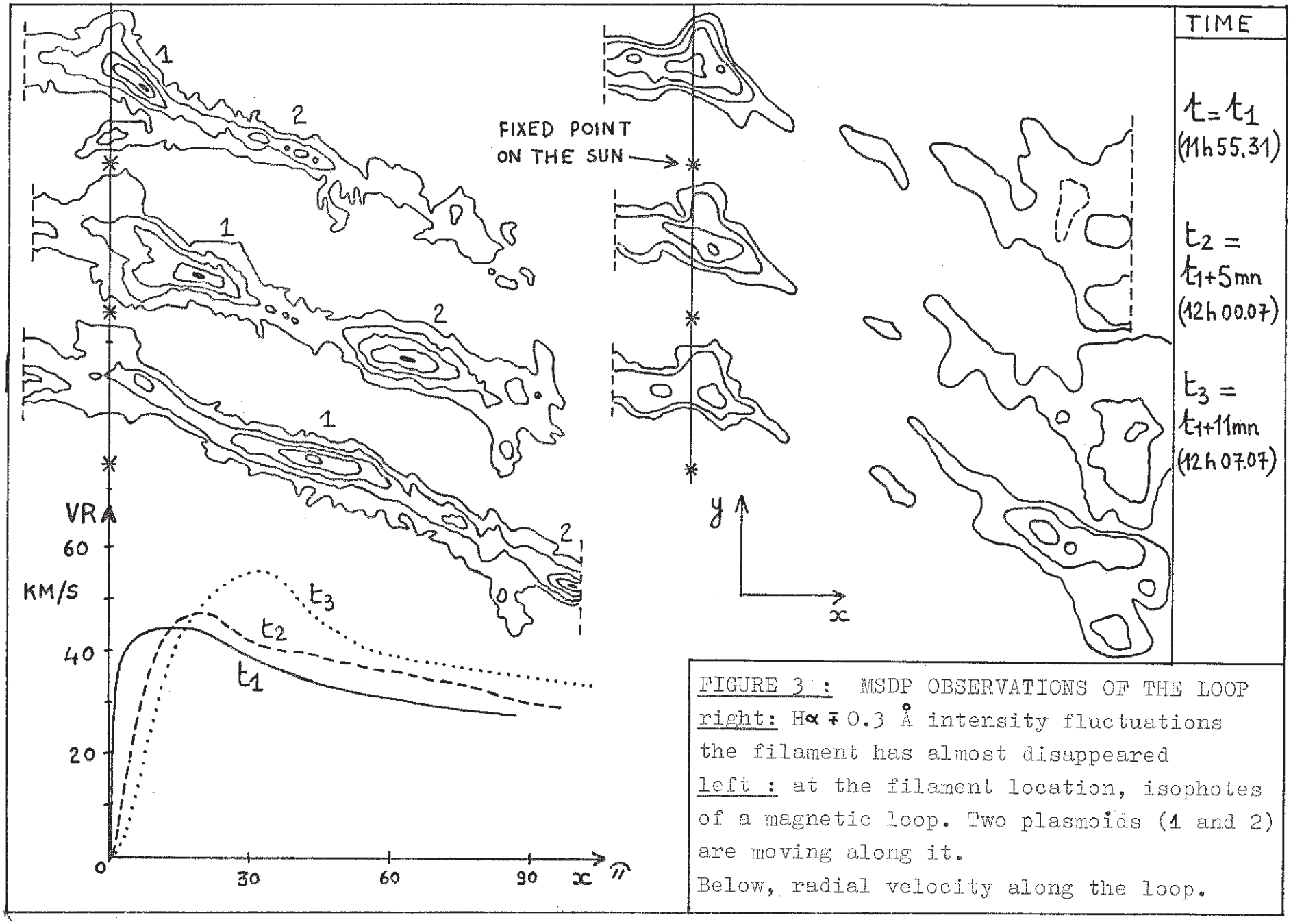

FIGURE 3 : MSDP OBSERVATIONS OF THE LOOP
right: Hα ∓ 0.3 Å intensity fluctuations
the filament has almost disappeared
left : at the filament location, isophotes of a magnetic loop. Two plasmoids (1 and 2) are moving along it.
Below, radial velocity along the loop.

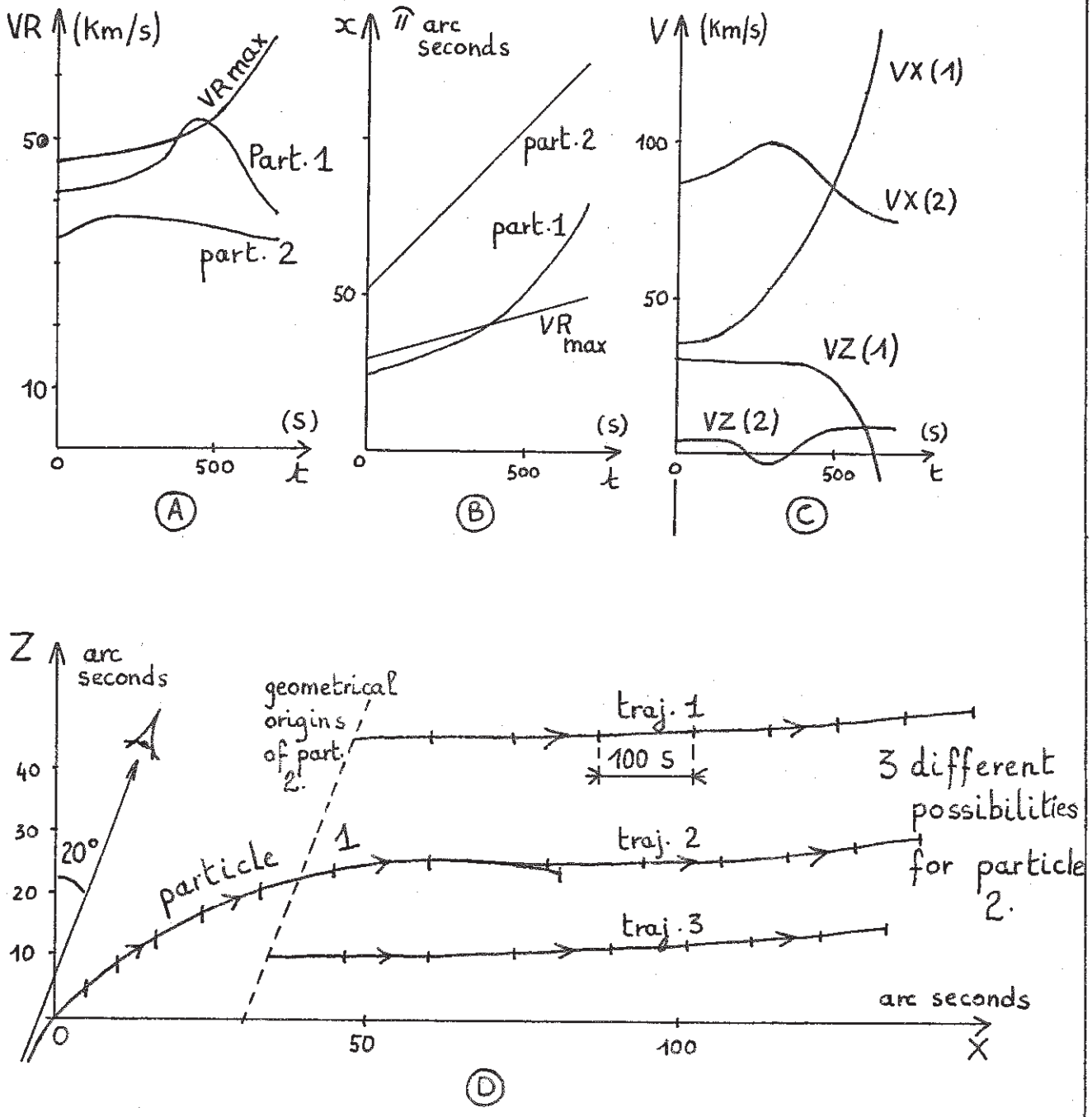

FIGURE 4 : A - radial velocities
B - horizontal motions } versus time
C - velocity vector
D - trajectories of particles 1 and 2 -
3 solutions are possible for particle 2

IV - UN MODELE DYNAMIQUE DE PROTUBERANCE QUIESCENTE

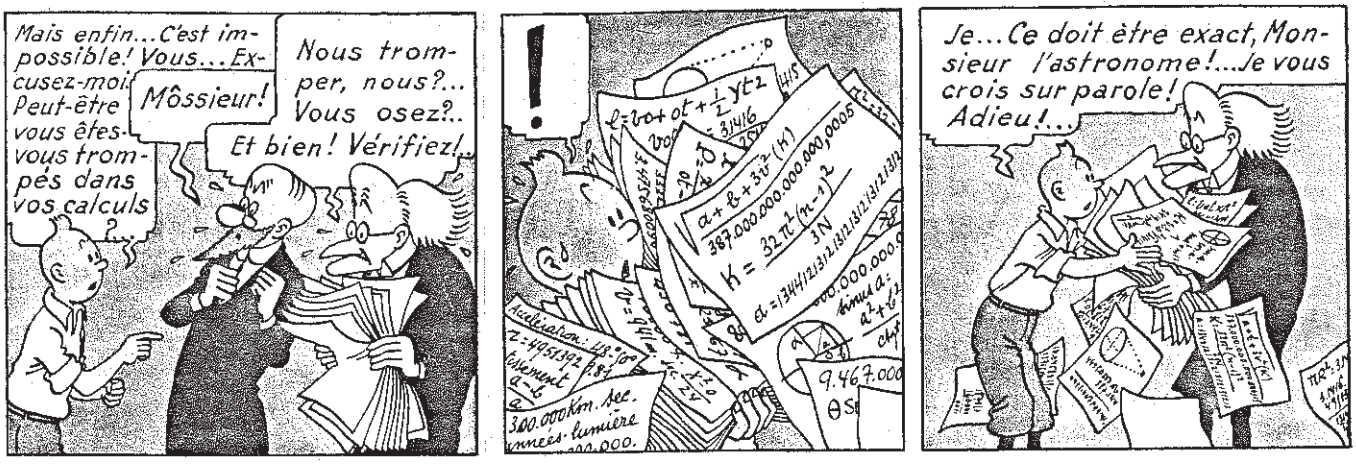

IV - 1 - ETAT DES MODELES : FORMATION DES FILAMENTS, MAGNÉTOSTATIQUE ET DYNAMIQUE.

Nous allons étudier brièvement les mécanismes physiques qui régissent la formation et la condensation des protubérances, puis nous décrirons brièvement l'état des modèles magnétostatiques et dynamiques. Le lecteur intéressé par davantage de détails peut se référer à Priest (1982, Chapitre 11).

a - formation des protubérances

Le mécanisme mis en jeu est l'instabilité thermique dont nous allons donner le principe (Field, 1965) : considérons une boucle coronale de longueur 2L, pression P_c, densité ρ_c et température T_c. Son équilibre thermique est gouverné par

$$h - \rho\, Q(T) = 0 \qquad (1)$$

où $T = T_c$, $\rho = \rho_c$, h étant le taux de chauffage par ondes et Q(T) le taux de refroidissement radiatif (optiquement mince) par unité de masse. La fonction Q(T) (Figure IV-1) a été calculée par de nombreux auteurs et moyennée par Hildner (1974). Elle est maximale pour des températures du type zone de transition.

The cooling function $Q(T) = \chi T^{\alpha}$ according to Hildner (1974)

Temperature range (K)	χ (MKS)	α
$T < 1.5\ 10^4$	$1.759\ 10^{-13}$	7.4
$1.5\ 10^4 < T < 8\ 10^4$	$4.290\ 10^{10}$	1.8
$8\ 10^4 < T < 3\ 10^5$	$2.860\ 10^{19}$	0
$3\ 10^5 < T < 8\ 10^5$	$1.409\ 10^{33}$	- 2.5
$T > 8\ 10^5$	$1.970\ 10^{24}$	- 1.0

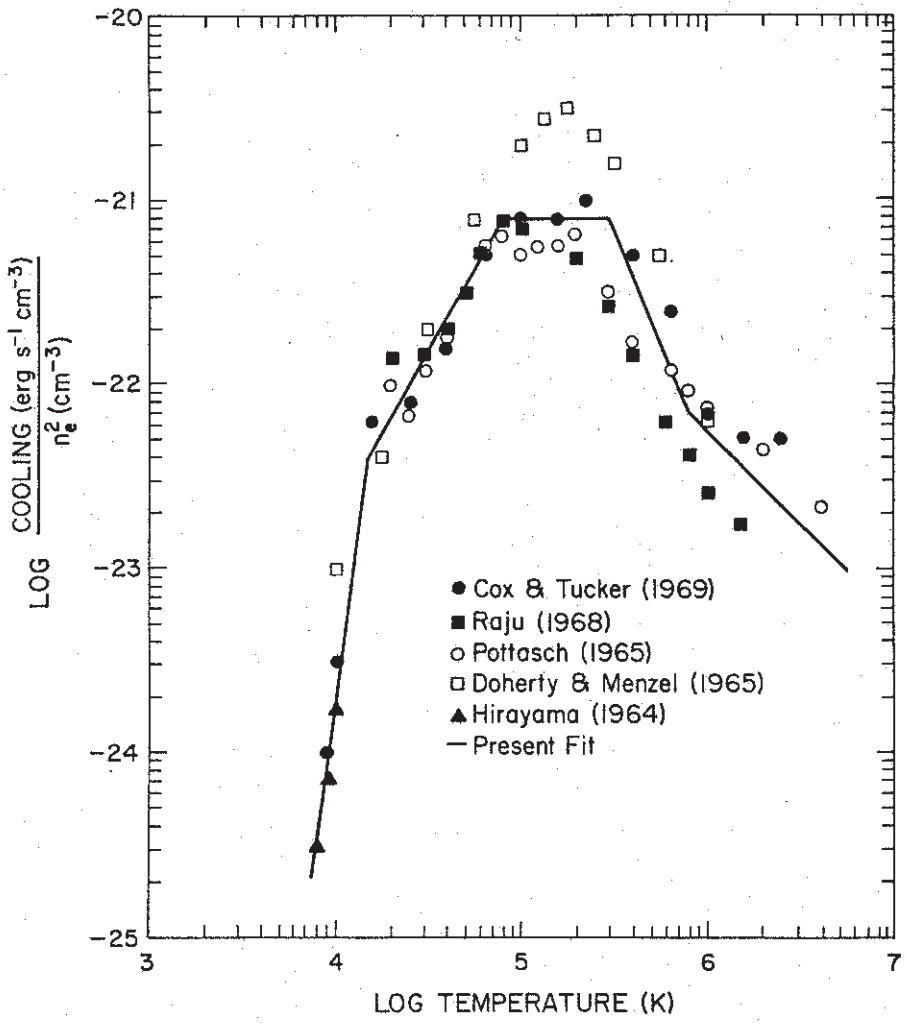

FIGURE IV-1

L'équation (1) possède une propriété intéressante due à la forme de Q(T) : à pression constante ($p \propto T^{-1}$), pour un taux de chauffage donné , deux équilibres sont possibles : coronal chaud (10^6K) et ténu (10^{-15}g cm^{-3}), et protubérantiel froid (8200 K) et dense ($1.22\ 10^{-13}$g cm^{-3}). La transition entre ces deux états peut s'effectuer grâce à l'instabilité thermique : la perturbation de l'équilibre (1) à pression constante, négligeant la conduction, aboutit à :

$$\frac{\gamma}{\gamma-1}\ \frac{\partial(T/T_c)}{\partial(t/\tau_R)} = 1 - \frac{T_c}{T}\ \frac{Q(T)}{Q(T_c)}$$

et montre que l'équilibre chaud est instable. L'instabilité se produit sur une échelle de temps radiative $\tau_R = p_c / \rho_c^2 Q(T_c)$ de l'ordre de 10^4s.

Si l'on incorpore l'effet de la conduction thermique parallèle aux lignes de champ, la perturbation de l'équilibre (1) s'écrit

$$\rho C_p \, \partial T/\partial t = h\rho - \rho^2 Q(T) + \frac{\partial}{\partial s}\left(k_{//} \frac{\partial T}{\partial s}\right) \qquad (2)$$

où C_p est la chaleur massique, $k_{//} = ko\ T^{5/2}$ ($ko = 3\ 10^{-11}$) la conductivité, et s l'abscisse curviligne le long de la boucle. Approximant le terme conductif par $ko\ T^{5/2}\ \frac{Tc-T}{L^2}$ où L est la demi longueur de la boucle, (2) devient, à pression constante :

$$\frac{\gamma}{\gamma-1} \frac{\partial(T/T_c)}{\partial(t/\tau_R)} = 1 - \frac{T_c}{T} \frac{Q(T)}{Q(T_c)} + \frac{\tau_R}{\tau_c}\left(\frac{T}{T_c}\right)^{7/2}\left(1 - \frac{T}{T_c}\right) \qquad (3)$$

$\tau_c = \dfrac{P_c\ L^2}{k_o\ T_c^{7/2}}$ représentant l'échelle de temps conductive.

L'étude de (3) montre que l'instabilité thermique ne peut survenir que si

$$\tau_R / \tau_c < 2 \qquad (4)$$

c'est à dire si l'apport conductif de chaleur est suffisamment faible devant les pertes radiatives.

(4) peut s'écrire aussi $L > Lm = 7.2\ 10^3\ T_c^{13/4} / P_c$ km, où T_c est mesurée en unité de 10^6K et P_c en dynes cm^{-2}. Typiquement, 2 Lm est de l'ordre de $50\ 10^3$ km. La <u>conduction</u> a donc un effet <u>stabilisant</u> qui l'emporte sur l'effet déstabilisant des pertes radiatives, tant que la longueur de la boucle 2L reste en deça d'une valeur critique 2Lm.

Ces principes de base ont été perfectionnés par plusieurs auteurs et adaptés à diverses géométries (boucles, arcades, "current sheets").
Hood et Priest (1979), inspirés par les observations de Foukal (1975), ont étudié la formation des filaments dans une boucle coronale et montrèrent l'existence d'une longueur L, d'une pression P ou d'un taux de chauffage h critiques à partir desquels tout état d'équilibre chaud n'existe plus (Fig. IV-2).

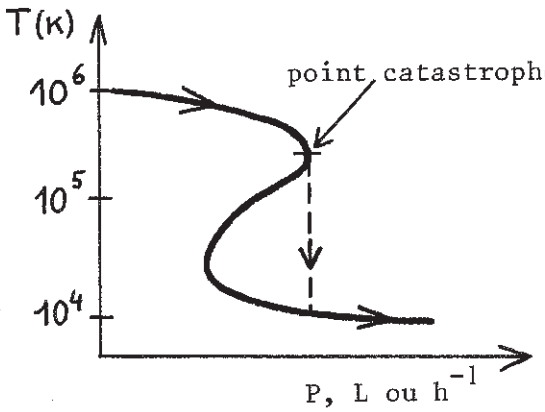

FIGURE IV-2
Température au sommet de la boucle

La conduction est alors incapable de stabiliser le processus de condensation. Cette analyse, valable pour les filaments en boucle, peut s'appliquer aussi aux protubérances quiescentes, si celles-ci sont formées d'une collection d'arches magnétiques (Figure II-4).

La même instabilité peut survenir lorsqu'on tord ("twist" d'angle φ) la boucle par l'intermédiaire de ses pieds au delà d'une valeur critique (mouvements photosphériques). Des résultats semblables à ceux de Hood et Priest (1979) ont été obtenus par Priest et Smith (1979) pour la formation des protubérances quiescentes dans une arcade coronale. L est alors la largeur de l'arcade et φ son "shear". Ils expliquèrent aussi l'extension en altitude des filaments : sous les protubérances, la longueur des lignes de force est assez courte pour que la conduction l'emporte sur les pertes radiatives et empêche l'instabilité thermique ; au-dessus, la densité, décroissant avec l'altitude, limite le rayonnement et le même mécanisme se produit. Kuperus et Tandberg-Hanssen (1967) proposèrent la condensation dans un "current sheet" formé dans une région active après une phase éruptive (Fig. IV-3).

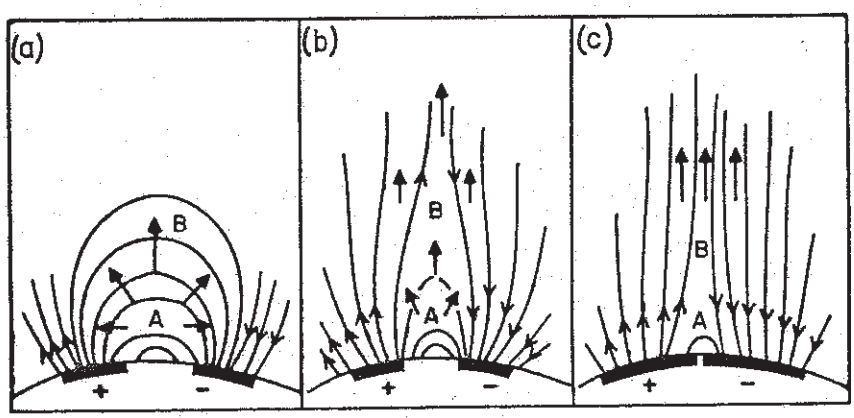

The possible magnetic field configuration over an active region during (a) the early phase of activity, (b) the main phase of activity, (c) the post-active phase.

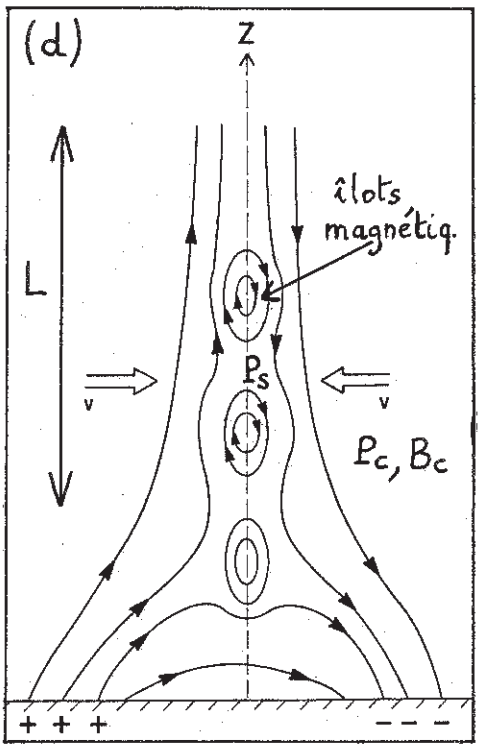

(d) filamentation du plasma par "tearing modes" et formation de la protubérance par coalescence des îlots.

FIGURE IV-3

Dans la phase (d), la condensation du plasma déclenchée par la surpression du "current sheet" ($P_s = P_c + B_c^2/2\mu$) pourrait être limitée par l'augmentation de pression magnétique qu'elle engendre (gel des lignes de force), si celle-ci n'était pas annihilée par reconnections dûes à l'instabilité de "tearing mode", qui crée, par la même occasion, une composante de champ horizontale pouvant supporter la matière froide. La phase de reconnections peut engendrer la création d'ilôts magnétiques, favorisant la condensation du plasma (isolation de l'apport extérieur d'énergie), dont la coalescence, dans la partie non linéaire de l'instabilité, peut aboutir à la formation d'un filament d'épaisseur typique quelques $\Lambda/100$ (Λ = échelle de hauteur coronale, 100 = facteur de compression). L'ancrage ("line-tying") des lignes de force dans la photosphère, s'opposant au mouvement transverse à l'axe z, pourrait aussi s'opposer à la condensation : Raadu et Kuperus (1973) ont montré que, malgré cet effet, l'instabilité thermique restait possible. L'ancrage peut même favoriser la condensation lorsque les protubérances se forment au dessus de la ligne d'inversion entre deux cellules de polarités opposées qui sont animées de mouvements d'approche (ceinture polaire). Une très forte compression du plasma, perpendiculairement à l'axe z, est alors obtenue. Smith et Priest (1977), incorporant l'effet de la conduction, ont montré que l'instabilité thermique survenait au delà d'une hauteur L critique du "current sheet". Enfin, Chiuderi et Van Hoven (1979) étudièrent la formation des filaments dans un champ force free possèdant du "shear" (cisaillement des lignes de force).

Disons pour conclure que les modèles de "current sheets" (du type Kuperus-Raadu) présentent plusieurs avantages théoriques sur les autres : les processus de formation, de filamentation ("tearing modes") et d'activation par instabilités MHD y sont plus clairs.

b - Magnétostatique

Les divers types de support magnétique proposés jusqu'ici ont déjà été présentés (Figure II-5).

Modèles à structure non hélicoïdale

Milne et al (1979) ont généralisé le modèle isotherme de Kippenhahn et Schlüter (1957) en y adjoignant une équation d'énergie, de façon plus élaborée que Lerche et Low (1977), et mirent en évidence deux résultats nouveaux : l'existence de valeurs maximales φ_m et β_m du shear φ et du β du plasma. Lorsque $\varphi > \varphi_m$, l'équilibre thermique est rompu et le filament peut devenir éruptif (section III-1-b). Lorsque $\beta > \beta_m$ l'équilibre magnétostatique est rompu et le plasma s'effondre en formant des "pieds". Le modèle de Kippenhahn et Schlüter a été aussi modifié par Low (1982) pour tenir compte de la structure fine. La stabilité a été examinée par Anzer (1969), malheureusement sans tenir compte de l'effet stabilisant dû à l'ancrage des lignes de force dans la photosphère, puis par Zweibel (1982). En particulier, un des deux critères trouvés par Anzer a reçu une vérification expérimentale (section II-1-b). Lerche et Low (1981) ont aussi proposé une méthode très générale pour l'étude de la stabilité. Le modèle de Kuperus et Raadu (1973), plus complexe, a été revu par Raadu (1979) et développé par nous mêmes (section IV-2). Aucune analyse de stabilité n'a été tentée.

Modèles à structure hélicoïdale

Anzer et Tandberg-Hanssen (1970), suivis par Lerche et Low (1980) ont étudié le support par un champ magnétique horizontal. Low (1981) a modifié ce modèle pour l'adapter au support des filaments par une configuration plus réaliste, une arcade coronale, aboutissant à une structure type Kippenhahn et Schlüter en hélice (figure II-5), déjà suggérée par Malville (voir revue d'Anzer, 1979).

Enfin, Kuperus et Raadu (1974), puis Van Tend et Kuperus (1978) ont modellisé le support dans un "current sheet" en utilisant l'image électrique du filament sous la photosphère.

Reconstitution du support à partir d'observations du champ magnétique.

Anzer (1972), utilisant la théorie des fonctions complexes a pu reconstituer un champ potentiel à partir de conditions aux limites fournies par des observations centre-bord, à l'extérieur d'une protubérance très simplifiée. Sa méthode pourrait être généralisée et constituer un outil puissant pour la détermination du support magnétique (en projet).

c - dynamique

La construction de modèles dynamiques est en général plus complexe que la simple étude de la magnétostatique. En effet, les aspects dynamiques sont liés indissolublement aux problèmes de support magnétique, qu'il faut de nouveau étudier, et de thermodynamique, par l'intermédiaire des processus de condensation et de refroidissement du plasma alimentant la protubérance.

C'est pourquoi très peu de travaux ont été entrepris dans cette direction pour rendre compte des observations (section II-1-c). Dans la plupart des cas, pour des raisons de simplicité, un seul des aspects (dynamique ou thermique) a été traité correctement. De plus, les modèles actuels sont tous des mécanismes de siphon, le mouvement s'effectuant parallèlement aux lignes de force d'une configuration magnétique statique. L'intéraction dynamique/support a donc toujours été négligée. En outre, la possibilité d'évolution du support magnétique, dûe à des causes externes (mouvements photosphériques) et son influence sur la dynamique n'ont jamais été considérées. Le modèle que nous présentons (section IV-2) tente de combler ces lacunes.

Le mécanisme de siphon proposé par Pickel'ner (1971) a été perfectionné par Ribes et Unno (1980), négligeant les aspects thermiques, et Uchida (1980), dont le traitement est plus complet. Priest et Smith (1979) étudièrent la condensation du plasma et ne donnèrent qu'une solution dynamique aux ordres de grandeur. Mais actuellement, aucun modèle n'est capable d'expliquer les mouvements stationnaires ascendants dans les filaments.

d - Conclusion

Alors que la formation et la magnétostatique des filaments, en temps que structure globale, semblent à peu près comprises, il n'en est pas de même de la dynamique : ce problème est beaucoup plus complexe car ne peut être traité sans la thermodynamique (condensation du plasma alimentant la structure) et est étroitement lié à l'évolution du support magnétique, considéré jusqu'ici comme statique.

Le modèle que nous proposons ici (section IV-2) tente de résoudre, pour la première fois, ces différents problèmes, tout en rendant compte des observations les plus récentes de vitesses et de champ magnétique.

La structure fine des filaments, ainsi que les "pieds" qui les relient à la chromosphère sont encore des problèmes ouverts. Pour faire progresser davantage la théorie, des observations plus précises seront nécessaires, tant pour élaborer des modèles nouveaux que pour effectuer une discrimination entre modèles existants (de beaux programmes pour THEMIS et le DPSM des canaries en perspective !).

IV - 2 - UN MODÈLE DYNAMIQUE DE PROTUBÉRANCE QUIESCENTE À RECONNECTIONS MAGNÉTIQUES STATIONNAIRES.

Article 3 (accepté) et article 4 (soumis).

Nous présentons d'abord une méthode, appliquée pour la première fois aux protubérances, de construction de supports magnétostatiques, à champ potentiel, basée sur l'utilisation des fonctions holomorphes. L'évolution de ces modèles sous l'influence de mouvements photosphériques est étudiée. Dans le cas d'un support du type Kippenhahn-Schlüter, un flux de matière photosphérique divergent en dessous des filaments pourrait expliquer les mouvements ascendants observés à travers leur corps (Martres et al, 1981 ; Malherbe et al, section II-2). Par contre, un flux photosphérique convergent serait nécessaire dans le cas de protubérances de type Kuperus-Raadu.

Or, ces dernières semblent, selon les récentes observations magnétiques de Leroy (1982) être plus fréquentes sur le Soleil que celle du type Kippenhahn-Schlüter. De plus, les filaments paraissent souvent se former au dessus des lignes d'inversion séparant des cellules géantes de polarités magnétiques opposées animées de mouvements d'approche (c'est le cas des protubérances des ceintures polaires notamment). Ces deux derniers résultats alliés à nos observations de champ de vitesse, sont donc un argument assez fort en faveur d'un modèle de type Kuperus-Raadu, dans lequel la dynamique est induite par l'évolution des lignes de force dont les pieds sont mûs par des mouvements photosphériques convergents.

Nous proposons, suivant Raadu (1979), un modèle à reconnections magnétiques stationnaires, dans lequel le chaud plasma coronal se condense et se refroidit en pénétrant dans le filament au dessus du point de reconnection. La matière dense et froide est alors transportée à l'intérieur de la protubérance par les mouvements ascendants du champ magnétique. Sa dynamique est étudiée dans l'article 3. Les processus de condensation et de refroidissement stationnaires, ainsi que la dynamique du plasma coronal alimentant la protubérance sont étudiés dans l'article 4.

A R T I C L E 3

CURRENT SHEET MODELS FOR SOLAR PROMINENCES

I- MAGNETOHYDROSTATICS OF SUPPORT AND EVOLUTION THROUGH QUASI-STATIC MODELS .

J.M. MALHERBE* AND E.R. PRIEST**

* Observatoire de Meudon, DASOP (LA 326)
92190 MEUDON - FRANCE
** University of St Andrews,
Department of applied Mathematics,
St ANDREWS KY 16 9SS - SCOTLAND

Accepted by : Astronomy & Astrophysics
The Main Journal
sous presse pour I983

Abstract

Several 2D current sheet models for solar prominences, supported against gravity by potential magnetic configurations, are presented. Simple magnetostatic solutions, both of Kuperus-Raadu type (KR) and of Kippenhaln-Schlüter type (KS), which have the advantage of being analytical, are built with the help of complex functions and discussed.

The evolution, induced by photospheric motions, of such magnetic structures, through series of equilibria, is studied.

We suggest that, in the case of KS models, slow (< 100 m s^{-1}) diverging photospheric flows below prominences could explain the upward motions reported by Malherbe et al (1983) in disk filaments ; while, in the case of KR models, slow converging flows could explain them. To account for such motions and magnetic field observations by Leroy et al (1982a) we propose, in Raadu's spirit (1979), a quasistatic reconnection model, in which new material entering the prominence condenses and is brought up through it by the moving magnetic field. The resulting dynamics is studied in a simple magnetic geometry of KR type. A fast input of coronal material, already suggested by Malherbe et al (1983), is predicted above the reconnection point, but it is strongly dependent on the details of the condensation process.

I - INTRODUCTION

Filaments are thin condensed sheets of chromospheric-like material ($T = 10^4 K, n_e = 10^{11}$ cm^{-3}). They are suspended against gravity in the low corona by magnetic lines of force rooted in the photosphere, and lie above an inversion line of magnetic polarity. Their typical dimensions are : 60 to 600 Mm long (1 Mm = 10^6 m), 10 to 100 Mm high and 2 to 15 Mm thick. Basic properties can be found in Tandberg-Hanssen (1974), Jensen et al (1979) and Engvold (1982).

The geometry of magnetic lines is controversial : basic magnetostatic theories were proposed by Kippenhaln and schlüter (1957) and Kuperus and Raadu (1973), with quite different properties : in a KS prominence, the magnetic polarity is the same as in the underlying photosphere ; in a KR prominence, the polarity is opposite and a neutral point (B = 0) is present in the magnetic structure between the photosphere and the filament. The KS model was generalized by Milne et al (1979), to take into account energy balance, and modified by Low (1982) to explain fine structures reported by Dunn (1960). It was also modified by Anzer and Tandberg-Hanssen (1970), Lerche and Low (1980) and Low (1981) to produce helical structures, often observed in eruptive prominences, and suggested in quiescent ones by Malville (see Anzer's review, 1979).

The most recent observations of magnetic fields in quiescent prominences are due to Leroy et al (1982 a). From an analysis of the linear polarization of D_3 and Hβ lines using Hanlé effect, Leroy confirms that :

- the average field strength lies arround 8G.
- the field strength increases with height with a vertical gradient of about 0.5 G/10 Mm, in agreement with Zeeman measurements (1G/10 Mm) by Rust (1967).
- the average angle between the horizontal component of the magnetic field and the prominence long axis lies around 25°, in agreement with Tandberg-Hanssen and Anzer (1970).

New important results are due to Leroy (1982 a, b) :
- the magnetic vector is nearly horizontal inside prominences.
- The prominence support seems to be of KR type in 2/3 of observed cases, and of KS type in only 1/3 of cases.
- the field component along the polarity inversion line has a cyclic reversal.

Synoptic maps reveal also that prominences often appear above the inversion line between approaching giant (a few 100 Mm) cells of opposite polarity (Leroy, 1982c). For instance, this occurs commonly at the beginning of a new cycle, when new magnetic regions of low latitude push up against old ones near the poles to form the polar crowns.

The most extensive results concerning Hα velocity fields in disk filaments are due to Mein (1977), Martres et al (1981) and Malherbe et al (1981, 1983). From centre to limb observations of a filament, Malherbe et al (1983) derived a 3D-velocity field and concluded that :
- slow upward and vertical motions (0.5 km s^{-1}) occur through prominences (see also Lites, 1976).
- a fast input of material (5km s^{-1}) occurs at both edges of prominences.
- the angle between the horizontal component of the velocity vector and the filament axis lies around 20°, in agreement with magnetic field measurements.

The modelling of both velocity and magnetic field observations is the topic of this paper. Dynamical models of filaments have already been proposed by Pickel'ner (1971), Uchida (1980), Ribes and Unno (1980) (siphon mechanisms) and also by Priest and Smith (1979) (thermal non equilibrium onset at the top of coronal arcades). We want to suggest here, following Raadu (1979), that a steady-state reconnection model for current sheet prominences agrees with the observations of both Leroy et al (1982a) and Malherbe et al (1983).

The formation of prominences in current sheets has several theoretical advantages. A high compression perpendicular to the magnetic field is possible, and the prominence is

well isolated from the corona against heat conduction (Raadu and Kuperus, 1973). As the plasma condenses, dragging the magnetic field with it, the build-up of magnetic pressure, which would inhibit condensation may be relieved by the onset of tearing mode instability. This instability annihilates the field, and the reconnection may produce closed field lines supporting the plasma (see Priest, 1982, chapter 11) and filamentation (Kuperus and Tandberg-Hanssen, 1967) reported by Dunn (1960). The tearing mode instability may also trigger a "disparition brusque" or a flare (see Priest for a review, 1981). The formation of prominences in current sheets by thermal instability was investigated by Raadu and Kuperus (1973) (including line tying), Smith and Priest (1977), Chiuderi and Van Hoven (1979) and Somov and Syrovatsky (1980).

We present first in section II some basic properties of simple complex functions used in the following sections to represent a current sheet in a potential magnetic field. We show in section III that 2D magnetic configurations of KS type or KR type can easily be described by holomorphic functions of the complex variable $\zeta = x + iy$.

We study the magnetostatics of such models. Then we investigate in section IV their evolution, through series of equilibria, due to photospheric flows (diverging or converging), which are expected to move the line-tied foot points of magnetic lines. We show (section V) that velocity and magnetic observations may well be explained by a stationary reconnection model of KR type. The dynamics is examined in details, but the energetics, outside the scope of this paper, will be presented in the next one.

II - BASIC EQUATIONS AND COMPLEX FUNCTIONS

II-1. Magnetic support for 2D current-sheet prmominences.

We consider prominences as vertical thin sheets of dense material (figure 1) supported by magnetic fields in

the low corona. For a steady state ($\partial/\partial t = 0$) the equation of momentum gives

$$\rho(\bar{V}.\bar{\nabla})\,\bar{V} = -\bar{\nabla}P + \bar{j}\wedge\bar{B} + \rho\,\bar{g}$$

with $\bar{j} = (\bar{\nabla}\wedge\bar{B})/\mu$

where ρ is the density, P the gas pressure, $\bar{B}$ the magnetic field, $\bar{V}$ the velocity, $\bar{j}$ the current density, μ the magnetic permeability and $\bar{g}$ the gravity.
Outside the current sheet, in the corona, this equation reduces to :

$$\bar{j}\wedge\bar{B} = \bar{0}$$

when

$$V \ll Cs \quad , \quad V \ll Va \tag{1}$$

Cs and Va being the sound and Alfven speeds and

$$\beta = P_{kin} / P_{magn} \ll 1 . \tag{2}$$

In the corona ($T_c = 10^6$ K, $n_c = 10^9$ cm^{-3}), with $B_c \geq 6$G, we find $\beta \leq 0.1$, so condition (2) is verified. Observations by Tsubaki* of velocities around prominences in coronal lines, and also by Lites (1976) in transition zone lines showed that $V_c \leq 20$ km s^{-1}. So, with Cs = 166 km s^{-1} and Va = 415 km s^{-1} ($B_c = 6$G), condition (1) also holds.
Thus, a potential field

$$\bar{j} = (\bar{\nabla}\wedge\bar{B})/\mu = \bar{0} \tag{3}$$

may be used to represent magnetic configurations supporting current sheet prominences.
Using the coordinate system of Figure 1, we take $\partial/\partial z = 0$ (symmetry of translation),

$$\bar{B} = \mathrm{curl}\,(\Psi(x,y)\,\bar{e}_z) + B_z\,\bar{e}_z \tag{4}$$

*(1975)

and Bz = constant value.
The field lines are given by $\Psi(x, y)$ = const in the (x, y) plan. Equation (3) leads to

$$\Delta \Psi = 0 \qquad (5)$$

Then, $\Psi(x, y)$ is the real part of a holomorphic function $A(\zeta)$ of the complex variable $\zeta = x + iy$.
We define now

$$B = By + i\,Bx$$

as the complex magnetic field in (x, y) plan.
From relation (4), we find

$$B = B(\zeta) = -\frac{\partial A}{\partial \zeta}$$

So a 2-D potential field may be represented by :

$$\begin{cases} By + i\,Bx = B(\zeta) & \text{with } \zeta = x + iy \\ Bz = \text{const} \end{cases}$$

The fild lines are defined by $\mathbb{R}e\left(\int B(\zeta)\, d\zeta\right)$ = const
and orthogonal lines by $\mathbb{I}m\left(\int B(\zeta)\, d\zeta\right)$ = const
in the complex plan (x, y), where $\mathbb{R}e$ is the real part and $\mathbb{I}m$ the imaginary part.
Two different methods at least are available to determine $B(\zeta)$:

(a) - Anzer (1972) solves numerically equation(5) for KS prominences using a Keldych-Sédov integral (see Lavrentiev and Chabat, 1972, chapter III, p. 311), with simplified boundary conditions obtained from magnetic observations. His solution can be extended to include more accurate boundary conditions and adapted to produce KR configurations, which will be the subject of another paper.

(b) - Here we prefer to seek particular solutions $B(\zeta)$, that have the advantage of being analytical, in the spirit of Green (1965), Syrovatsky (1976) and also Priest and Raadu (1975), Tur and Priest (1976), who used such a technique for simulating preflare current sheets.

II-2. Two basic holomorphic functions to represent current sheets.

Two basic holomorphic functions will be used here to build more sophiticated potential fields supporting current sheet prominences; these are :

$$B_A(\zeta) = B_o \sqrt{p^2+\zeta^2}\,/\,\zeta$$

for an infinite current sheet in y-direction and

$$B_B(\zeta) = B_o \sqrt{(p^2+\zeta^2)(q^2+\zeta^2)}\,/\,\zeta$$

for a finite current sheet in y-direction, where B_o, p, q are real positive constants.
The field lines associated with these functions are displayed in Figure 2a (for $B_A(\zeta)$) and 2b (for $B_B(\zeta)$). The current sheet is represented by the double determination of the square roots : the magnetic field is vertical and has opposite directions on both sides of the sheet. The circular field lines above the polarity inversion line are represented close to the origin by the function $1/\zeta$. Magnetic configurations corresponding to $B_A(\zeta)$ are favourable for the condensation of prominences in current sheets (see Kuperus and Tandberg-Hansen, 1967 ; Raadu and Kuperus, 1973 ; Smith and Priest, 1977). But inside the sheet, the magnetic field, given by $B_A(\zeta)$ or $B_B(\zeta)$, is vertical and cannot support any material : we therefore need to add to it a horizontal component Bx (see section III).

II-3. The supporting force for dense material in the prominence sheet.

The supporting force is the y-component of the Lorentz force $\bar{f} = \bar{j}_p \wedge \bar{B}$, $\bar{j}_p$ being the current density in the sheet.

Since $\bar{j}_p = (\bar{\nabla} \wedge \bar{B})/\mu = \left(\partial B_z/\partial y\,,\ -\partial B_z/\partial x,\ \partial B_y/\partial x - \partial B_x/\partial y\right)/\mu$

we find $f_y = \dfrac{B_x}{\mu}\dfrac{\partial B_y}{\partial x} - \dfrac{\partial}{\partial y}\left(\dfrac{B_x^2 + B_z^2}{2\mu}\right)$ (per unit volume)

Also $\overline{B}_p(y) = (B_x(0,y), 0, B_z)$ is the magnetic field inside the sheet (fig. 1), and its strength is $B_p(y) = \left(B_x(0,y)^2 + B_z^2\right)^{1/2}$.

Integrating over an arbitrary small prominence width W, the Lorentz force per unit surface is

$$F_y(y) = \int_{-w/2}^{w/2} f_y(x,y)\,dx \approx 2\,\frac{B_x(0,y)}{\mu}\,B_y(0^+,y) - \nabla_y\left(\frac{B_p^2}{2\mu}\right) w \qquad (6)$$

where By(0^+, y) is the vertical field component at the right edge of the sheet. Dense material can be supported if this force balances gravity, so that :

$$F_y(y) = \rho(y)\, g\, w$$

Introducing the angle φ between the magnetic vector $\overline{B}p$ and its component Bx along x direction (figure 1), and the angle α between $\overline{B}p$ and the vertical component By(0^+, y) of the magnetic field outside the sheet (figure 1), we find

$$B_x(0,y) = B_p(y)\cos\varphi$$
$$B_y(0^+,y) = B_p(y)\ \mathrm{tg}\,\alpha(y)$$

and we deduce the following relationship between $\alpha(y)$ and $\rho(y)$:

$$\mathrm{tg}\,\alpha(y) = \frac{w}{\cos\varphi}\left(\frac{B_p(y)\,\nabla_y B_p(y)/\mu + \rho(y)\,g}{2\,B_p^2(y)/\mu}\right) \qquad (7)$$

Observations by Leroy et al (1982a) provide Bp = 8G, the vertical gradient ∇_y Bp = 0.5G/10 Mm and the angle φ = 65°. For a typical value of ρ ($6.7\ 10^{-13}$ g cm^{-3} with $n_e = 10^{11}$ cm^{-3} and a ionization degree of 1/3), the magnetic gradient term in (7) is small compared to the gravity one :

$$\rho g \,/\, (B_p\,\nabla_y B_p/\mu) \approx 58$$

Depending on W values, a wide range of α values is possible (see Table 1).

III - MAGNETOSTATIC MODELS OF PROMINENCE SUPPORT

We show in this section how it is possible to describe current sheet prominences supported in a potential field by the help of simple holomorphic functions.

We prescribe the prominence horizontal magnetic field component Bx(o, y) to increase with height, as observed by Leroy et al (1982a) and Rust (1967). This condition corresponds to the first Anzer's stability criterion (Anzer, 1969), but we do not seek to verify his second one (namely $\partial B_y(o^+,y)/\partial y \leq 0$), which has not yet been observed to hold in prominences. Moreover, for simplicity, we do not prescribe the magnetic field $|B(\zeta)|$ to vanish when $|\zeta| \to +\infty$, because we may cut our model at an arbitrary finite distance. In the following B_0, B_1, p, q, h are real positive constants and $\zeta = x + iy$ is the complex variable.

III-1. KR Models

In such models, the horizontal component of the magnetic field exhibit a polarity reversal between the photosphere and the prominence sheet.

III-1. a) An infinite current sheet in the y-direction :

We modify the previous function $B_A(\zeta)$ to

$$B_1(\zeta) = B_0\sqrt{p^2+\zeta^2}/\zeta + i B_1 (\zeta - ih)/\zeta$$

The field lines are displayed in Figure 3a (for h < p) and Figure 3b (for h = p). When h > p, the prominence cannot be supported. The fact that the field strength $|B_1(\zeta)|$ becomes infinite when $|\zeta| \to 0$ is not a serious fault because the altitude of the photosphere (here zero) is arbitrary in the coordinate system and may be taken to be positive. A neutral point (B = 0) exists below the sheet (h < p) or at the sheet's

base (h = p); its altitude is

$$n = \frac{h + \left(B_o^4 p^2 / B_1^4 + (p^2 - h^2) B_o^2 / B_1^2\right)^{1/2}}{1 + B_o^2 / B_1^2}$$

We prefer this second configuration, because it is more favourable to the understanding of prominence formation and condensation (see paper II). This model will be studied in detail in section V.

III-1. b) For a finite current sheet in the y-direction :

We now modify the previous function $B_B(\xi)$. At least 3 types of model may be investigated : the first has open field lines towards the corona (figure 3c) and is described by

$$B_2(\xi) = B_o \sqrt{(p^2+\xi^2)(q^2+\xi^2)} \,/\, \xi + B_1 (\xi - ip)$$

The second has closed field lines down to the photosphere (figure 3d) and is given by

$$B_3(\xi) = - B_o \frac{\sqrt{(p^2+\xi^2)(q^2+\xi^2)}}{\xi(\xi+ih)^2} - B_1 \frac{\xi - ip}{\xi(\xi+ih)}$$

with the condition $q \leq 2p$

Finally, configurations with helical structure (a magnetic island) may represented by :

$$B_4(\xi) = - B_o \frac{\sqrt{(p^2+\xi^2)(q^2+\xi^2)}}{\xi(\xi+ih)^2} + B_1 \frac{\xi - ip}{\xi(\xi-iq)}$$

with the condition q/p < B1/Bo (see Figure 3e).
The fact that $|B_4(\xi)| \to \infty$ when $\xi \to iq$ (at the top of the prominence) is not a serious fault because here the current sheet is infinitely thin (for simplicity) and the singularity would disappear if the finite thickness of the sheet were incorporated.

III-2. KS Models

In such models, the direction of the horizontal component of the magnetic field in the prominence is the same as in the photosphere.

III-2. a) Without helical structure :

The simple functions $B_A(\xi)$ and $B_B(\xi)$ can be modified as follows to provide a prominence support :

$$B_5(\xi) = i B_0 \frac{\sqrt{p^2+\xi^2}}{\xi(\xi+ih)} - \frac{B_1}{\xi}$$

gives an infinite current sheet in the y-direction (see Figure 4a).

and $$B_6(\xi) = -B_0 \frac{\sqrt{(p^2+\xi^2)(q^2+\xi^2)}}{\xi(\xi+ih)^2} - \frac{B_1}{\xi}$$

gives a finite current sheet in the y-direction (see figure 4b).

These two models do not satisfy the first Anzer criterion but they have an interesting property :

for $B_5(\xi)$, when $p/h < B_1/Bo$ the configuration is of KS type.
$p/h > B_1/Bo$ the configuration is of KR type.

The same conditions hold for $B_6(\xi)$, replacing p/h by pq/h^2.

These different solutions may be related to bifurcations between multiple equilibria (see Low, 1977 ; Heyvaerts et al, 1980), when, for instance, h varies due to motions in the convective zone.

III-2. b) With helical structure :

Such a configuration may be described by

$$B_7(\xi) = -B_0 \frac{\sqrt{(p^2+\xi^2)(q^2+\xi^2)}}{\xi(\xi+ih)^2} + \frac{B_1}{\xi}\frac{\xi+ih'}{\xi-iq}$$

with the conditions

$$q^2 p/(h^2 h') < B_1/B_0 < 1$$

(see Figure 4c).

and $$h'q > h^2$$

This kind of geometry is similar topologically to those used by Low (1981) or Lerche and Low (1980), for a prominence that has the shape of a cylinder rather than a sheet.

IV - QUASI-STATIC EVOLUTION OF MAGNETIC STRUCTURES DUE TO PHOTOSPHERIC MOTIONS.

IV-1. The velocity field

Observations by Martres et al (1981) and Malherbe et al (1981, 1983) show that slow upward and vertical motions (V_p = 0.5 km s^{-1}) occur inside filaments with a long lifetime of several days. The dynamical time-scale of such motions $t_{dyn} = H/V_p$ (where H is a typical prominence height of 10 Mm) is a few hours, a small duration compared to the lifetime. Thus stationary models are needed to investigate the global dynamics of solar prominences.

We now suppose that slow photospheric motions below the filament (diverging or converging) induce evolution of its magnetic structure (section III) through a series of equilibria ($V \ll V_a$), due to the line-tying of foot points. Such motions may be caused by supergranular or giant cell motions, or dynamo effects in the convective zone (Heyvaerts and Mercier, 1977). With $\partial/\partial t = 0$, the induction equation becomes

$$\partial \bar{B}/\partial t = \bar{\nabla} \wedge (\bar{V} \wedge \bar{B}) + \Delta \bar{B}/(\mu\sigma) = \bar{0}$$

The magnetic Reynolds number $R_m = 10^{-3} V(\text{km s}^{-1})\ L(\text{km})\ T^{3/2}$ is higher than 10^6 both inside the prominence (V = 0.5 km s^{-1}, L = 2 10^3 km, T = 10^4 K) and outside (V $\geqslant$ 10 km s^{-1}, L = 10^4 km, T = 10^6K). So the magnetic lines are frozen in the plasma and the diffusive term is negligible everywhere in the induction equation (except near a reconnection point, if present), which reduces to

$$\bar{\nabla} \wedge (\bar{V} \wedge \bar{B}) = \bar{0} \qquad (8)$$

We now take for simplicity $B_z = 0$ $(\varphi = 0)$.

With $\begin{cases} \bar{B} = B\,\bar{e}_b \\ \bar{V} = V_{//}\,\bar{e}_b + V_\perp\,\bar{e}_n \end{cases}$

$V_{//}$ being the velocity component along the field lines and $V_\perp$ the perpendicular one, equation (8) reduces to

$$V_\perp B = C \qquad (9)$$

C being a constant.

This relationship may also be written in vectorial form

$$\bar{E} + \bar{V} \wedge \bar{B} = \bar{j}/\sigma = \bar{0}$$

which implies

$$\bar{V}_\perp = V_\perp \bar{e}_n = \bar{E} \wedge \bar{B} / B^2 \quad \text{with} \quad \bar{E} = E_z \bar{e}_z$$

and E_z = constant.

Using complex variables, with B = By + i Bx, $V_\perp = V_\perp y + iV_\perp x$ and $\zeta = x + iy$

$$V_\perp(\zeta) = -i E_z B(\zeta) / |B(\zeta)|^2$$

Now assume $V_{//} = 0$, so that equation (9) gives $V_\perp \sqrt{B_x^2 + B_y^2} = C$ outside the prominence and Vp Bx = C inside, where Vp(y) is the plasma velocity inside the prominence sheet. We deduce

$$V_\perp(0^+, y) = V_p(y) \left(1 + B_y(0^+, y)^2 / B_x^2\right)^{-1/2} = V_p(y) \cos\alpha(y)$$

with $tg\,\alpha(y) = B_y(0^+, y) / B_x$ (see section I)

Then

$$\underline{V(0^+, y) = V_\perp(0^+, y) < V_p(y)}$$

With $Vp(y) \approx 0.5$ km s^{-1}, our model cannot explain the fast input of material (≈ 5 km s^{-1}) on both sides of the sheet reported by Malherbe et al (1983), unless $V_{//} \neq 0$. The calculation of $V_{//}$ using continuity, momentum and energy equations will be the topic of paper II.

Equation (9) predicts a decreasing velocity with height in the filament ; the gradient would be

$$\nabla_y V_p = - V_\perp \nabla_y B_x / B_x$$

or numerically - 50 m s^{-1}/10 Mm .
Such a small gradient would not actually be observable.

IV-2. Evolution of KS models without islands.

Upward motions may be produced inside KS prominences by a moving magnetic field due to diverging photospheric motions (typical velocity of 100 m s^{-1}) below the filament (Figure 5a). But the occurrence of such a diverging flow does not seem really to be very probable, at least below polar crown prominences, against which old remnant magnetic regions are pressed by the emergence of new active regions at low latitudes.

IV-3. Evolution of models with helical structure (magnetic islands).

Upward motions may also be produced inside prominence sheets, inbedded in helical structures, by a moving magnetic field caused by diverging photospheric flows for KS models (Figure 5b) or converging flows for KR models (Figure 5d). However, this leads to a progressive accumulation of material at the O-type singular points unless it flows out of the(x,y) plan along the long axis z of the prominence. Thus, such a picture seems to be less likely, though by no means impossible.

V - A STEADY-STATE RECONNECTION MODEL FOR KR PROMINENCES

At least at high latitudes, a converging flow below prominences seems to be more probable than a diverging one : prominences often appear along boundaries between regions of opposite polarities, which are pressed together near the poles (for instance, the polar crowns at the beginning of a new cycle).

A slow converging flow below a KR prominence is expected to induce a stationary process of magnetic reconnections at the neutral point (Raadu, 1979), producing upward motions in the prominence sheet (Figure 5c).

We now study the solution provided by the simplified 2D configuration $B_1(\xi)$ (see section III and fig. 3b) with h = p :

$$B(\xi) = B_o \frac{\sqrt{p^2+\xi^2}}{\xi} + i B_1 (\xi - ip)/\xi$$

with $\xi = x + iy$, the field lines of which are given by :

$$\mathrm{Re}\left\{ B_o\left[\sqrt{p^2+\xi^2} + p\,\mathrm{Ln}\left(\frac{\xi}{p+\sqrt{p^2+\xi^2}}\right)\right] + i B_1\left(\xi - ip\,\mathrm{Ln}\,\xi\right)\right\} = \text{constant}$$

We are interested in the upper plane $y \geqslant 0$, but we can restrict ourselves to the quadrant $y \geqslant 0$, $x \geqslant 0$ because of symmetry conditions :

$$B_x(-x,y) = B_x(x,y) \quad \text{and} \quad B_y(-x,y) = -B_y(x,y)$$

V-1. Velocity field of the prominence sheet

The magnetic field $\overline{B_e}$ at the right edge of the sheet $(\xi = iy, y \geqslant p)$ is given by

$$\overline{B_e} = \left(B_1 \frac{y-p}{y} , B_o \sqrt{y^2-p^2}/y \right)$$

so $$tg\,\alpha(y) = B_{e,x}/B_{e,y} = \frac{B_o}{B_1}\sqrt{\frac{y+p}{y-p}}$$

Inside the sheet, the magnetic field is horizontal and given by $\overline{B_p} = (B_1(y-p)/y , 0)$ and B_p increases with height from 0 to B1 with the vertical gradient $B_1\, p/y^2$.

The material velocity $V_p(y)$ inside the prominence is given by $V_p B_p = C$ with C = constant value = $V_\infty B_\infty$; V_∞ and B_∞ may be deduced from observations which refer generally to high altitude features in prominences, both for velocity and magnetic measurements.

Thus according to Leroy (1982a) and Malherbe et al (1983), we choose

$$B_\infty = B_1 = B_{observed} \cos\varphi = 3.5\ G \ (\text{with } B_{obs} = 8\ G \text{ and } \varphi = 65°)$$

$$V_\infty = V_{observed} = 0.5\ km\ s^{-1}$$

then, in the sheet,

$$V_P(y) = V_\infty\ y/(y-p) \qquad (10)$$

at the edges of the sheet, we find

$$V_\perp(y) = V_P(y) \Big/ \sqrt{1 + \frac{B_o^2}{B_1^2}\ \frac{y+p}{y-p}}$$

V-2. Density inside the prominence sheet

The equation of momentum along the y-direction gives :

$$\rho_P V_P\ dV_P/dy = -\rho_P g - dP/dy + f_y$$

where ρ_P is the prominence density and fy is the Lorentz force per unit volume (see Equation 6) :

$$f_y = \frac{2\ B_{P,x}\ B_{e,y}}{\mu\ w} - \frac{B_{P,x}\ \nabla_y\ B_{P,x}}{\mu}$$

then, assuming a constant gaz pressure P, we obtain

$$\rho_P(y) = \left(\frac{2\ B_{P,x} B_{e,y}}{\mu w} - \frac{B_{P,x}\ \nabla_y B_{P,x}}{\mu} \right) \Big/ \left(g + V_P\ \nabla_y V_P \right)$$

with u = y/p, we deduce

$$\rho_P(u) = \frac{(u-1)^4}{u^2}\ \frac{B_1^2}{Pg} \left[\frac{\frac{2p\ B_o}{\mu w\ B_1} \sqrt{u^2-1} - 1/u}{(u-1)^3 - u\ V_\infty^2/pg} \right] \qquad (11)$$

when $u \longrightarrow \infty$

$$\rho_p \longrightarrow \rho_{p\infty} = \frac{2 B_o B_1}{w g \mu} \qquad (12)$$

For typical values w = 2500 km, p = 2 w = 5000 km, $\rho_{p\infty} = 6.7\ 10^{-13}$ g cm^{-3}, equation (12) gives Bo = 8.27 G.

Then α decreases with heigh from 90° to α_∞ = 67°. Using the perfect gas law, the sheet temperature Tp(y) may be obtained from

$$P = \frac{k}{m} \rho_{p\infty} T_{p\infty} = \frac{k}{m} \rho_p(y)\ T_p(y)$$

where Tp_∞ = 6000 K and P = 0.33 dynes cm^{-2}.

V-3. Input of coronal material both sides of the sheet

Hot coronal material $\left(n_c = 10^9\ cm^{-3},\ \rho_c = 1.67\ 10^{-15}\ g\ cm^{-3},\ T_c = 10^6 K\right.$ enters both sides of the sheet where it is expected to cool and condense to form the prominence. The process of condensation will not be described here (see paper II) but coronal flow estimates may be obtained by using mass balance. With a coronal velocity of V_c along x, the continuity equation $\vec{\nabla}.(\rho\vec{V}) = 0$ reduces to

$$2 \rho_c V_c / w + \partial(\rho_p V_p)/\partial y = 0$$

This predicts an estimate for the coronal velocity of :

$$V_c(y) = -\frac{w}{2\rho_c} \frac{\partial}{\partial y}(\rho_p V_p)$$

which can be calculated using equations (10) and (11).

The previous results for Vp(y), $V_\perp(y)$ and Vc(y) are displayed in Figure 6, and functions Bp(y), $\rho p(y)$ and Tp(y) are plotted in Figure 7. The results become invalid, say, below y = 2p, because the oversimplified behaviour of Bp(y) around y = p does not allow us to describe the physics of the reconnection point. For instance, the Alfvèn speed at this point provides an upper limit for Vp. The altitude at which $\nabla_y Bp = (\nabla_y Bp)$ observed = 0.5 G/10Mm is given in Fig.6 and 7 ($y/p \approx 5.77$).

As shown in figure 6a, we expect a strong input of coronal material ($\geq$ 10 km/s) at the sheet's base, just above the reconnection site. The condensation process of this material will be developped in paper II. Since $V_\perp \leq Vc$ (when $y/p < 9.7$), we expect to have a strong component $V_{//}$ for the inflow.

V-4. Velocity field below the reconnection point

The magnetic field with $\xi = iy (y \leq p)$ is given by

$$\overline{B_b} = \left(- B_0 \frac{\sqrt{p^2 - y^2}}{y} - B_1 \frac{p-y}{y} , \; 0 \right)$$

and so $$V_b = V_\infty \, B_1 \, y \Big/ \left(B_0 \sqrt{p^2 - y^2} + B_1 (p-y) \right)$$

the velocity vector is vertical and downwards directed.

These functions are plotted in Figure 8a.
The solution is invalid, say below $y/p = 0.45$, because our magnetic field becomes infinite when $y \to 0$. This might be avoided by changing the photospecric altitude (take, for instance, y phot = p/2).

V-5. Velocity field in the photosphere

The photospheric magnetic field ($\xi = x$) is given by

$$\overline{B}_{phot} = \left(B_1 , B_0 \frac{\sqrt{p^2+x^2}}{x} + B_1 \frac{p}{x} \right)$$

and so V phot = $V_\infty B_1 \Big/ \left(B_1^2 + \left(B_0 \frac{\sqrt{p^2+x^2}}{x} + B_1 \frac{p}{x} \right)^2 \right)^{1/2}$

The functions Bphot(x) and Vphot(x) are sketched in Figure 8b. A typical value of Vphot lies around 100 m s^{-1}. The model is invalid when $x/p < 0.3$ for the same reasons as in V-4.

Conclusion

2D current sheet models for solar prominences, supported by potential magnetic configurations have here been investigated, with the help of complex functions.

Two approaches were possible, namely using Anzer's method (1972) to solve numerically Laplace's equation (with boundary conditions obtained from magnetic field observations), or seeking simple solutions, which have the advantage of being analytical. Choosing this second way, we showed first how to find simple holomorphic functions to represent 2D magnetic structures of Kippenhaln-Schlüter type or Kuperus-Raadu type. Then, after looking at the evolution, induced by photospheric motions, of the magnetic field through a series of equilibria, we suggested that slow diverging flows ($< 100\,m\,s^{-1}$) below KS prominences could explain the upward motions reported by Martres et al (1981) and Malherbe et al (1981, 1983) in disk filaments. Alternatively, slow converging photospheric flows could explain them in a KR model.

To account for such motions, and also for magnetic measurements by Leroy et al (1982 a), we have proposed, following Raadu (1979), a quasi-static reconnection model, in which new coronal material is expected to condense and cool while entering the prominence just above the reconnection site. The dynamics of cold material, carried upwards through the filament by the moving magnetic field, was investigated by using a simple magnetic configuration of KR type. Nevertheless, the fast inflow ($5km\ s^{-1}$), occurring at both sides of prominences, and reported by Malherbe et al (1983), cannot be well modelled here, because it strongly depends on energetics and the condensation process : this will be the topic of paper II.

Acknowledgements

This work was begun while one of the authors (JMM) was a visitor at the University of St Andrews. He wants to thank all the staff members for their hospitality. He would also like to thank Dr. P. Mein, Dr. B. Schmieder and Pr. J. Heyvaerts for helpful discussions, and inspiring comments and suggestions.
Both authors are also indebted to G. Prieur for typing the manuscript.

REFERENCES :

ANZER, U. : 1969, Solar Phys., 8, 37.

ANZER, U. : 1972, Solar Phys., 24, 324.

ANZER, U. : 1979, in Physics of Solar Prominences, IAU coll. n° 44, 322, Jensen, Maltby, Orrall eds.

ANZER, U., TANDBERG-HANSSEN, E. : 1970, Solar Phys., 11, 61.

CHIUDERI, C., VAN HOVEN, G. : 1979, Astrophys. J. Letters, 232, L 69.

DUNN, R.B. : 1960, Thesis, Harvard University.

ENGVOLD, O. : 1982, in trans. of the IAU, 18, in Press.

GREEN, R.M. : 1965, IAU coll. n° 22, 398.

HEYVAERTS, J.,LASRY, J.M., SCHATZMAN, M.,WITOMSKY, G. : 1980, Lecture Notes Math., 782, 160.

HEYVAERTS, J., MERCIER, C. : 1977, Astron. Astrophys., 61, 685.

JENSEN, E., MALTBY, P., ORRALL, F.Q. : 1979, Physics of Solar Prominences, IAU Coll. n° 44.

KIPPENHAHN, R., SCHLUTER, A. : 1957, Z. Astrophys., 43, 36.

KUPERUS, M., TANDBERG-HANSSEN, E. : 1967, Solar Phys., 2, 39.

LAVRENTIEV, M., CHABAT, B. : 1972, Méthodes de la théorie des fonctions d'une variable complexe, MIR, Moscou, USSR.

LERCHE, I., LOW, B.C. : 1980, Astrophys. J., 238, 1088.

LEROY, J.L., BOMMIER, V., SAHAL-BRECHOT, S. : 1982a, Solar Phys., in press.

LEROY, J.L. : 1982 b and c, private communications.

LITES, B. : 1976, Astrophys. J. Letters, 210, L111.

LOW, B.C. : 1977, Astrophys. J., 212, 234.

LOW, B.C. : 1981, Astrophys. J., 246, 538.

LOW, B.C. : 1982, Solar Phys., 75, 119.

MALHERBE, J.M., SCHMIEDER, B., MEIN, P. : 1981, Astron. Astrophys., 102, 124.

MALHERBE, J.M., SCHMIEDER, B., RIBES, E., MEIN, P. : 1983, Astron. Astrophys., in press.

MARTRES, M.J., MEIN, P., SCHMIEDER, B., SORU-ESCAUT, I. : 1981, Solar Phys., 69, 301.

MEIN, P. : 1977, Solar Phys., 54, 45.

MILNE, A.M., PRIEST, E.R., ROBERTS, B. : 1979, Astrophys. J., 232, 304.

PICKEL'NER, S.B. : 1971, Solar Phys., 17, 44.

PRIEST, E.R. : 1981, 3rd European Solar Meeting, Oxford, 203, Jordan ed.

PRIEST, E.R. : 1982, Solar Magnetohydrodynamics, chapter 11, D. Reidel Publ. C°, Dordrecht, Holland.

PRIEST, E.R., Raadu, M.A. : 1975, Solar Phys., 43, 177.

PRIEST, E.R., SMITH, E.A. : 1979, Solar Phys., 64, 267.

RAADU, M.A. : 1979, In Physics of Solar Prominences, IAU Coll n° 44, 167, Jensen, Maltby, Orrall eds.

RAADU, M.A., KUPERUS, M. : 1973, Solar Phys., 28, 77.

RUST, D.M. : 1967, Astrophys. J., 150, 313.

RIBES, E., UNNO, W. : 1980, Astron. Astrophys., 91, 129.

SYROVATSKY, S.I. : 1976, in proc. P.N. Lebedev Phys. Institute, 74, 1.

SMITH, E.A., PRIEST, E.R. : 1977, Solar Phys., 53, 25.

SOMOV, B.V., SYROVATSKY, S.I. : 1980, Pis'ma Astron. Zh., 6, 592.

TANDBERG-HANSSEN, E. : 1974, Solar Prominences, D. Reidel Publ. C°, Dordrecht, Holland.

TANDBERG-HANSSEN, E., ANZER, U. : 1970, Solar Phys., 15, 158.

TSUBAKI, T. : 1975, Solar Phys., 43, 147.

TUR, T.J., PRIEST, E.R. : 1976, Solar Phys., 48, 89.

UCHIDA, Y. : 1980, in proc. Japan France Seminar on Solar Phys., 169, Moriyama, Hénoux eds.

FIGURE CAPTIONS

Figure 1 : Schematic representation of a prominence, showing the coordinate system used throughout the paper.
The vertical y axis is in the opposite direction to gravity. The x axis is normal to the prominence sheet, while the z axis runs along the prominence length.

Figure 2 : The field lines for the two basic functions used throughout the paper.
(a) an infinite current sheet in the y-direction beginning at altitude p above the photosphere.
(b) a finite current sheet in the y-direction of height (q-p).

Figure 3 : Current sheet models for KR type prominences.
(a) and (b) : Infinite current sheets in the y-direction, with a neutral point below the prominence or at its base.
Finite current sheets in the y-direction, with (c) open field lines, (d) closed field lines or (e) helical structures.

Figure 4 : Current sheet models for KS type prominences.
(a) : Infinite current sheets in the y-direction.
(b) and (c) : Finite current sheets in the y-direction. (c) shows helical structures.

Figure 5 : Dynamical models.
(a) and (b) show the evolution of KS models induced by diverging photospheric motions.
(c) and (d) give the evolution of KR models induced by converging photospheric motions.
The arrows represent the velocity field, perpendicular to magnetic lines.

Figure 6 : The plasma velocity Vp(y) inside the prominence sheet (upwards directed) and the velocity $V_{\perp}$ (y) perpendicular to magnetic lines at both edges of the sheet, together with the velocity Vc(y) of the coronal input of material.

Figure 7 : The prominence temperature Tp(y), magnetic field strength Bp(y) and density $\rho p(y)$.

Figure 8 : (a) Below the reconnection point, the velocity $V_b(y)$ (downwards directed) and magnetic field strength $B_b(y)$.

(b) In the photosphere, the velocity $V_{phot}(y)$ perpendicular to magnetic lines (converging flow) and field strength $B_{phot}(y)$.

Table 1

W (Mm)	1	2.5	5	10	15
α (degrees)	23.5	47.4	65.3	77.1	81.3

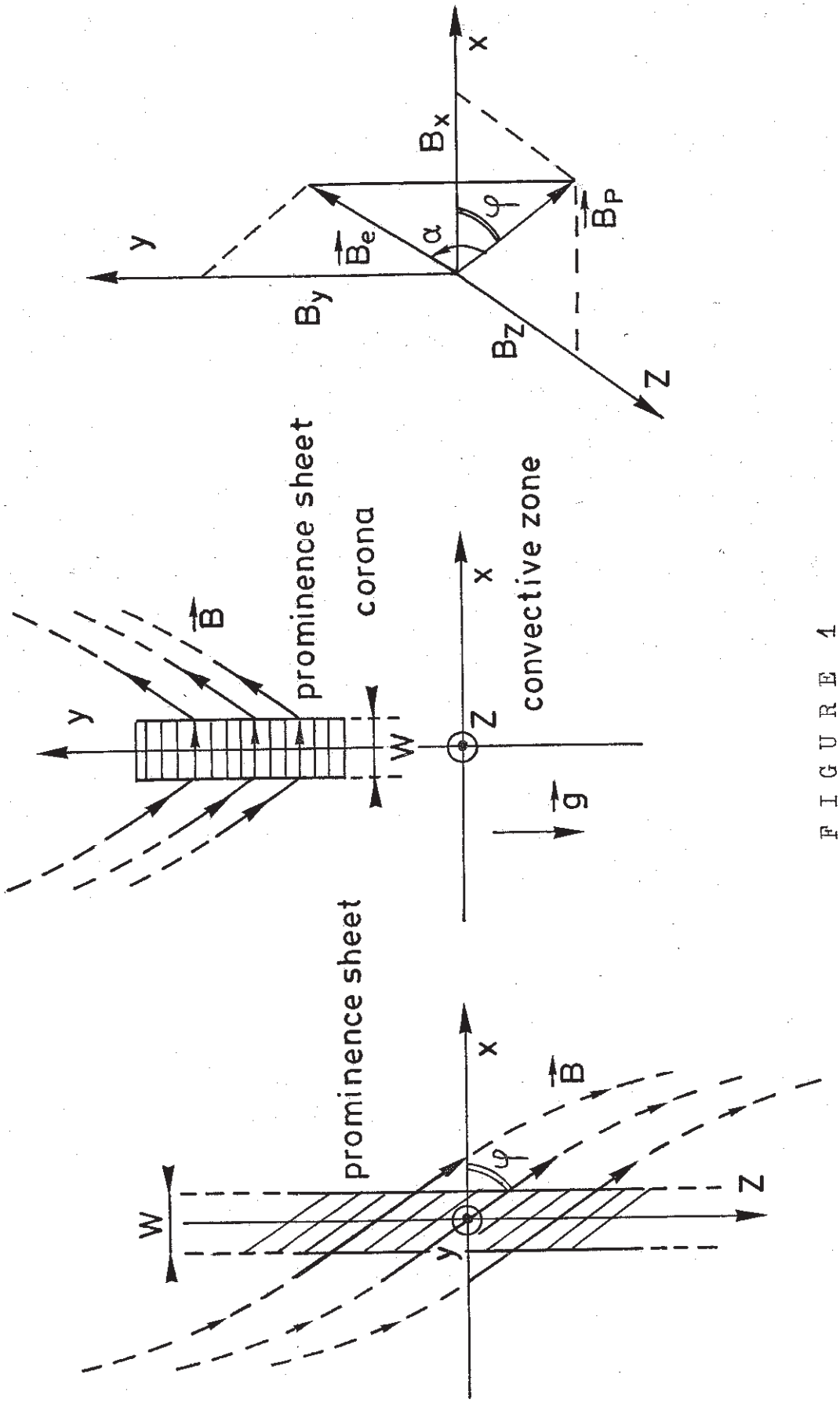
x
B_x
B_P
φ
α
B_e
y
B_y
B_z
z
prominence sheet
corona
convective zone
B
y
W
x
z
g
prominence sheet
B
x
φ
z
W
y

FIGURE 1

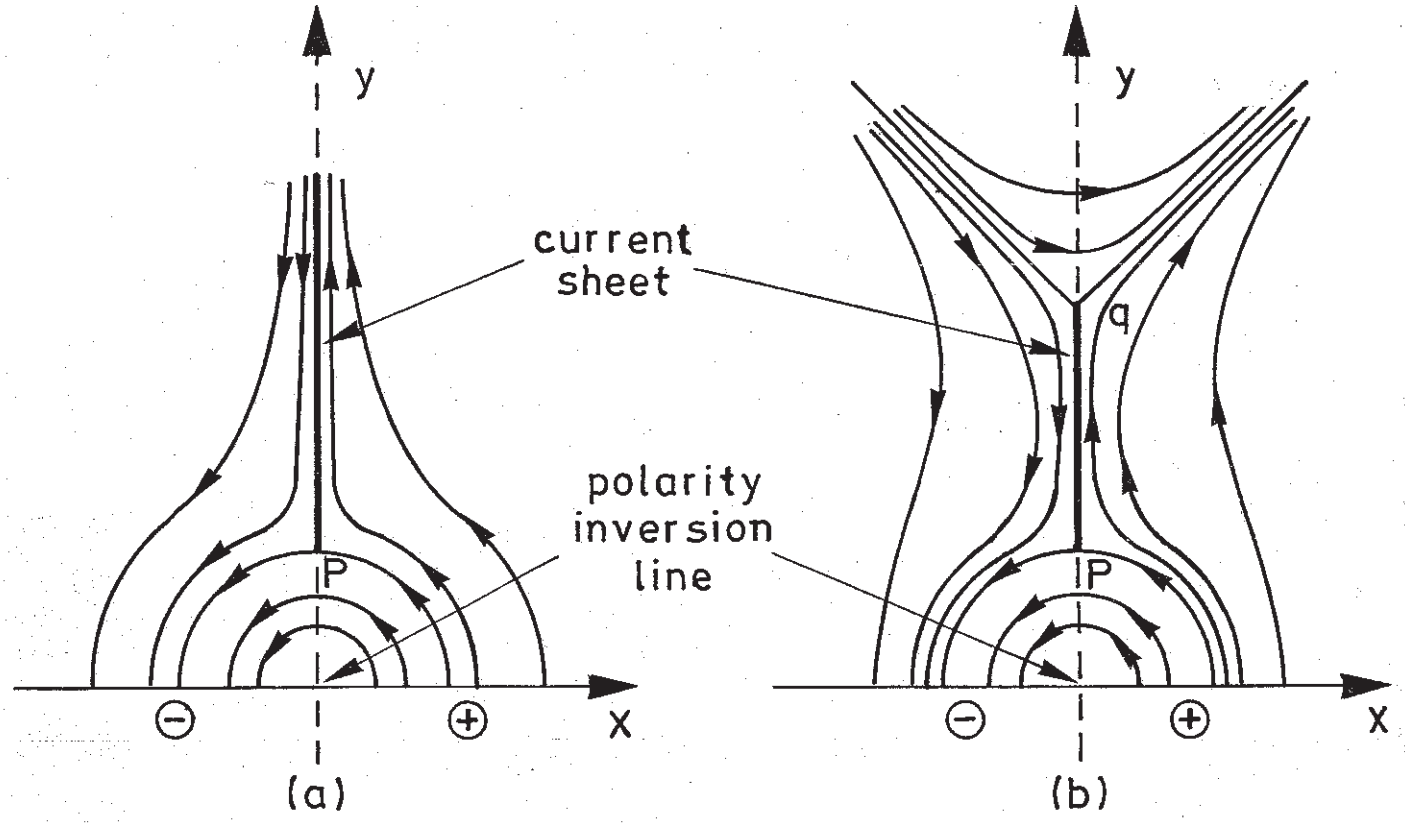

FIGURE 2

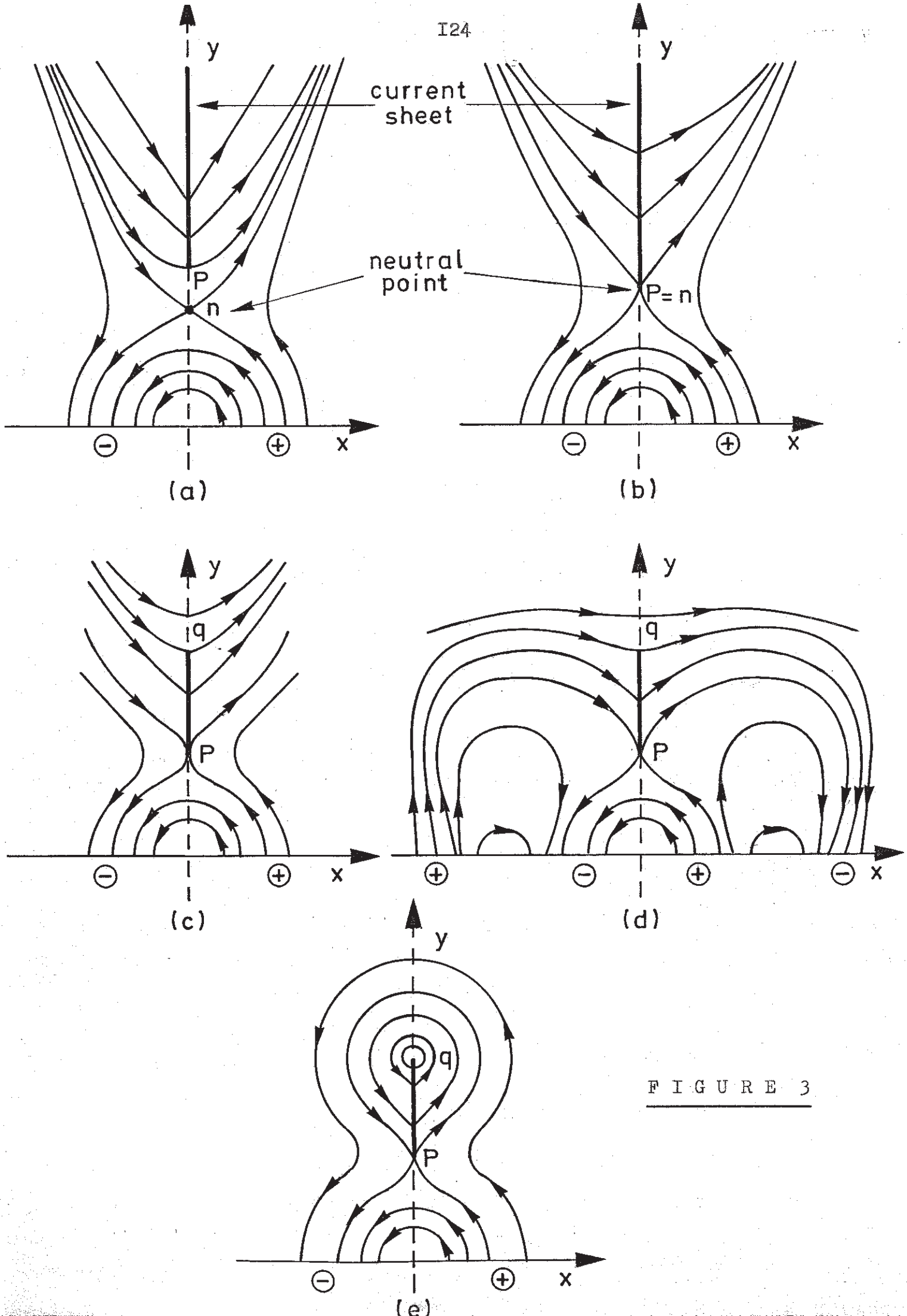

FIGURE 3

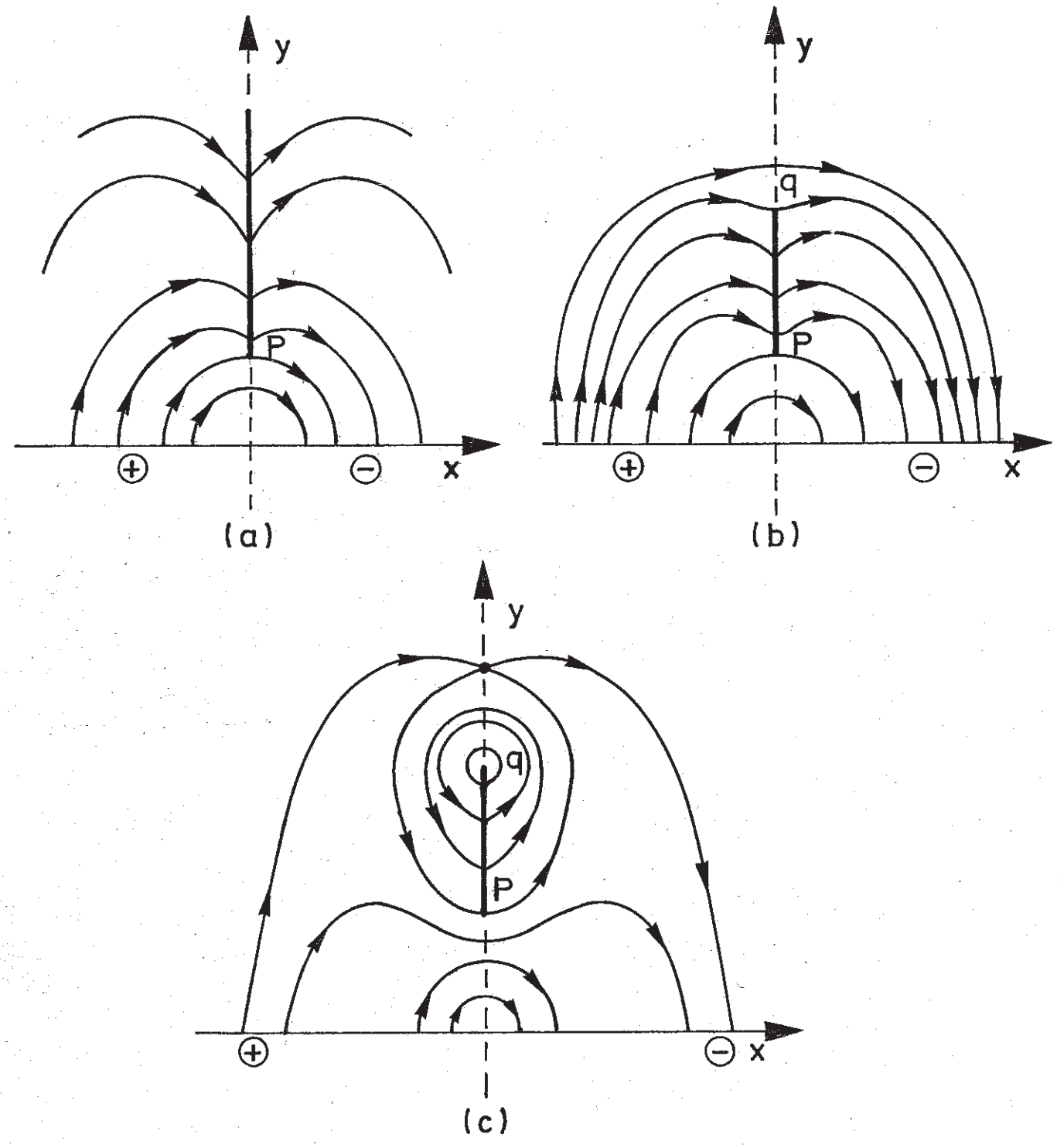

FIGURE 4

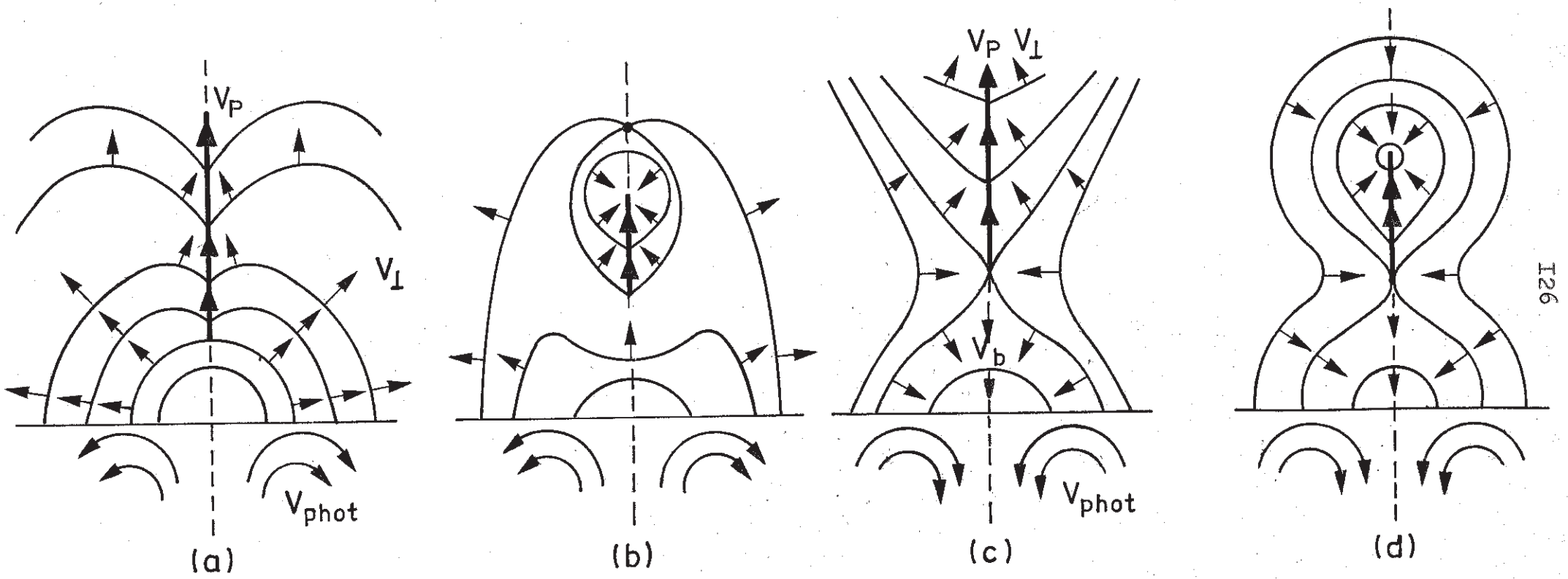

I26

FIGURE 5

F I G U R E 6

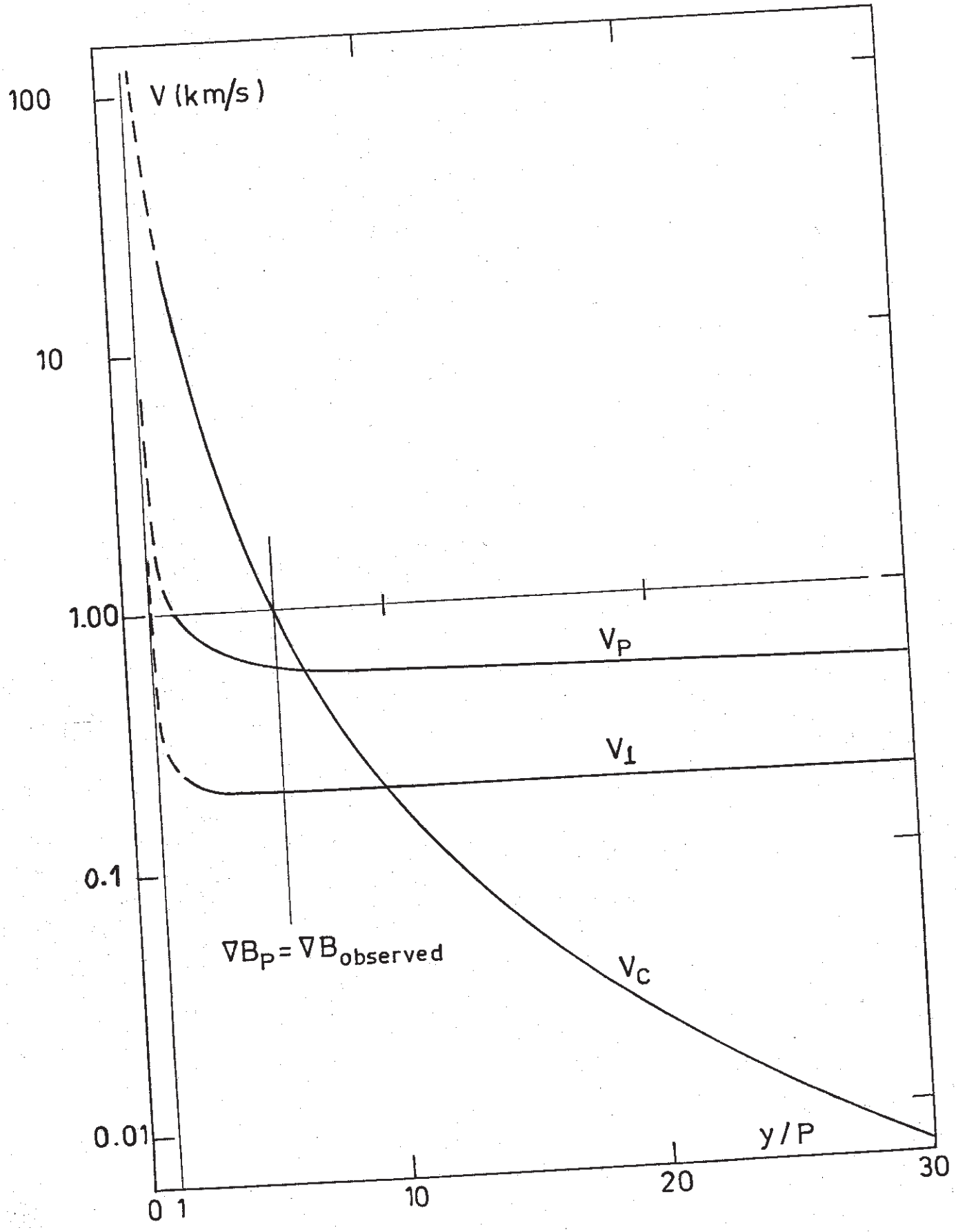
V (km/s)
100
10
1.00
0.1
0.01
0 1
10
20
30
y/P
V_P
V_1
V_C
$\nabla B_P = \nabla B_{observed}$

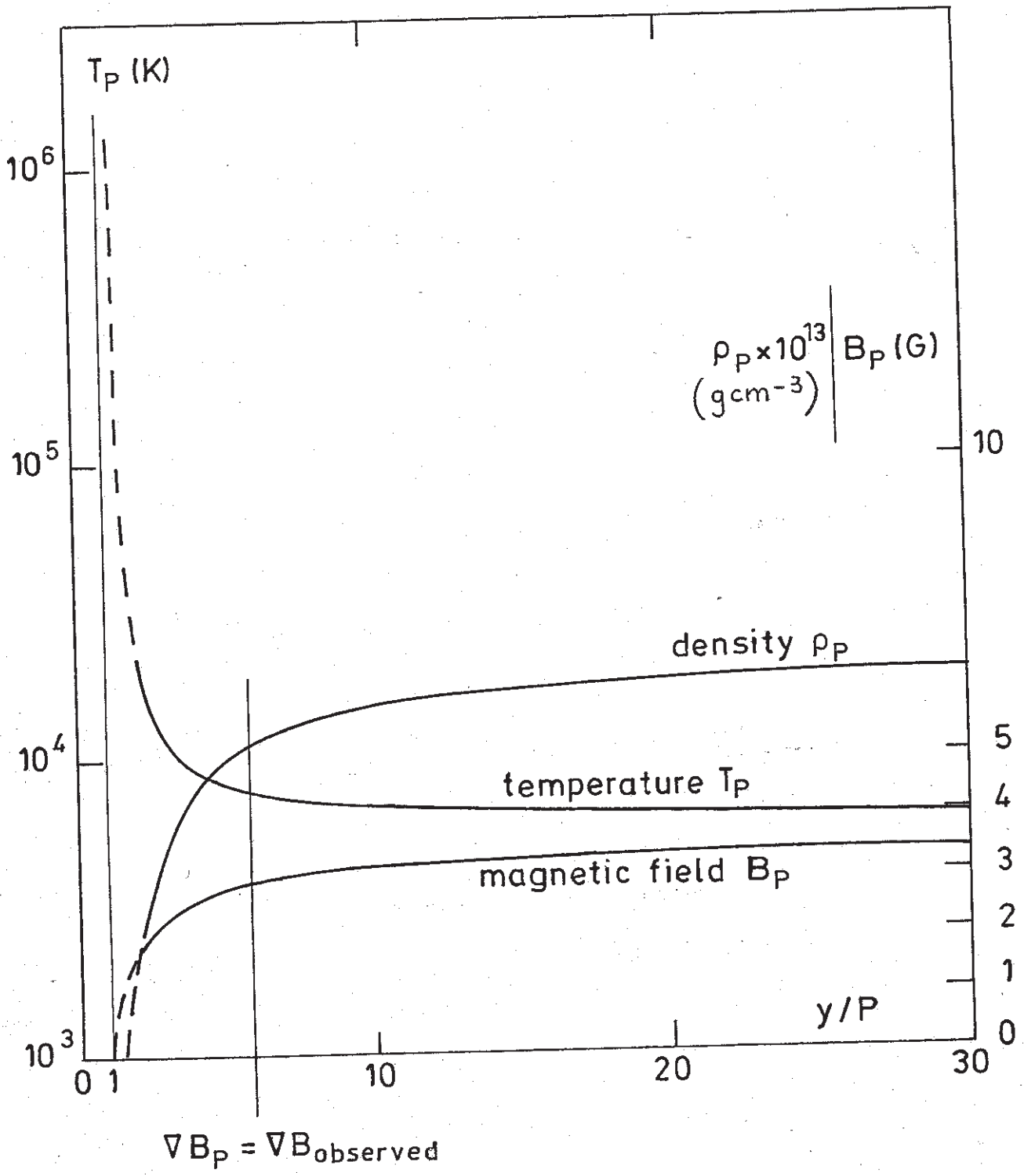
T_P (K)
10^6
10^5
10^4
10^3
$\rho_P \times 10^{13}$ $(g cm^{-3})$
B_P (G)
10
5
4
3
2
1
0
density ρ_P
temperature T_P
magnetic field B_P
y/P
0 1
10
20
30
$\nabla B_P = \nabla B_{observed}$

FIGURE 7

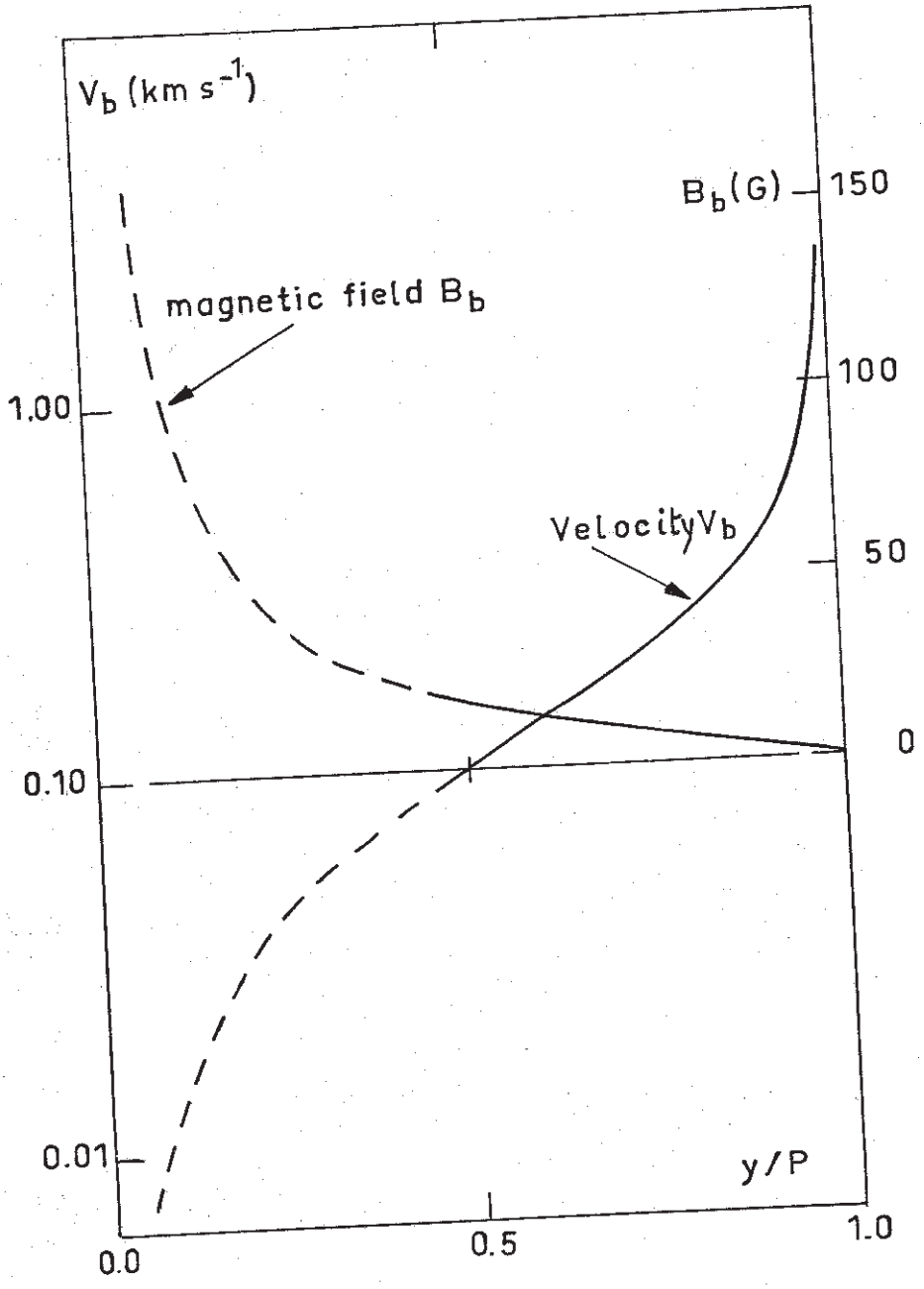
V_b (km s^{-1})
B_b(G)
150
100
50
0
magnetic field B_b
Velocity V_b
1.00
0.10
0.01
0.0
0.5
1.0
y/P

FIGURE 8a

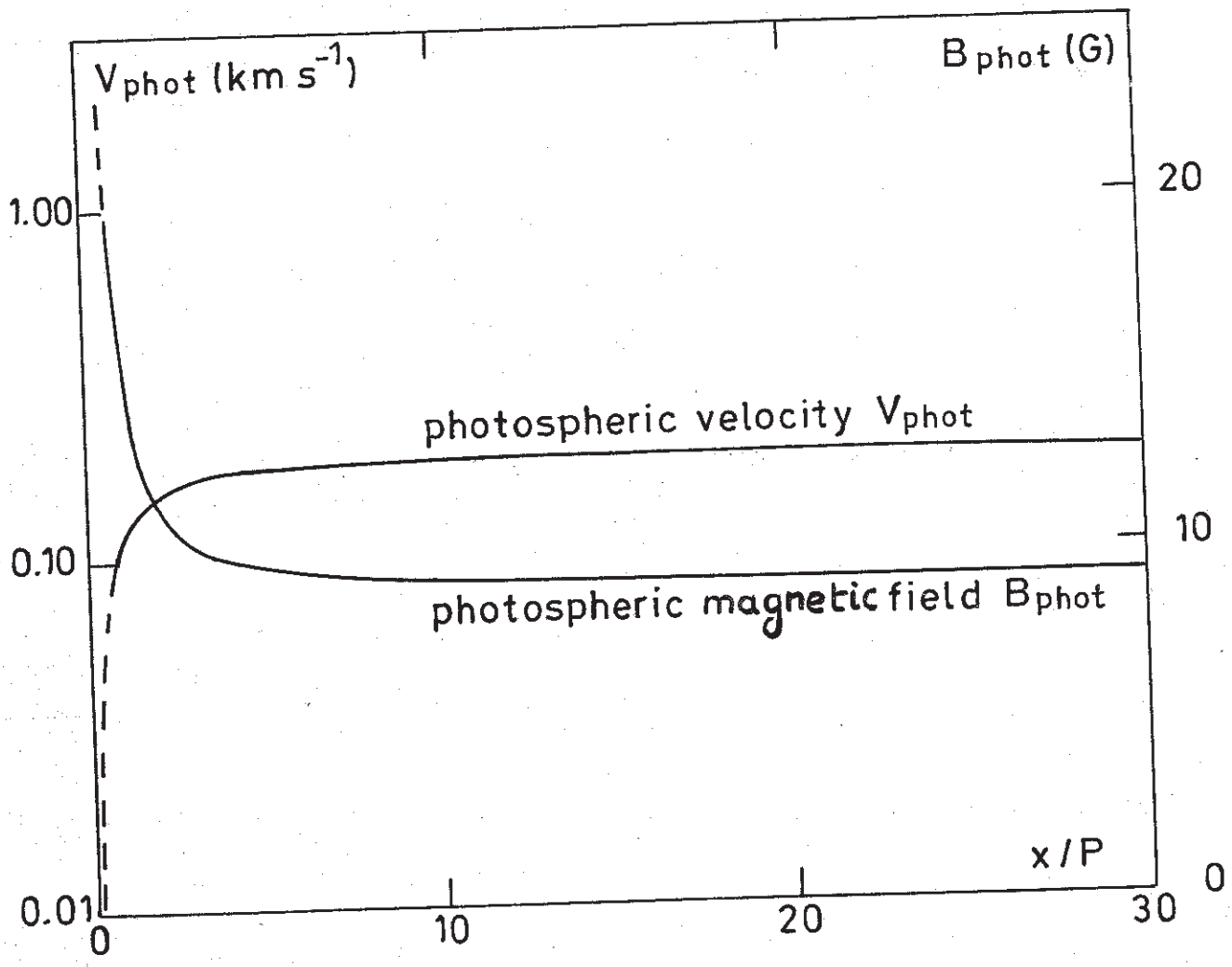
Vphot (km s-1)
Bphot (G)
1.00
0.10
0.01
20
10
0
photospheric velocity Vphot
photospheric magnetic field Bphot
x/P
0
10
20
30

FIGURE 8 b

A R T I C L E 4

CURRENT SHEET MODELS FOR SOLAR PROMINENCES

II - ENERGETICS AND CONDENSATION PROCESS

J.M. MALHERBE*, E.R. PRIEST**, AND J. HEYVAERTS***

* Observatoire de Meudon, DASOP (LA 326),
92190 MEUDON - FRANCE

** University of St Andrews, Department of Applied
Mathematics, St ANDREWS KY 16 9SS - SCOTLAND

*** Institut d'Astrophysique du CNRS,
98 bis Bd Arago, 75014 PARIS - FRANCE

Submitted to : Astronomy & Astrophysics
The Main Journal

ABSTRACT

A steady state dynamic model for solar prominences of Kuperus and Raadu type was previously proposed by MALHERBE and PRIEST (1983), but only the motion through series of quasi-static states was investigated there. We study here the mechanisms for formation, condensation and cooling of plasma in this model. As hot coronal material approaches the filament sheet, it is expected to cool and condense. Cold material is then carried up through the prominence by rising magnetic field lines due to converging photospheric motions below the filament. Two possible ways are suggested of triggering a thermal instability and so producing such a stationary condensation process : a larger pressure in the sheet, or a smaller wave heating in the reconnected field than in the surrounding corona. This paper presents a simple model to simulate the plasma condensation : the thermodynamics of the cooling process, as well as the dynamics of new material entering the prominence sheet, are described in detail.

I - INTRODUCTION

In paper I (MALHERBE and PRIEST, 1983), current sheet models, built with the help of complex functions, were presented to explain the observations of magnetic fields (LEROY et al, 1982) and velocity fields (MARTRES et al, 1981; MALHERBE et al, 1981, 1983a) in solar prominences. Simple magnetostatic solutions, both of Kuperus-Raadu (KR) type (1973) and Kippenhahn-Schlüter (KS) type (1957) were proposed. The evolution, induced by photospheric motions, of such magnetic structures through series of equilibria, was studied. It was suggested that, in the case of KS models, slow diverging photospheric motions, ($100 ms^{-1}$) below prominences could explain the upflows ($\rangle$ $0.5 kms^{-1}$) reported in disk filaments by MARTRES et al (1981) and MALHERBE et al (1981, 1983a); while, in the case of KR models, slow converging photospheric motions could explain them. But, according to LEROY et al (1982), KR prominences seem to be more frequent on the Sun than KS ones. Converging flows below filaments also seem to be more probable than diverging ones, at least in the polar regions, where prominences often appear along boundaries between regions of opposite polarity, which are pressed together near the poles to form the polar crown. We therefore proposed, in Raadu's spirit (1979), a quasi-static reconnection KR model, in which new coronal material was expected to condense and cool while entering the prominence above the reconnection point ($B = o$), and it was then carried up through the filament by the moving magnetic field (see figure 1). But only the dynamics were investigated. A fast and continuous input of coronal material was predicted above the neutral point (in agreement with observations by MALHERBE et al, 1983a), but it is strongly dependent on the details of the energetics and the condensation process, which are the topic of this paper.

The condensation of prominences by thermal instability has been examined by several authors (see PRIEST for a review, chapter 11, 1982). HOOD and PRIEST (1979) studied the formation of prominences in coronal loops and found that a thermal equilibrium was no longer possible when the pressure, the length or the twist of a hot loop were becoming too great, or the heating too small. The state of non equilibrium ensued when thermal conduction was no longer able to inhibit the condensation process. The result was the formation of a cool core. PRIEST and SMITH (1979) suggested that the same mechanism could account for the formation of prominences in coronal arcades : for instance, shearing an arcade beyond a critical value could reduce the stabilizing effect of

conduction and create a region of non equilibrium, where material could cool and condense to form a filament (However, the process depends on the base boundary conditions, which need further study).

The formation of prominences in current sheets was investigated by KUPERUS and TANDBERG-HANSSEN (1967), Raadu and Kuperus (1973), SMITH and PRIEST (1977), CHIUDERI and VAN HOVEN (1979) and SOMOV and SYROVATSKY (1980). The condensation of filaments in current sheets has several theoretical advantages : a high compression perpendicular to the magnetic field is possible, due to the onset of tearing mode instability which may occur as the plasma condenses dragging the field with it. It may inhibit the build-up of magnetic pressure by annihilation of field lines and create magnetic islands to support the dense and cool plasma. SMITH and PRIEST (1977) showed that thermal instability could occur inside a current sheet when its length exceeds a critical value. Here we want to suggest that thermal instability may also be initiated above the neutral point of our reconnection model, followed, as hot coronal material enters the sheet, by a stationary condensation process.

Thus, we describe in section II two possible mechanisms which may trigger, by thermal instability, the formation of our prominence model. Basic dynamical properties follow from mass balance. We present in Section III an approximate model, using simplified continuity and energy equations, for the simulation of the hydrodynamics and energetics of the condensing plasma.

II - 2 POSSIBLE MECHANISMS FOR TRIGGERING A THERMAL INSTABILITY

II - 1 - The mechanism and time scale of thermal instability.

Consider a hot coronal plasma with temperature T_c, density ρ_c in thermal equilibrium under a balance between wave-heating h and optically thin radiative cooling $\rho_c Q(T_c)$ (per unit of mass), so that:

$$h - \rho_c Q(T_c) = 0$$

The cooling function $Q(T) = \chi T^{\alpha}$ has been calculated by several authors and averaged by HILDNER (1974), splitting the temperature range into five regions (see table 1).

Perturb this equilibrium at constant gas pressure P_c neglecting thermal conduction, for simplicity only :

$$\rho C_p \, \partial T/\partial t = h - \rho Q(T) \qquad (1)$$

$$\text{and} \quad \rho = m P_c / k T \qquad (2)$$

where k is the Boltzmann's constant, m the mean atomic mass and $C_p = (k/m)\left(\gamma/(\gamma-1)\right)$, (with $\gamma = 5/3$) is the calorific capacity per unit mass.

Equations (1) and (2) then reduce to (subscript c referring to coronal values) :

$$\frac{\gamma}{\gamma-1} \frac{P_c}{\chi_c \rho_c^2 T_c^{\alpha_c}} \frac{\partial}{\partial t}\left(\frac{T}{T_c}\right) = \left(1 - \frac{\chi (T/T_c)^{\alpha-1}}{\chi_c T_c^{\alpha_c - \alpha}}\right)$$

When $\alpha < 1$, a thermal instability may occur. It may be triggered from a hot equilibrium ($\alpha = -1$ in coronal conditions), but not from a cold one ($\alpha = 7.4$ in prominence conditions).

The instability runs on the radiative cooling time-scale

$$\tau_R = \frac{P_c}{\chi_c \rho_c^2 T_c^{\alpha_c}} \qquad (3)$$

numerically of the order of 10^4 s in coronal conditions (see PRIEST, 1982, chapter 7 for a more extensive review).

II - 2 - Triggering the thermal instability.

Two mechanisms at least may be suggested to trigger the thermal instability : increasing the density ρ by reconnection at constant temperature T (mechanism 1), or reducing the heating h (mechanism 2), as shown approximately by equation (1). The instability is favoured by the behaviour of the cooling function Q(T) which increases (at high temperatures) when T decreases.

II - 2 - a - mechanism 1 : compression of the sheet.

Assuming that the prominence height is large compared to its width, the force balance along the x direction (Figure 1) gives :

$$P + \frac{B_y^2}{2\mu} = \text{const.}$$

where By is the y-component of the magnetic field $\vec{B}$, and μ the magnetic permeability.

With subscripts c and p refer ing respectively to the corona and the prominence, we obtain, with $By_p \approx 0$:

$$P_p / P_c = 1 + \varepsilon^2 / \beta \quad > 1 \qquad (4)$$

where $\beta = P_c / (B_c^2 / 2\mu) = (C_s / V_a)^2$ and $\varepsilon = B_{yc} / B_c$, B_c being the field strength (a few G), C_s the sound speed ($\approx$ 130 kms^{-1}) and V_a the Alfven speed ($\approx$ 500 kms^{-1}) in the corona.

Mechanism 1 may be initiated at the reconnection point : w being the prominence width ($\approx$ 5000 km), the Alfven time-scale $\tau_a = W/V_a$ ($\approx$ 10s) and the sonic time-scale $\tau_S = W/C_s$ ($\approx$ 40s) are much smaller than the cooling time-scale τ_R ($\approx 10^4$s, equation 3). This implies that the temperature may be regarded as a constant near the reconnection site. Relation (4) becomes

$$\rho_p / \rho_c = 1 + \varepsilon^2 / \beta \quad > 1$$

So the condensation process is expected to begin just above the reconnection point.

II - 2 - b - <u>mechanism 2 : reduction of wave-heating</u>.

In a state of thermal equilibrium, wave and Joule heating balance radiation and conduction. In the case of prominences supported against gravity by potential magnetic fields (paper I), Joule heating J is only present in the filament. J may be estimated by :

$$J = \frac{j_p^2}{\sigma} \approx \frac{B_p^2}{\mu^2 w^2 \sigma}$$

where j_p is the current density and $\sigma = 8\ 10^{-4}\ T^{3/2}$ the electric conductivity. Numerically, with B = 10 G, W = 2500 km, T = 8000 K, we obtain $J = 1.27\ 10^{-10}\ Wm^{-3}$, while radiative cooling $\rho^2 \chi T^{\alpha}$ lies around $5.98\ 10^{-3} Wm^{-3}$. Thus, Joule heating appears to be negligible.

The hatched area around the prominence in figure 1, delimited by the singular field lines reconnecting at the neutral point, is well isolated against dissipation of waves. Alfvèn waves and MHD show mode waves propagate

upwards along the magnetic field, and so avoid the reconnected plasma. The MHD fast mode waves (see HEYVAERTS, 1980) may propagate across the field lines, but, once the prominence starts to form, they may all be dissipated in the surface layers of the prominence and not reach the core.

Thus, we expect a smaller wave-heating inside the hatched region of figure 1 than outside.

II - 3 - An order of magnitude solution for the dynamics of the condensation process.

The coronal plasma enters the prominence above the neutral point where it condenses, cools and is carried up through it by magnetic field motions. New coronal material is pumped along field lines both sides of the sheet by the depression produced by the condensation process.

II - 3 - a - height of condensation.

V_p being the plasma velocity inside prominences, (see MALHERBE et al, 1983a), the height of condensation D may be approximated by

$$D = V_p \, \tau_R \approx 5000 \text{ km}$$

with $V_p = 0.5$ km s^{-1} and $\tau_R \approx 10^4$ s (eq3)

Over this range of altitudes, the temperature and density are expected to vary from coronal to prominence values.

II - 3 - b - Mass balance

We define the velocity both sides of the prominence sheet as

$$\vec{V} = V_\perp \, \vec{e_n} + V_{//} \, \vec{e_b}$$

where $V_{//}$ is the velocity component along magnetic lines and $V_\perp$ is the perpendicular one (see figure 1). The properties of $V_\perp$ were studied in paper I : a relationship between $V_\perp$ and the field strength B was established, namely $V_\perp B = \text{const}$, leading to $V_\perp = Vp \cos \alpha$, α being the angle between the prominence magnetic vector $\vec{Bp}$ and the magnetic field $\vec{Bc}$ both sides of the sheet (figure 1).

$V_{//}$ may then be estimated using mass balance between the hot and condensing

material entering the sheet, and the cold and dense plasma flowing up through it :

$$2 V_x \rho_c D = \rho_p V_p w \qquad (5)$$

where

$$Vx = - V_{//} \cos\alpha \cos\varphi - V_{\perp} \sin\alpha \cos\varphi \qquad (6)$$

φ being the angle between the prominence magnetic field $\vec{Bp}$ and its x-component (fig. 1).

From equations (5) and (6), we derive a relationship between $V_{//}$ and Vp :

$$V_{//} = V_p \left(\frac{\rho_p}{2\rho_c} \frac{w}{D} \frac{1}{\cos\alpha \cos\varphi} - \sin\alpha \right)$$

Also, the horizontal (V_h) and vertical (V_v) components of $\vec{V}$ are given by :

$$V_h = V_p \frac{\rho_p}{2\rho_c} \frac{w}{D} \frac{1}{\cos\varphi}$$

$$V_v = V_p \left(1 - \frac{\rho_p}{2\rho_c} \frac{w}{D} \frac{tg\,\alpha}{\cos\varphi} \right)$$

The angle φ may be deduced from observations (LEROY et al, 1982), and α is given by (see paper I, section II-3) :

$$tg\,\alpha = \frac{w}{\cos\varphi} \frac{\rho_p g + B_p \nabla_y B_p / \mu}{2 B_p^2 / \mu}$$

where $\nabla_y B_p$ is the vertical gradient of the prominence field strength.

With $\varphi = 65°$, $B_p = 8$ G, $\nabla_y B_p = 0.5$ G/10Mm (LEROY et al, 1982) and with $\rho_p / \rho_c = 100$, $w = 2500$ km and Vp = 0.5 km s^{-1}, we find $\alpha = 47.4°$ and
$V_{\perp} = 0.34$ km s^{-1}, $V_{//} = 43.3$ km s^{-1}, $V_h = 29.6$ km s^{-1} and $V_v = -31.7$ km s^{-1}.
Then, in absolute value, $V = 43.3$ km s^{-1}.

Thus, a subsonic coronal flow is expected to occur both sides of the prominence, in agreement with observations by TSUBAKI (1975) in coronal lines, and LITES (1976) and MALHERBE et al (1983b) in transition zone lines.

III - APPROXIMATE MODEL FOR THE COOLING MECHANISM

We study here the equilibrium energy balance of coronal material around the sheet; the hot plasma is found to be thermally unstable and an approximate model for the cooling process is proposed.

III - 1 - Equilibrium energy balance.

For simplicity we suppose that the magnetic field is uniform on both sides of the current sheet so that :

$$\alpha = tg^{-1} \left(B_y / B \right) = const$$

$$\varphi = tg^{-1} \left(B_z / B_x \right) = const$$

The equilibrium energy balance may be written, neglecting thermal conduction perpendicular to magnetic lines, as :

$$h\rho - \rho^2 \chi T^{\alpha} + \vec{\nabla} . \left(\left(k_{//} \vec{\nabla} T . \vec{e_b} \right) \vec{e_b} \right) = 0 \qquad (7)$$

where $\vec{e_b} = \vec{B} / B$ and $k_{//} = ko\ T^{5/2}$ is the thermal conductivity parallel to field lines : for fully ionized hydrogen, $ko = 3\ 10^{-11}$ (ORRALL and ZIRKER, 1961). Assuming all variables depend on x alone, equation (7) reduces to

$$h\rho - \rho^2 \chi T^{\alpha} + \frac{d}{dx} \left(\frac{B_x^2}{B^2} k_{//} \frac{dT}{dx} \right) = 0$$

Furthermore, we approximate the heat conduction term by

$$\frac{B_x^2}{B^2} k_{//} \frac{T_c - T}{L^2}$$

where L is a length-scale characteristic of coronal formations around prominences.

If wave-heating balances radiation in the corona, we may take $h_c = \rho_c \chi_c T_c^{\alpha c}$. We introduce a reduction factor δ ($0 \leq \delta \leq 1$) for the heating around prominences, so that $h = \delta h_c$.
Assuming that the gas pressure P remains constant during the condensation process, a relationship between coronal and prominence temperatures (Tc, T) and densities (ρ_c, ρ) is given by the perfect gas law and equation (4) :

$$\rho_c T_c \left(1 + \varepsilon^2 / \beta \right) = \rho T = const$$

Then, equation (7) becomes :

$$\delta - q(\bar{T})\,\eta + \frac{\tau_R}{\tau_c}\,\frac{\cos^2\alpha\,\cos^2\varphi}{\eta}\,\frac{\bar{T}^{7/2}\,(1-\bar{T})}{(L/H_c)^2} = 0 \qquad (8)$$

where $\bar{T} = T/T_c$, H_c is the coronal height-scale ($\approx$60 Mm) and $\eta = 1+\varepsilon^2/\beta$ is the prominence compression factor (section II-2).

$\tau_c = P_c H_c^2 / k_0 T_c^{7/2}$ and $\tau_R = P_c/\rho_c^2 \chi_c T_c^{\alpha_c}$ (see equation 3)

are respectively the coronal conductive and radiative time-scales, and

$q(\bar{T}) = \chi \bar{T}^{\alpha-1}/\chi_c T_c^{\alpha_c-\alpha} = T_c\,Q(T)/T\,Q(T_c)$ is a normalized cooling function.

In cases when $\delta = 1$ (compression only) or $\eta = 1$ (reduced heating only), it can be shown that the equilibrium described by equation (8) ceases to exist when

$$L > L_m = H_c \cos\varphi \cos\alpha \left(\tau_R/2\tau_c\right)^{1/2}$$

Such a result is similar to those obtained by HOOD and PRIEST (1979), SMITH and PRIEST (1977) and PRIEST and SMITH (1979). When $L > L_m$, thermal conduction is no longer able to stabilize the radiative cooling process.

From coronal conditions, with

$$\tau_R = 1.5\ 10^4\ s\ ,\ \tau_c = 3\ 10^3\ s\ ,\ \alpha = 47.4^\circ\ ,\ \varphi = 65^\circ,$$

we obtain $L_m/H_c = 0.44$ or $L_m = 26.4$ Mm .

Since L_m is probably of the order of H_c, the plasma is likely to be thermally unstable.

Moreover, at a fixed L value, a critical value of φ :

$$\varphi_m = \cos^{-1}\left(\frac{L}{H_c \cos\alpha}\left(\frac{2\tau_c}{\tau_R}\right)^{1/2}\right)$$

may exist, beyond which no equilibrium is possible, in agreement with PRIEST and SMITH (1979).

III - 2 - Stability of equilibrium

The stability of thermal equilibrium, when it exists, may be investigated, following SMITH and PRIEST (1977) :

Perturb equilibrium (7) at constant gas pressure :

$$\rho C_p \, \partial T/\partial t = h\rho - \rho^2 \chi T^{\alpha} + \vec{\nabla}.\left((k_{//} \vec{\nabla} T . \vec{e_b}) \vec{e_b} \right) \qquad (9)$$

Using the same simplifications and notations as in section III-1, equation (9) reduces to :

$$\partial \overline{T}/\partial t = F(\overline{T}, \eta, \delta) \qquad (10)$$

where $F(\overline{T}, \eta, \delta) = \frac{\gamma - 1}{\gamma} \left(\delta - q(\overline{T}) \eta + \frac{\sigma_R}{\sigma_c} \frac{\cos^2\alpha \cos^2\varphi}{\eta} \frac{\overline{T}^{7/2}(1-\overline{T})}{(L/H_c)^2} \right)$

At equilibrium temperature $\overline{T}_e$,

$F(\overline{T}_e, \eta, \delta) = 0$

A second order development of equation (10) provides :

$$\frac{\partial}{\partial t}(\overline{T} - \overline{T}_e) = (\overline{T} - \overline{T}_e) \left(\frac{\partial F}{\partial \overline{T}} \right)_{\overline{T} = \overline{T}_e} + \frac{1}{2} (\overline{T} - \overline{T}_e)^2 \left(\frac{\partial^2 F}{\partial \overline{T}^2} \right)_{\overline{T} = \overline{T}_e}$$

We shall now treat only the case $\delta = 1$ (initial compression). The case $\eta = 1$ (reduced heating) would lead to similar results.

In a state of equilibrium, $F(\overline{T}, \eta(\overline{T})) = 0$

Then

$$\frac{\partial F}{\partial \overline{T}} = - \frac{\partial F}{\partial \eta} \frac{\partial \eta}{\partial \overline{T}}$$

- If $\partial\eta/\partial\overline{T} \neq 0$, the equilibrium is stable when $\partial F/\partial \overline{T} < 0$ and unstable when $\partial F/\partial \overline{T} > 0$.

- If $\partial\eta/\partial\overline{T} = 0$, $\frac{\partial F}{\partial \overline{T}} = 0$ and a second order treatment is necessary. We find

$$\frac{\partial^2 F}{\partial \overline{T}^2} = - \frac{\partial F}{\partial \eta} \frac{\partial^2 \eta}{\partial \overline{T}^2}$$

the equilibrium is stable when $\partial^2 F/\partial \overline{T}^2 > 0$ and unstable when $\partial^2 F/\partial \overline{T}^2 < 0$.

The results of this stability analysis are summarized in Figure 2.

III - 3 - Temperature of cold equilibrium

At prominence temperatures, wave-heating balances radiative cooling. The temperature is given by

$$T = \left(\frac{\delta}{\eta} \frac{\chi_c T_c^{\alpha_c - 1}}{\chi} \right)^{\frac{1}{\alpha - 1}} = \left(\frac{\delta}{\eta} \right)^{0.156} \times 8.2\ 10^3\ K \quad \text{(table 2)}.$$

If wave-heating were completely absent ($\delta = 0$), which may be the case in the densest parts of prominences, heat conduction should balance radiation, but it would produce too much cold filaments, because the cooling function Q(T) (table 1) is appropriate only for optically thin plasmas. So a modification would be required to reduce the radiative losses in the central optically thick parts of prominences (take for instance $\alpha = 17.4$, as in MILNE et al, 1979).

III - 4 - The cooling time of prominence material.

Assuming constant gas pressure, the prominence condensation may be modelled using the energy equation :

$$\rho C_p \, dT/dt = h\rho - \rho^2 Q(T) + \vec{\nabla} \left((k_{//} \vec{\nabla} T . \vec{e_b}) \vec{e_b} \right) \qquad (11)$$

where

$$dT/dt = \partial T/\partial t + (\vec{V} . \vec{\nabla}) T \qquad (12)$$

For a steady state, $\partial/\partial t = 0$.

We assume that magnetic field motions are vertical, so that $\vec{V} = Vz\ \vec{ez} + V_{//}\ \vec{e_b}$, Vz being a constant and $V_{//}$ being the velocity along field lines. Symmetry conditions in the sheet impose $V_{//} = 0$.

Then equation (12) becomes $dT/dt = V_z \partial T/\partial z = \partial T/\partial \tau$ where $\tau = z/V_z$.

Using the approximations of section III-1 for evaluating the conductive term, and choosing L as the height scale (L = Hc T/Tc), we obtain the temperature evolution T (τ) from the following relation :

$$\overline{\tau} = \frac{\gamma}{\gamma - 1} \int_1^{\overline{T}} du \Big/ \left(\delta - q(u) \eta + \frac{\tau_R}{\tau_c} \frac{\cos^2\alpha \cos^2\varphi}{\eta} \; u^{3/2} (1 - u) \right)$$

which must be integrated numerically, and where $\overline{\tau} = \tau / \tau_R$.

The temperature behaviour is sketched in Figure 3 for different values of η (sheet compression factor) and δ (heating reduction factor). The cooling time $\overline{\tau}_{cool}$ is plotted in Figure 4a for various values of η and δ. It decreases with η at fixed δ. The heating reduction factor δ has a weak influence on $\overline{\tau}_{cool}$ for high η values, but has an important one at low η compression rates. This conclusion is similar for the effect of shear φ (see figure 4b). Shearing the structure, or reducing the heating factor δ, or increasing the compression factor η diminish the prominence cooling time.

Typical $\overline{\tau}_{cool}$ values may lie in the range $0.1\ \tau_R$ to τ_R, numerically 10^3 s to 10^4 s, corresponding to cooling altitudes from 500 km to 5000 km (with Vz = 0.5 km s^{-1}).

III - 5 - Input velocity of coronal material.

Coronal material flows down along magnetic lines when approaching the sheet, while it condenses and cools. The condensation mechanism may be described by equations (11) and (12), where $\partial/\partial t = 0$ and $(\vec{V}.\vec{\nabla})T = \partial T/\partial z + V_{//}\,\partial T/\partial s$. An approximate solution consists in replacing $V_{//}\,\partial T/\partial s$ by $-V(T_c - T)/H$, where V is the absolute velocity and H the height scale. The velocity V is deducible from the continuity equation

$$\vec{\nabla}.(\rho\vec{V}) = 0$$

which can be approximated by

$$\partial\rho/\partial z - V\rho_c/H = 0$$

Assuming constant gas pressure, the velocity is given by

$$\overline{V} = -\frac{\eta}{\overline{T}^2}\,\frac{\partial\overline{T}}{\partial\overline{z}} \qquad (13)$$

where $\overline{V} = V/C_S$ and $\overline{z} = z/\tau_D$, $\tau_D = H_c/C_S$ being the coronal dynamical time-scale. Using equations (11) to (13), the evolution of temperature and velocity both sides of the sheet may be deduced from

$$\overline{z} = \frac{\gamma}{\gamma-1}\int_1^{\overline{T}} \frac{\left(1+\eta\,(1-\overline{T})/\overline{T}^2\right)\,d\overline{T}}{\frac{\tau_D}{\tau_R}\left(\delta - q(\overline{T})\,\eta\right) + \frac{\tau_D}{\tau_c}\,\frac{\cos^2\alpha\cos^2\varphi}{\eta}\,\overline{T}^{3/2}(1-\overline{T})}$$

and $$\overline{V} = -\frac{\eta}{\overline{T}^2}\,\frac{\gamma-1}{\gamma}\,\frac{\frac{\tau_D}{\tau_R}\left(\delta - q(\overline{T})\,\eta\right) + \frac{\tau_D}{\tau_c}\,\frac{\cos^2\alpha\cos^2\varphi}{\eta}\,\overline{T}^{3/2}(1-\overline{T})}{1+\eta\,(1-\overline{T})/\overline{T}^2}$$

Functions $\overline{T}(\overline{\tau})$ and $\overline{V}(\overline{\tau})$ are sketched in Figure 5a for $\eta = 1.5$ and $\delta = 0$ or 1. The velocity reaches its maximum for $T = 3\ 10^5$ K. Its effect is to increase the cooling time τ_{cool} on both sides of the sheet. τ_{cool} is measured at the inflexion point of curves $\overline{T}(\overline{\tau})$ and plotted versus η in figure 5b, as well as the velocity maximum, which appears to be almost independent of δ. On the contrary, it increases strongly with the sheet compression factor η and becomes supersonic when η exceeds 4.2. In that case, a shock wave would be expected.

If such a condensing flow is observable, the comparison with EUV observations of subsonic motions by LITES (1976) and MALHERBE et al (1983b) suggests that the compression factor η could be small ($\ll 2$), implying that the vertical component of the coronal magnetic field could be smaller than 3 G.

CONCLUSION

We have here discussed the formation and the condensation of plasma in the dynamic prominence model of MALHERBE and PRIEST (1983). A stationary process was investigated : as coronal material approaches the filament, we suggest that a thermal instability can trigger the cooling of the plasma. Such a mechanism may be initiated by either a larger gas pressure in the sheet or a smaller wave-heating than in the neighbouring corona. Such a condensation process holds for a Kuperus-Raadu magnetic geometry. For Kippenhahn-Schlüter prominences, a possible dynamic formation has been described by PRIEST and SMITH (1979).

A further improvement of our simple model would consist of producing a 1-D numerical model with boundary conditions fixed in the corona around the sheet or, better, at an infinite distance from it. First, we plan to solve the equations of continuity, energy, and motion along the field lines of a prescribed magnetic configuration depending on variable x only. A second step could consist in a 2-D numerical simulation. It would allow us to investigate the hydrodynamics of cold material flowing up inside the prominence, together with the cooling phase and motions of new coronal material entering the sheet. This will be the subject of another paper.

Also, a better knowledge of wave-heating around prominences is required as well as a more precise determination of the magnetic support. The effect of the finite height of a prominence could also be incorporated (see PRIEST and SMITH, 1979, for a static description), but it would raise a new thermodynamical problem.

ACKNOWLEDGEMENTS

This work was begun while one of the authors (JMM) was a visitor at the University of St. Andrews. He wants to thank all the staff members for their hospitality. He would also like to thank Dr. P. MEIN and Dr. B. SCHMIEDER for helpful discussions and suggestions. Numerical computations were performed on the VAX 11 system of INAG at Meudon.

The authors are indebted to M. LEVEQUE for typing the manuscript.

REFERENCES

CHIUDERI, C., VAN HOVEN, G. : 1979, Astrophys. J. Letters, 232, L69.

HEYVAERTS, J. : 1980, Ann. Phys., 5, 337.

HILDNER, E. : 1974, Solar Phys., 35 123.

HOOD, A.W., PRIEST, E.R. : 1979, Astron. Astrophys., 77,233.

KIPPENHAHN, R., SCHLÜTER, A. : 1957, Z. Astrophys., 43, 36.

KUPERUS, M. TANDBERG-HANSSEN, E. : 1967, Solar Phys., 2, 39.

LEROY, J.L., BOMMIER, V., SAHAL BRECHOT, S. : 1983, Solar Phys., in Press.

LITES, B. : 1976, Astrophys. J. Letters, 210, L111.

MALHERBE, J.M., SCHMIEDER, B., MEIN, P. : 1981, Astron. Astrophys., 102, 124.

MALHERBE, J.M., SCHMIEDER, B., RIBES, E., MEIN, P. : 1983a, Astron. Astrophys., in press.

MALHERBE, J.M., SCHMIEDER, B., MEIN, P. : 1983b, in preparation.

MALHERBE, J.M., PRIEST, E.R. : 1983, Astron. Astrophys., in press.

MARTRES, M.J., MEIN, P., SCHMIEDER, B., SORU-ESCAUT, I. : 1981, Solar Phys., 69, 301.

ORRALL, F.Q., ZIRKER, J.B. : 1961, Astrophys. J., 134, 72.

PRIEST, E.R. : 1982, Solar Magnetohydrodynamics, D. Reidel Pub. C°, Dordrecht, Holland.

PRIEST, E.R., Smith, E.A. : 1979, Solar Phys., 64, 267.

RAADU, M.A. : 1979, in Physics of Solar Prominences, IAU Coll. n° 44, 167, Jensen, Maltby, Orrall eds.

RAADU, M.A., KUPERUS, M. : 1973, Solar Phys., 28, 77.

SMITH, E.A., PRIEST, E.R. : 1977, Solar Phys., 53, 25.

SOMOV, B.V., SYROVATSKY, S.I. : 1980, Pis'ma Astron. Zh., 6, 592.

TSUBAKI, T. : 1975, Solar Phys., 43, 147.

Table 1

The cooling function $Q(T) = \chi T^{\alpha}$ according to Hildner (1974)

Temperature range (K)	χ (MKS)	α
$T < 1.5\ 10^4$	$1.759\ 10^{-13}$	7.4
$1.5\ 10^4 < T < 8\ 10^4$	$4.290\ 10^{10}$	1.8
$8\ 10^4 < T < 3\ 10^5$	$2.860\ 10^{19}$	0
$3\ 10^5 < T < 8\ 10^5$	$1.409\ 10^{33}$	- 2.5
$T > 8\ 10^5$	$1.970\ 10^{24}$	- 1.0

Table 2

The prominence temperature versus δ (heating reduction factor) and η (compression factor).

η \ δ	1	0.5	0.1	0.01	0
1	8202	7360	5724	3994	1550
1.1	8081	7252	5639	3935	1491
1.25	7921	7108	5528	3857	1415
1.5	7699	6908	5372	3749	1314
2	7360	6605	5136	3584	1168
5	6379	5724	4451	3106	804

FIGURE CAPTIONS

Figure 1 : Schematic representation of the prominence, showing the coordinate system used throughout the paper.
The vertical y axis is in the opposite direction to gravity.
The x axis is normal to the prominence sheet, while
the z axis runs along the filament length.
The solid headed arrows represent the velocity field.

Figure 2 : The equilibrium temperature T of the sheet as a function of η (compression factor) or δ (heating reduction factor).
According to L or φ values, a hot equilibrium is possible in case (a), but impossible in case (b). As δ or η increases, the path followed by the solution is indicated by the arrows (from A to B or C).

Figure 3 : The temperature evolution of the sheet during the cooling process with wave-heating (continuous line) or without (dashed line), for different values of the compression factor η .

Figure 4 : The cooling time $\tau_{cool}(\varphi, \delta, \eta)$ of the prominence sheet.
(a) as a function of δ and η .
(b) effect of shear φ : the ratio $\tau_{cool}(\varphi=0°)/\tau_{cool}(\varphi=90°)$ as a function of δ and η .

Figure 5 : The cooling process on both sides of the sheet.
(a) velocity and temperature evolutions for $\eta = 1.5$, with heating (continuous line) or without (dashed line).
(b) the cooling time and the velocity maximum V_m as functions of δ and η .

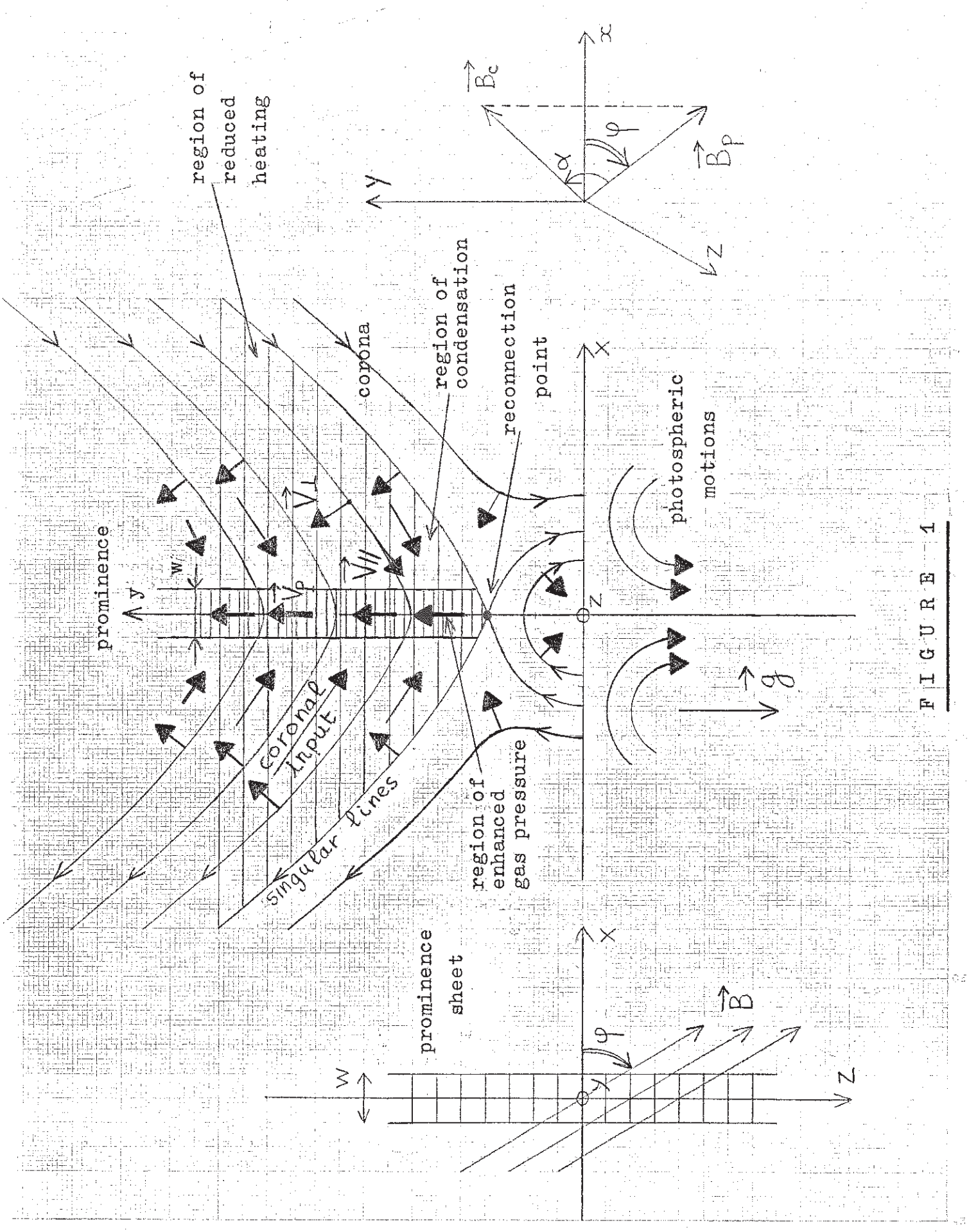
region of reduced heating
corona
region of condensation
reconnection point
photospheric motions
prominence
coronal input
singular lines
region of enhanced gas pressure
prominence sheet
$\vec{B}_c$
$\vec{B}_p$
$\vec{B}$
$\vec{V}_\perp$
$\vec{V}_{//}$
$\vec{V}_p$
$\vec{g}$
x
y
z
w
φ
α

FIGURE 1

FIGURE 2

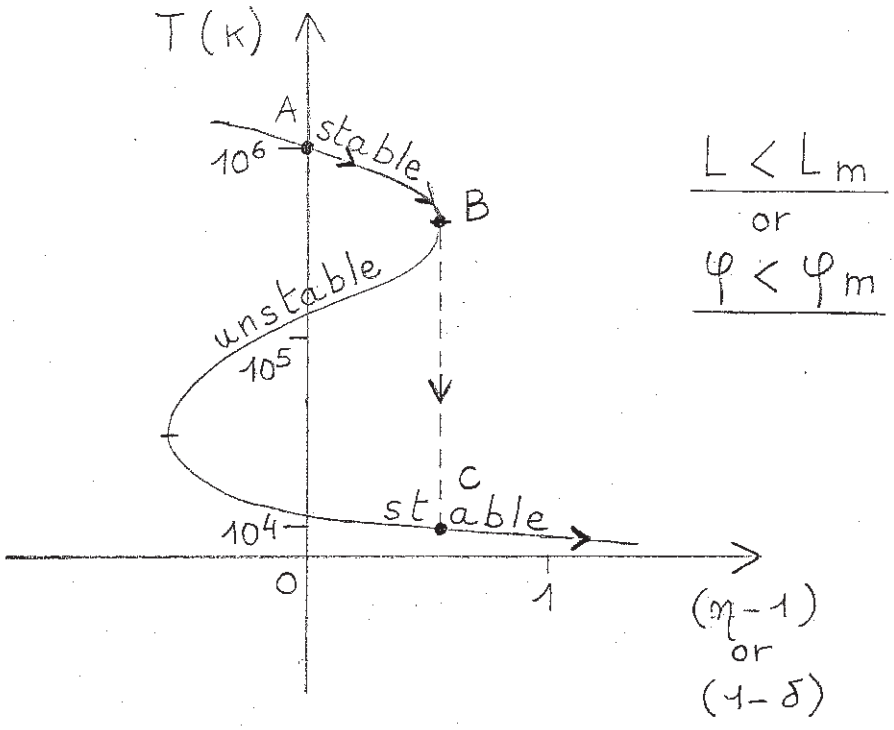
T(K)
A
stable
10^6
B
unstable
10^5
C
stable
10^4
0
1
$(\eta-1)$
or
$(1-\delta)$
$L < L_m$
or
$\varphi < \varphi_m$

(a)

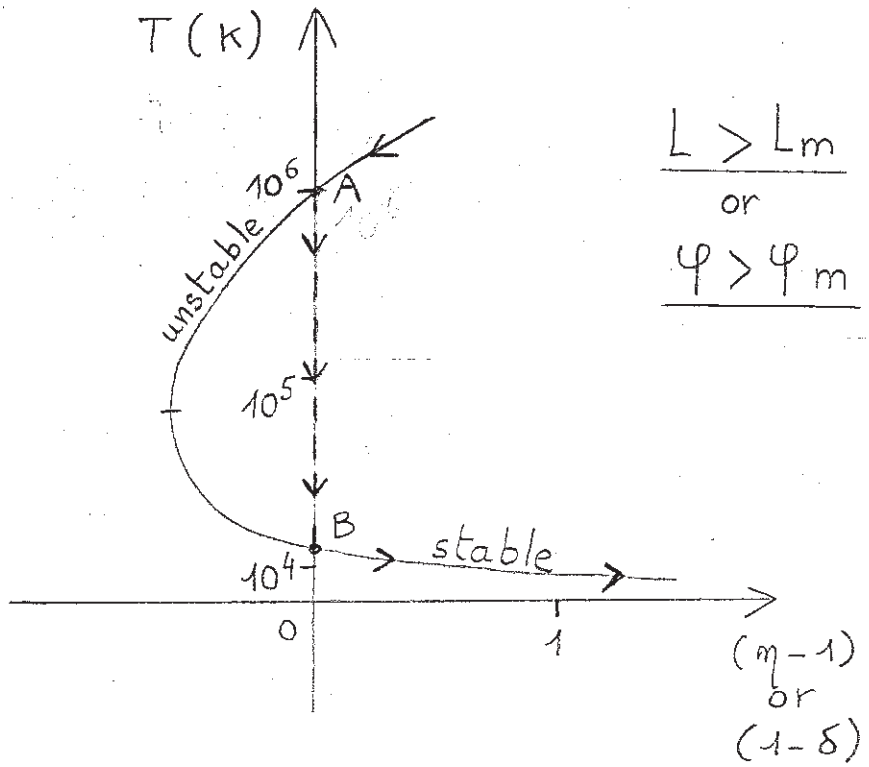
T(K)
10^6
A
unstable
10^5
B
stable
10^4
0
1
$(\eta-1)$
or
$(1-\delta)$
$L > L_m$
or
$\varphi > \varphi_m$

(b)

FIGURE 3

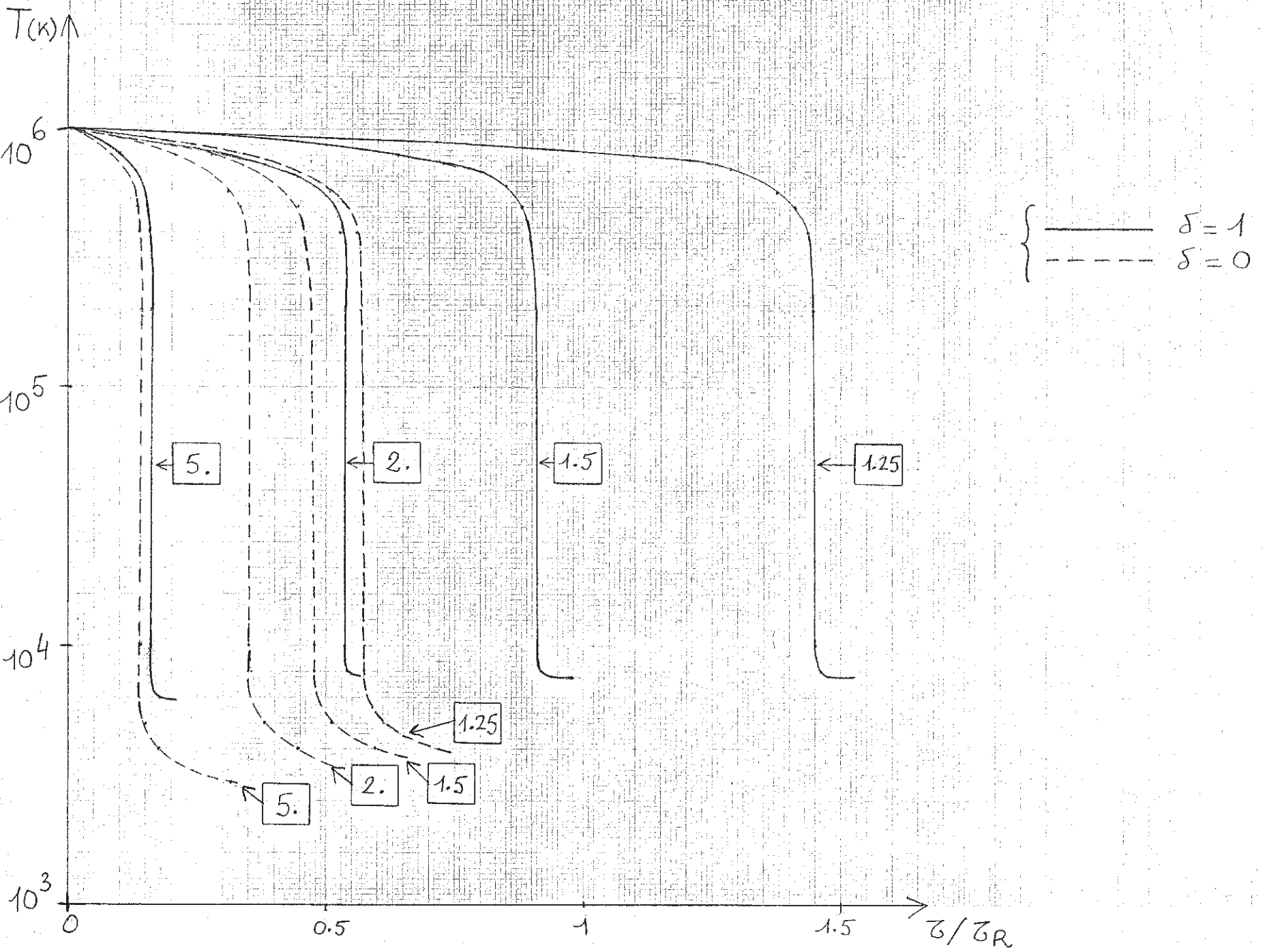

FIGURE 4

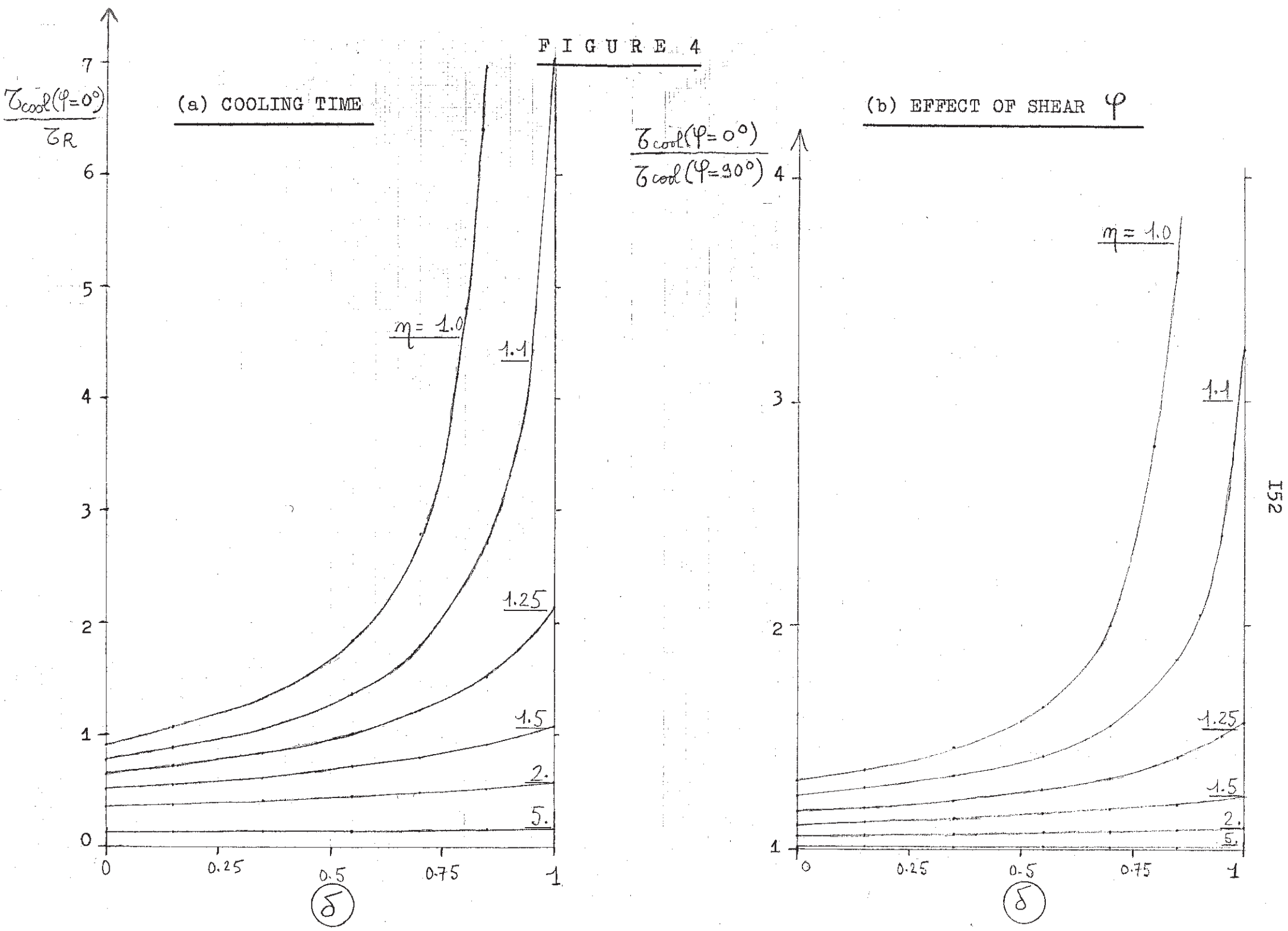
(a) COOLING TIME
$\frac{\tau_{cool}(\varphi=0°)}{\tau_R}$
7
6
5
4
3
2
1
0
m = 1.0
1.1
1.25
1.5
2.
5.
0
0.25
0.5
0.75
1
δ
(b) EFFECT OF SHEAR φ
$\frac{\tau_{cool}(\varphi=0°)}{\tau_{cool}(\varphi=90°)}$
4
3
2
1
m = 1.0
1.1
1.25
1.5
2.
5.
0
0.25
0.5
0.75
1
δ

FIGURE 5

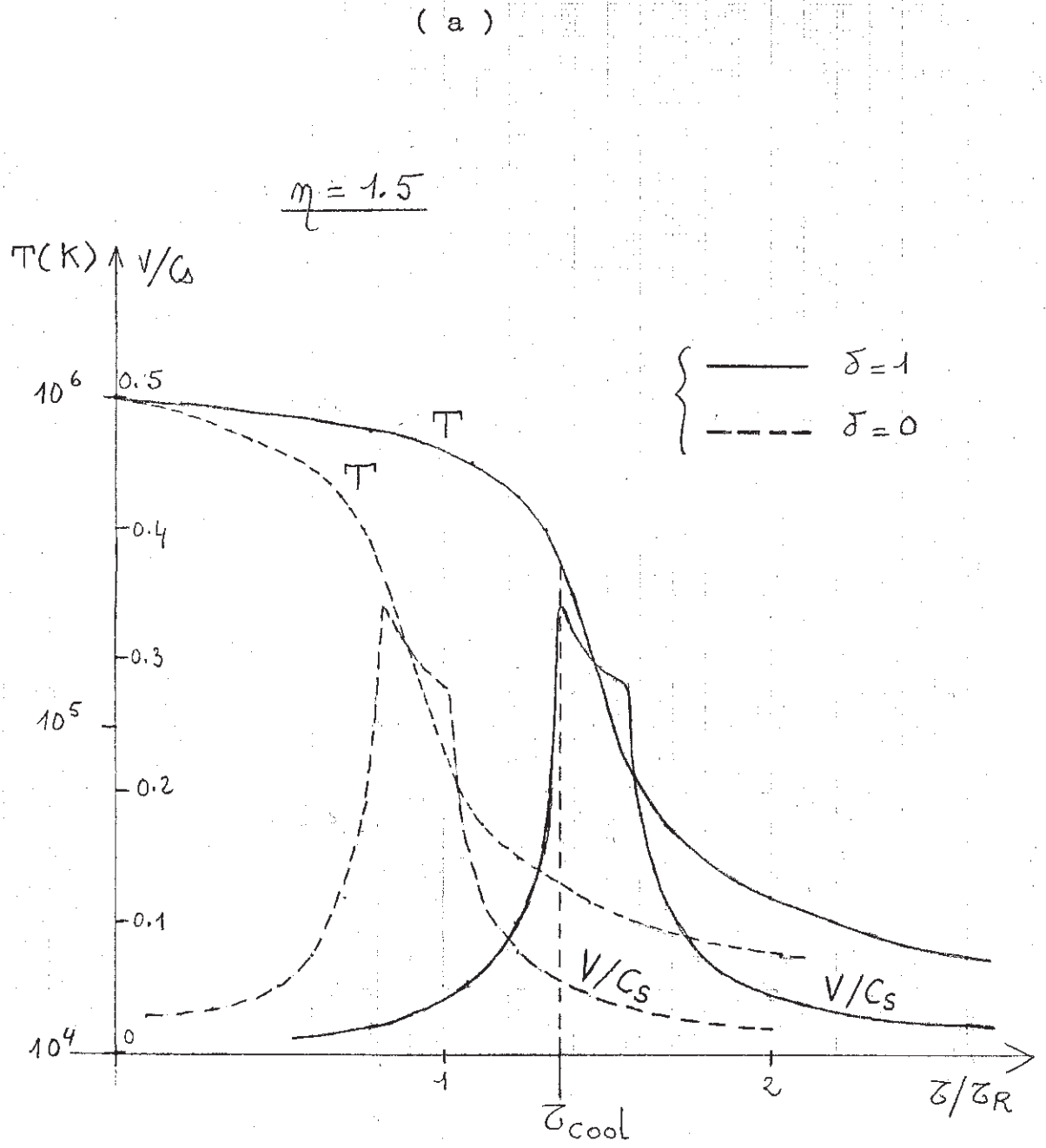
(a)
η = 1.5
T(K)
V/Cs
10^6
10^5
10^4
0.5
0.4
0.3
0.2
0.1
0
T
T
δ = 1
δ = 0
V/Cs
V/Cs
1
2
τ/τR
τcool

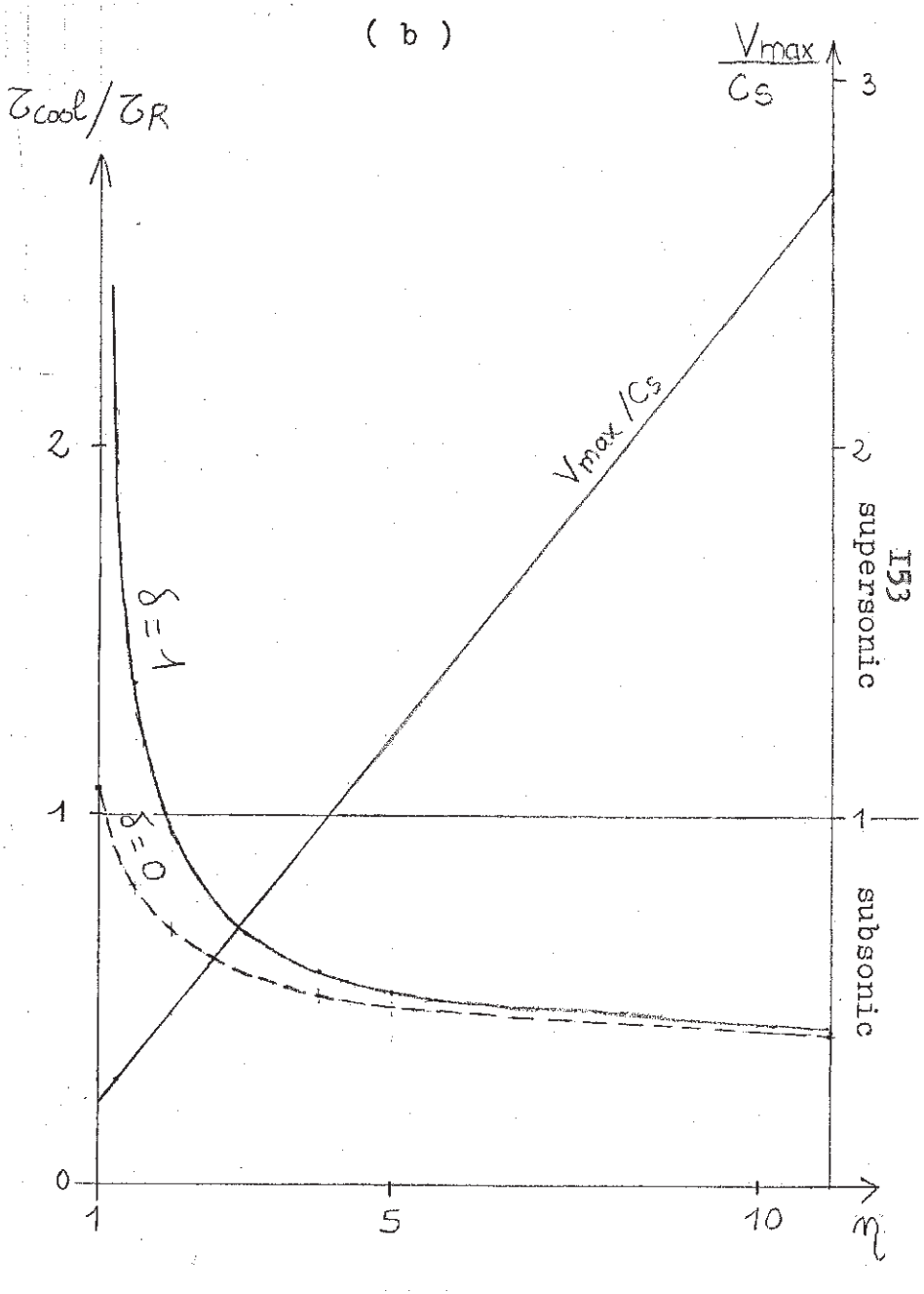
(b)
τcool/τR
Vmax/Cs
3
2
1
0
Vmax/Cs
δ = 1
δ = 0
1
5
10
η
supersonic
subsonic

V - CONCLUSIONS ET PERSPECTIVES

Nous avons orienté notre travail principalement vers l'élaboration d'un modèle d'équilibre dynamique de protubérance solaire.

Dans un premier temps, nous nous sommes efforcés d'accroître nos connaissances sur le champ des vitesses dans les filaments, à partir d'observations essentiellement au DPSM de la Tour Solaire de Meudon.

Nous avons entrepris une étude statistique du champ des vitesses à partir d'observations centre-bord, qui nous ont permis, moyennant l'hypothèse de stationnarité, d'obtenir les 3 composantes du vecteur vitesse. Un modèle de circulations globales de matière a pu en être déduit, que nous n'avons pu expliquer à l'aide des rares théories existantes.

Nous avons essayé, dans un second temps, de construire un nouveau modèle pour rendre compte des mouvements observés. Nous n'avons pas cherché, comme le faisaient en vain les modèles actuels, à utiliser un mécanisme de siphon dans un champ magnétique statique ; au contraire, nous avons envisagé les conséquences dynamiques de l'évolution du support magnétique, suggérée d'ailleurs observationnellement. Cette évolution pourrait être engendrée par des mouvements photosphériques entrainant les pieds des lignes de force, à cause de la forte densité et conductivité du plasma. Nous avons donc étudié l'évolution de plusieurs supports de type Kippenhahn-Schlüter ou Kuperus-Raadu, sous l' influence de mouvements photosphériques convergents (c'est le cas, sous les protubérances des ceintures polaires, au moins), et nous en avons conclu qu'un support de type Kuperus-Raadu était nécessaire pour reproduire les mouvements observés, ce qui, de plus, est en accord avec les déterminations expérimentales de champ magnétique. Nous avons donc proposé un modèle dynamique à reconnections magnétiques stationnaires, dans lequel le plasma protubérantiel est transporté par les mouvements ascendants des lignes de force. Les processus de condensation et de refroidissement du chaud plasma coronal alimentant le filament sur ses bords, au dessus du site de reconnections, ainsi

que son mouvement (couplé à la thermodynamique) ont été examinés.

Bien entendu, des observations plus nombreuses et plus performantes seront nécessaires pour valider ce modèle.

En ce qui concerne l'étude du champ des vitesses, le DPSM s'avère être un outil très adapté pour les raies chromosphériques ; nous attendons beaucoup des instruments du Pic du Midi et, en 1984, des Canaries pour améliorer la qualité de nos observations. Nous pensons aussi étendre cette étude à la zone de transition autour des filaments, encore mal connue, grâce à des observations UV sur SMM2 (en 1984) coordonnées avec le DPSM.

Une meilleure connaissance du support magnétique est particulièrement cruciale pour l'élaboration des modèles. Bien que la technique Hanlé soit très féconde pour les mesures au limbe, elle ne permet pas d'étudier les structures dont l'altitude est inférieure à 10 000 Km, donc les "pieds" des filaments dont l'existence reste mal comprise. Des mesures sur le disque sont donc nécessaires et nous attendons de THEMIS, avec la détermination des 3 composantes du champ, un progrès certain.

Mais, d'ores et déjà, une étude plus poussée du support magnétique que par le passé semble possible. Nous pensons étendre la méthode d'Anzer (1972) à l'étude de supports force-free plus généraux et ainsi, à partir d'observations centre-bord, reconstituer la structure magnétique. Nous envisageons aussi, pour trouver une réponse aux mouvements descendants dans les fins filets verticaux observés au limbe, d'étudier la condensation desprotubérances dans une arcade coronale et la diffusion du plasma au travers des lignes de force par microinstabilités (Rayleigh-Taylor). Enfin, la stabilité des divers modèles proposés devrait aussi être analysée, en tenant compte de l'ancrage photosphérique des lignes de force, mais c'est là une difficile entreprise.

oooooooooooooo

BIBLIOGRAPHIE GENERALE

ANZER, U. : 1969, Solar Phys., 8, 37

ANZER, U. : 1972, Solar Phys., 24, 324

ANZER, U. : 1979, in Physics of Solar Prominences, IAU coll. 44, 322, Jensen, Maltby, Orrall eds.

ANZER, U., TANDBERG-HANSSEN, E. : 1970, Solar Phys., 11, 61

BECKERS, J.M. : 1968, Solar Phys., 3, 367

BOMMIER, V., SAHAL-BRECHOT, S. : 1979, in Physics of Solar Prominences, IAU Coll. 44, 87, Jensen, Maltby, Orrall eds.

BRUZEK, A. : 1951, Z. Astrophys., 13, 277

BRUZEK, A. : 1957, Z. Astrophys., 42, 76

CARLQVIST, P. : 1979, Solar Phys., 63, 353

CHIUDERI, C., VAN HOVEN, G. : 1979, Astrophys.J. Letters, 232, L69

DUBOIS, M.A., SAMAIN, A. : 1980, Ann. Phys., 5, 409

DUNN, R.B. : 1960, Thesis, Harvard University

ENGVOLD, O. : 1976, Solar Phys., 49, 283

ENGVOLD, O. MALVILLE, J.M. :1977, Solar Phys. 52, 369

ENGVOLD, O., MALVILLE, J.M., LIVINGSTON, W. : 1978, Solar Phys. 60, 57

FIELD, G.B. : 1965, Astrophys. J., 142, 531

FOUKAL, P.V. : 1975, Solar Phys. 43, 327

HEYVAERTS, J., LASRY, J.M., SCHATZMAN, M., WITOMSKY, G. : 1980, Lecture Notes Math., 782, 160

HEYVAERTS, J., MERCIER, C. : 1977, Astron. Astrophys., 61, 685

HEYVAERTS, J., PRIEST, E.R., RUST, D.M. :1977, Astrophys. J., 216, 123

HILDNER, E. : 1974, Solar Phys., 35, 123

HOOD, A.W., PRIEST E.R. : 1979, Aston. Astrophys. 77, 233

HOOD, A.W., PRIEST E.R. : 1980, Solar Phys., 66, 113

HOOD, A.W., PRIEST, E.R. : 1981a, Geophys. Astrophys. Fluid Dynamics, 17, 297

HOOD, A.W., PRIEST, E.R. : 1981b, Solar Phys., 73, 289

HYDER, C.L. : 1966, Z. Astrophys. 63, 78

JENSEN, E., MALTBY, P., ORRALL, F.Q. : 1979, Physics of Solar Prominences, IAU Coll. 44.

JORDAN, S.D. : 1981, in The Sun as a Star, 301, monograph series on nonthermal phenomena in stellars atmospheres, CNRS and NASA publ.

KAHLER, S.W., WEBB, D.F., MORE, R.L. : 1979, Bull. American Astron. Soc., 11, 659

KIPPENHAHN, R., SCHLUTER, A. : 1957, Z. Astrophys., 43, 36

KLECZEK, J., KUPERUS, M. : 1969, Solar Phys. 6, 72

KUBOTA, J. : 1980, in proc. Japan France Sem. on Solar Phys. 178, Moriyama and Henoux eds.

KUPERUS, M., and HEYVAERTS, J. : 1980, Ann.Phys., 5, 483

KUPERUS, M., RAADU, M.A. : 1974, Astron. Astrophys., 31, 189

KUPERUS, M., TANDBERG-HANSSEN, E. : 1967, Solar Phys.2, 39

LERCHE, I.,LOW, B.C. : 1977, Solar Phys., 53, 385

LERCHE, I., LOW, B.C. : 1980, Astrophys. J., 238, 1088

LERCHE, I., LOW, B.C. : 1981, Solar Phys., 69, 327

LEROY, J.L. : 1982, private communication

LEROY, J.L., BOMMIER, V., SAHAL-BRECHOT, S. : 1982, Solar Phys. in press.

LITES, B. : 1976, Astrophys. J. Letters, 210, L111

LOW, B.C. : 1977, Astrophys.J., 212, 234

LOW, B.C. : 1981, Astrophys.J., 246, 538

LOW, B.C. : 1982, Solar Phys., 75, 119

MALTBY, P. : 1976, Solar Phys., 46, 149

MARTRES, M.J. : 1956, l'Astronomie, 70, 401

MARTRES, M.J., RAYROLE, J., SORU-ESCAUT, I. : 1976, Solar Phys. 46, 137

MARTRES, M.J., MEIN, P., SCHMIEDER, B., SORU-ESCAUT I. : 1981, Solar Phys. 69, 301

MARTRES, M.J. : 1982, private communication

MEIN, P. : 1977, Solar Phys., 54, 45

MEIN, N., SCHMIEDER, B. : 1981, Astron. Astrophys., 97, 310

MILNE, A.M., PRIEST, E.R., ROBERTS, B. : 1979, Astrophys.J., 232, 304

MOORE, R.L., LABONTE, B.J. : 1980, in proc. IAU Coll. 91, 207, Dryer and Tandberg-Hanssen eds.

MORETON, G.E. : 1960, Astron.J., 65, 494

MORETON, G.E. : 1965, in proc. IAU Coll. 22, 371

MOURADIAN, Z., MARTRES, M.J., SORU-ESCAUT, I. : 1980, in proc. Japan France sem. on Solar Phys., 195, Moriyama and Henoux eds.

NAKAGAWA, Y., MALVILLE, J.M. : 1969, Solar Phys., 9, 102

PICKEL'NER, S.B. : 1971, Solar Phys., 17, 44

PRIEST, E.R. : 1981, in proc. 3rd European Solar Meeting, 203, Oxford, C. Jordan Ed.

PRIEST, E.R. : 1981, Solar Flare Magnetohydrodynamics, Gordon and Breach eds, London, England

PRIEST, E.R. : 1982, Solar Magnetohydrodynamics, D. Reidel Publ. Co., Dordrecht, Holland

PRIEST, E.R., SMITH, E.A. : 1979, Solar Phys. 64, 267

RAADU, M.A. : 1979, in proc. IAU Coll. 44, 167, Jensen, Maltby and Orrall eds.

RAADU, M.A., KUPERUS, M. : 1973, Solar Phys., 28, 77

RIBES, E., UNNO, W. : 1980, Astron. Astrophys., 91, 129

ROBERTS, B. : 1980, Ann. Phys. 5, 453

RUST, D.M. : 1967, Astrophys. J., 150, 313

SCHMAHL, E.J., MOURADIAN, Z., MARTRES, M.J., SORU-ESCAUT, I. : 1982, Solar Phys. 81, 91

SECCHI, A. : 1875, Le Soleil, Gauthier-Villars, Paris, Vols 1 and 2.

SHIBATA, K., NISHIKAWA, T., KITAI, R., SUEMATSU, Y. : 1982, Solar Phys. 77, 121

SLONIM, Y.M. : 1980, Soviet Astron. Letters, 6, 21

SMITH, E.A., PRIEST, E.R. : 1977, Solar Phys. 53, 25

STEINOLFSON, R.S., SCHMAHL, E.J., WU, S.T. : 1979, Solar Phys., 63, 187

TANDBERG-HANNSEN, E. : 1974, Solar Prominences, D. Reidel Publ. Co., Dordrecht, Holland

TSUBAKI, T. : 1975, Solar Phys. 43, 147

UCHIDA, Y. : 1980, in proc. Japan France sem. on Solar Phys., 169, Moriyama and Henoux eds.

VAN TEND, W., KUPERUS, M. : 1978, Solar Phys. 59, 115

VIAL, J.C. : 1981, Thèse d'état, Université Paris 7

VIAL, J.C., GOUTTEBROZE, P., ARTZNER, G., LEMAIRE, P. : 1979, Solar Phys. 61, 39

WEBB, D.F., JACKSON, B.V. : 1981, Solar Phys. 73, 341

XIAOMA, G., BOSHU, L., YOUGI, D., SUCHUAN, L., ZHI, L. : 1982, in proc. of the SMY Symp., 24st Cospar meet., in press.

ZWEIBEL, E.G. : 1982, Astrophys. J. Letters, 258, L53.

oooooooooooooooo

REFERENCES DES ARTICLES ET COMMUNICATIONS CONSTITUANT LA THESE

Articles

1 - Malherbe, J.M., Schmieder, B., Mein, P. : 1981, Astron. Astrophys., 102, 124

2 - Malherbe, J.M., Schmieder, B., Ribes, E., Mein, P. : 1983, Astron. Astrophys., in press

3 - Malherbe, J.M., Priest, E.R. : 1983, Astron. Astrophys., in press

4 - Malherbe, J.M., Priest, E.R., Heyvaerts, J. : submitted to Astron. Astrophys.

Communications présentées oralement

1 - Malherbe, J.M., Schmieder, B., Mein, P. : 1983, SMM Workshop, Greenbelt, USA

2 - Malherbe, J.M., Simon, G., Mein, P., Mein, N., Schmieder, B., Vial, J.C. : 1982, in proceedings of the 24th Cospar Meeting, Ottawa, Canada.

3 - Malherbe, J.M., Schmieder, B., Mein, P. : 1982, in proceedings of 24th Cospar Meeting, Ottawa, Canada.

Posters

- Malherbe, J.M., Simon, G., Mein, P., Mein, N., Schmieder, B., Vial, J.C. : 1982, poster, IAU Coll. 102, Zürich, Switzerland.

oooooooooooooooooo